



**Data acquisition software development
and physics studies for future lepton
colliders**

Tom Coates

Submitted for the degree of Doctor of Philosophy
University of Sussex
July 2019

Declaration

I hereby declare that this thesis has not been and will not be submitted in whole or in part to another University for the award of any other degree.

Signature:

Tom Coates

UNIVERSITY OF SUSSEX

TOM COATES, DOCTOR OF PHILOSOPHY

DATA ACQUISITION SOFTWARE DEVELOPMENT AND PHYSICS

STUDIES FOR FUTURE LEPTON COLLIDERS

SUMMARY

In this thesis, a software framework called Data Quality Monitoring for High Energy Physics (DQM4hep) is presented, intended as a generic and adaptable online monitoring and data quality monitoring framework for high-energy physics experiments and testbeams. The framework and its development and deployment is discussed, using a number of testbeams as examples. The first group of these testbeams took place within the AIDA-2020 and CALICE collaborations, using the framework on the CALICE-AHCAL prototype. Following this, the framework was also used in the IDEA combined testbeam at the CERN Super Proton Synchrotron. The result of these testbeams was proof that the framework is capable of being adapted easily to a wide variety of detector types and experiments, demonstrating that it has fulfilled the requirements of the AIDA-2020 collaboration. Following this, it was also shown that DQM4hep can be used for online analysis of the IDEA testbeam, performing a similar role to more traditional offline analysis using ROOT.

Also presented is a physics analysis as part of the detector and physics for the Compact Linear Collider collaboration (CLIDdp). The analysis was performed using the hadronic decay channel of the $e^+e^- \rightarrow t\bar{t}h$ process at a centre-of-mass energy of 1.4 TeV. The goal of this analysis was to obtain an updated sensitivity on the measurement of the top-Higgs Yukawa coupling at the planned Compact Linear Collider. The analysis used Monte Carlo generated physics samples and several stages of modern processing, including Pandora Particle Flow Algorithms. Combined with a similar study of the semi-leptonic decay channel, the uncertainty of the coupling measurement was found to be 3.86%.

Acknowledgements

I'd first like to thank my supervisor Fabrizio Salvatore, for being exactly as hands-on and hands-off as I needed, when I needed it, and without whose help, guidance and faith I wouldn't have been able to do this. Thanks to all at the FLC group at DESY in Hamburg, but especially to Katja Krüger, Adrian Irles-Quiles (now at LAL Orsay), and Rémi Eté. Also thanks to the members of the IDEA collaboration, especially Romualdo Santoro. Thanks also the CLIDdp collaboration, but especially Yixuan Zhang and Victoria Martin.

I would like to thank the UK's Science and Technology Funding Council for supporting my studentship and providing me with the funding to perform this research. Thanks also to Linear Collider UK for providing vital funding for travel for the linear collider community in the UK.

I would also like to thank the whole AIDA-2020 collaboration for providing the working environment for a large portion of the work of this thesis and always scheduling their annual meetings in sunny countries with good food. Special thanks to all of the members of Work Package 5 for their support and expertise, and to David Cussans and Matthew Wing for their leadership and organisation of the activities within the group.

Similarly, I would like to thank all of the organisers of the Beam Telescopes and Test Beams workshop for providing a forum for researchers to discuss our work and learn from each other.

Finally, thanks to my highschool physics teachers Mr Coombes and Mr Thomas, who nurtured my early love for physics. I'd like to take this opportunity to apologise for never doing my homework, and hope that this thesis makes up for it.

Contents

1 Future Colliders	1
1.1 The Standard Model	2
1.1.1 The Standard Model as a quantum field theory	2
1.1.2 The Higgs mechanism	4
1.1.3 The Yukawa coupling	5
1.1.4 The completed Standard Model	6
1.2 The physics case for a lepton collider	6
1.2.1 Higgs physics	7
1.2.2 Top physics	8
1.2.3 Supersymmetry	9
1.3 The International Linear Collider	9
1.3.1 ILC detectors	11
1.4 The Compact Linear Collider	13
1.5 The Future Circular Collider	14
1.6 The Circular Electron Positron Collider	15
2 Data acquisition software	23
2.1 Introduction	24
2.1.1 Online monitoring and data quality monitoring	25
2.1.2 The AIDA-2020 project	26
2.2 Overview of DQM4hep	27
2.2.1 Architecture	27
2.2.2 Visualisation and graphical user interface	30
2.3 Analysis modules	33
2.3.1 Running an analysis module	34
2.3.2 Creating analysis modules	35
2.3.3 SimpleModule – a worked example	38

2.4	Data quality monitoring	46
2.4.1	Quality tests	46
2.4.2	Running quality tests	49
2.4.3	Writing quality tests	51
2.5	Documentation and user manual	54
2.5.1	Doxygen documentation	54
2.5.2	User manual	54
2.6	Adaptation to other detectors	55
3	AIDA-2020 testbeams	57
3.1	Introduction	57
3.2	The beamline facilities	59
3.2.1	DESY II	59
3.2.2	CERN-SPS	59
3.3	May 2016 testbeam at DESY II	59
3.3.1	Data format	60
3.3.2	Results	61
3.4	July 2016 testbeam at DESY II	63
3.5	May 2017 testbeam at CERN SPS	66
4	IDEA testbeam	71
4.1	Introduction	71
4.2	Detector components	74
4.2.1	RD52 dual-readout calorimeter	74
4.2.2	Preshower	74
4.2.3	Muon chamber	74
4.2.4	Drift chamber	75
4.2.5	Ancillary detectors	75
4.3	Monitoring	75
4.3.1	File readers	75
4.3.2	Analysis modules	76
4.4	Results	77
4.4.1	ADC to energy calibration	77
4.4.2	Tower ADC calibration	78

5 Physics studies for the Compact Linear Collider	89
5.1 Introduction	90
5.2 The $e^+e^- \rightarrow t\bar{t}H$ process	91
5.2.1 Higgstrahlung	92
5.3 Generation of Monte Carlo samples	93
5.4 Event reconstruction	94
5.4.1 Lepton identification	95
5.4.2 Tau identification	98
5.4.3 Jet clustering	100
5.4.4 Flavour tagging	100
5.4.5 Reconstruction of Higgs, top and W boson candidates	100
5.5 Event selection	101
5.5.1 PandoraPFOs	102
5.5.2 Event shape	102
5.5.3 Durham jet distance parameter	103
5.6 Results	103
6 Discussion	109
Bibliography	113
Acronyms	121

Chapter 1

Future Colliders

Progress is not a straight line.

An Wang

In the post-LHC era, particle physics is at somewhat of an impasse. The Standard Model (SM) has held up to most experiments and observation, and had been tested to a high precision. There are tantalising hints at a theory beyond the Standard Model – in the form of CP-violation, dark matter, and the non-zero neutrino mass and potential violations of lepton flavour universality – but as of yet all new ways to probe the SM for its weaknesses, to see the greater theory behind it, have yielded very little.

There are many planned investigations to attempt to identify physics Beyond the Standard Model that use the Large Hadron Collider (LHC), or plan to leverage the upgrades for the High Luminosity Large Hadron Collider (HL-LHC). However, now that the Higgs boson has been identified successfully, one of the most fruitful avenues for further research is the construction and operation of a lepton collider at the energy frontier, with sufficient centre of mass energy to produce Higgs bosons in large numbers and to interrogate them in greater detail than ever.

This is what motivates the several proposals for future lepton colliders around the world today, that would operate to complement and expand the reach of particle physicists beyond what the LHC is currently capable of. These proposed lepton colliders are broadly split into two groups: linear colliders and circular colliders.

Linear colliders use two accelerator arms pointed towards a single interaction point, and in general are capable of high centre of mass energies. The main candidates for this style of collider are the International Linear Collider (ILC) and the Compact Linear Collider (CLIC).

Circular colliders use a similar layout to the LHC, with a circular accelerator capable

of creating collisions at multiple different interaction points around the circumference of the ring, which permits multiple detectors. The downsides of a circular collider are that lighter particles like electrons have much higher energy losses via synchrotron radiation, limiting the centre of mass energies that a circular lepton collider can operate at. However, in exchange they tend to have much higher luminosities, allowing greater numbers of collisions and higher yields of certain processes or channels. The main candidates for circular colliders are the Future Circular Collider (FCC) and the Circular Electron Positron Collider (CEPC).

The above proposals for new colliders share many of the same motivations, design considerations, features, and challenges, as does the ongoing international effort in research and development to make these colliders a reality.

1.1 The Standard Model

The Standard Model of particle physics divides nature into two domains: particles and forces. The four fundamental forces are electromagnetism, the strong interaction, the weak interaction, and gravitation¹.

The particle domain is split into two – the spin-half particles or *fermions*, and the integer spin particles or *bosons*. The fermions are further split into two – the quarks and the leptons. These categories are defined by their relationship to the four fundamental forces: leptons can interact via the electroweak interaction only, while quarks can interact via both the electroweak and the strong interaction [2].

There are also the force carriers, which are the mechanism through which the fundamental interactions propagate. For instance, when two particles undergo an electromagnetic interaction, they exchange photons (γ). Likewise, weak interactions involve the exchange of W or Z bosons, and strong interactions the exchange of gluons (g).

A table summarising the particles of the Standard Model is shown in Fig. 1.1.

1.1.1 The Standard Model as a quantum field theory

The Standard Model is conceived as a quantum field theory. This describes a number of quantum fields, whose values are defined over all space. In this conception of particle physics, all particles are in fact excitations of the underlying fields. So the Standard Model can be thought of as a system of several overlapping fields:

¹Gravitation is not contained within the SM, although there is an ongoing effort to reconcile the Standard Model with general relativity [1].

- the *fermion fields* (ψ), whose quanta are the fermions (the leptons and quarks)
- the *electroweak fields*, whose quanta are the W_1 , W_2 , W_3 , B bosons
- the *gluon field* (G_a), whose quanta is the gluon

The interactions of these quantum fields can be described by the Lagrangian density \mathcal{L} , usually referred to simply as the Lagrangian.

We can mathematically formulate the Standard Model by writing out a Lagrangian expression for the Standard Model \mathcal{L}_{SM} . We can define this Lagrangian as a combination of individual Lagrangians for the fields described above:

$$\mathcal{L}_{SM} = \mathcal{L}_\psi + \mathcal{L}_{EW} + \mathcal{L}_{QCD} \quad (1.1)$$

where the \mathcal{L} terms in order are the fermion or Dirac term, the electroweak term, and the quantum chromodynamic (or strong) term².

However, a problem arises if we try to define the masses of the fermions in the fermion Lagrangian \mathcal{L}_ψ . This can be seen if we try to add a mass term and write it out fully:

$$m\bar{\psi}\psi = m(\bar{\psi}_L + \bar{\psi}_R)(\psi_L + \psi_R) = m(\bar{\psi}_L\psi_R + \bar{\psi}_R\psi_L) \quad (1.2)$$

This term then couples both to left-handed and right-handed fields. But these fields transform differently – applying the same transformation to these fields has different results depending on the chirality of the field. The gauge symmetry is broken and the fermion mass term is *not* invariant under electroweak symmetry – the exact form depends on the choice of gauge. If we cannot write a mass term that is consistent with the theory and respects its symmetries, then it follows the fermions do not have mass. However this represents a clear conflict with empirical evidence.

In the bosons we find a similar problem. We cannot write a mass term in the electroweak Lagrangian \mathcal{L}_{EW} , as that mass term will also break the gauge symmetry in a similar way. This presents no problem for the photon γ , which is known to be massless, but the other electroweak bosons – the W^+ , W^- and Z^0 – are known to be massive.

Therefore this formulation of SM predicts that *all* particles should be massless. Given that we know with certainty that all of the quarks, the charged leptons, and the W and Z bosons are massive, it follows that these particles do not have an intrinsic mass but instead acquire their mass from some interaction.

²Quantum chromodynamics (or QCD) is the field studying the strong interaction, and the dynamics and properties of colour charges, that govern the forces binding quarks together.

1.1.2 The Higgs mechanism

The problem of particle masses is solved by the introduction of the scalar Higgs field with four degrees of freedom:

$$\phi = \frac{1}{\sqrt{2}} \begin{pmatrix} \phi^+ \\ \phi^0 \end{pmatrix} \quad (1.3)$$

where the superscripts of ϕ denote electric charge. If we describe the Higgs field with a Lagrangian, we can separate it into a kinetic term and a potential term:

$$\mathcal{L}_H = T_H - V(\phi) \quad (1.4)$$

The Higgs potential $V(\phi)$ is found to be of an unusual but characteristic shape – often called the Mexican hat potential (see Fig. 1.2).

If we think of the Higgs beginning at the origin – at the apex of the sombrero – then this potential is symmetrical. But the Higgs can ‘roll down’ the slope into the trough to occupy a lower-energy state. Once this transition occurs, the potential is no longer symmetrical. This is the spontaneous symmetry breaking, and the result is that at low energies, the Higgs field has a nonzero vacuum expectation value $\langle \phi^0 \rangle = v$.

It is notable that this is the *only* parameter of the Standard Model that is not dimensionless – the vacuum expectation value of the Higgs field is in units of mass, and thus sets the scales of all other masses in the SM.

Once the symmetry is broken, three of the four degrees of freedom of the Higgs field mix with the bosons of the electroweak fields, giving them mass. The fourth degree of freedom emerges as a scalar boson: the Higgs boson H^0 .

Thus the W and Z bosons have masses that are defined in terms of the Higgs vacuum expectation value v and the strength of their coupling to the Higgs field g :

$$m_W = \frac{gv}{2} \quad (1.5)$$

$$m_Z = \frac{v}{2} \sqrt{g^2 + g'^2} \quad (1.6)$$

This is the “mixing” of the degrees of freedom of the Higgs field – the four degrees of freedom that would normally yield Goldstone bosons [4] instead mix with the W^+ , W^- , and Z^0 bosons, giving them mass. The fourth remaining degree of freedom emerges as the Higgs boson itself.

1.1.3 The Yukawa coupling

While the Higgs mechanism as described above explains the masses of the W and Z bosons, this does not explain the masses of the quarks and leptons. As we cannot add a consistent mass term to the fermion fields, and the degrees of freedom of the Higgs field do not mix with them, the fermions must acquire mass via some other mechanism.

This is solved by the Yukawa coupling. This is an interaction between the Higgs scalar field ϕ and the fermion field ψ that takes the form

$$V \approx g\bar{\psi}\phi\psi \quad (1.7)$$

where g is a coupling constant.

However, due to the spontaneous symmetry breaking of the Higgs mechanism, the Yukawa potential will have a minimum nonzero value ϕ_0 . The Higgs field can thus be thought of as a combination of the basic field term ϕ and a term representing the nonzero vacuum expectation value ϕ_0 :

$$\tilde{\phi} = \phi - \phi_0 \quad (1.8)$$

If the Yukawa coupling (Eq. 1.7) is re-written using this formulation of the Higgs field, it becomes

$$V \approx g\bar{\psi}\phi\psi - g\bar{\psi}\phi_0\psi \quad (1.9)$$

As ϕ_0 is a constant, the second term instead becomes $g\phi_0\bar{\psi}\psi$ which then simplifies to $g\phi_0$, resembling a mass term. Similarly to the W and Z bosons, fermion masses are then defined in terms of the Higgs vacuum expectation value v and the strength of their coupling to the Higgs field g :

$$m_i = -\frac{f_i v}{\sqrt{2}} \quad (1.10)$$

where i refers to the family of fermions – either the charged leptons, up-type quarks, or down-type quarks.

Returning back to the Lagrangian in Eq. 1.1, instead of attempting to write a mass term, we instead add a Yukawa coupling Lagrangian \mathcal{L}_{YU} . This Lagrangian is gauge-invariant, avoiding the problem of a fermion mass term.

1.1.4 The completed Standard Model

In light of the necessity of the Higgs field, and the part it plays in generating the masses of the fermions and vector bosons via spontaneous symmetry breaking, we must then rewrite the SM Lagrangian from Equation 1.1 to include the effects of the Higgs field and the Yukawa coupling:

$$\mathcal{L}_{SM} = \mathcal{L}_\psi + \mathcal{L}_{EW} + \mathcal{L}_{QCD} + \mathcal{L}_H + \mathcal{L}_Y \quad (1.11)$$

This then constitutes a full Lagrangian density for all Standard Model fields.

1.2 The physics case for a lepton collider

With the observation of a Higgs boson with a mass of 125 GeV, based on data from the Large Hadron Collider [5] [6], the Standard Model of particle physics is now functionally complete – all of its major predictions have been tested. This is a testament to its quality as a theory, where its predictive power and accuracy is one of the best in all of the sciences [2].

But despite this, a multitude of observations [7] [8] have shown that the Standard Model cannot be a complete theory of nature [9]. Many phenomena have been observed that the Standard Model cannot predict, or that don't seem to interact with the Standard Model in any way.

Particle physicists are now forced to seek answers to three questions that the Standard Model cannot solve:

1. What is dark matter? Astrophysics observations support the existence of a neutral, weakly-interacting substance that composes around 85% of all mass in the universe. Yet this substance cannot be explained by any known form of matter within the Standard Model [10].
2. Why is there so little antimatter? The symmetries inherent in the Standard Model predict that the Big Bang would have created an equal quantity of matter and antimatter. Yet the universe today is dominated by matter. [11]
3. Why does the Higgs field fill space and give mass to elementary particles? The existence of the Higgs field and the coupling of the Higgs boson to other particles can be understood from the Standard Model but their origin or cause is still unexplained.

In order to answer these questions, new theories of physics Beyond the Standard Model (BSM) have been made, and need to be experimentally tested. Particle collider experiments at the energy frontier are one important tool for testing these theories³, and the Large Hadron Collider (LHC) has already been used extensively in searches for new physics, in the forms of new particles, rare and exotic decays, supersymmetry, and dark matter.

However, the running of a lepton collider at the energy frontier would be complementary to the LHC’s continuing physics programme – there are many events or channels that are inaccessible or difficult to examine in one environment that are much simpler or higher precision in the other. In this way, a lepton collider would help to improve and refine measurements already taken at the LHC, while also allowing physicists to examine new channels and decays that were not accessible to it. A number of processes and their discovery potential can be seen in Table 1.1.

This follows a historical pattern in particle physics – as the energy frontier advances, hadron colliders are used to discover new physics and new phenomena, followed by lepton colliders to examine these phenomena in higher precision.

1.2.1 Higgs physics

Of specific interest to searches at lepton colliders would be the Higgs boson itself. Many BSM models predict differences from the Standard Model in the Higgs sector – such as several Higgs bosons with different masses, composite Higgs, charged Higgs etc. The comparatively ‘quiet’ environment of a lepton collider allows higher precision measurements of the properties of the Higgs boson, placing better constraints on the presence of new physics. In addition, lepton colliders can operate at specific thresholds and “hot spots” for Higgs production, permitting a much greater number of events yielding Higgs bosons, and thus a greater sample to examine.

Additionally, the most common decay of the Higgs boson, at a branching ratio of 57.7%, is the $H \rightarrow b\bar{b}$ process. Despite the high branching ratio, the huge QCD backgrounds in a hadron collider have made this decay incredibly difficult to observe at the LHC – in fact, the $H \rightarrow b\bar{b}$ decay has only fairly recently been experimentally confirmed by the ATLAS experiment [14]. However, in a lepton collider these QCD backgrounds are significantly smaller [15], meaning this decay channel is much easier to analyse, opening up a huge number of Higgs events for analysis and examination.

³In addition to colliders, there are an array of experiments looking at CP-violation in the lepton sector such as neutrinos, as well as direct and indirect dark matter detection experiments [12] [13].

Another highly interesting process uniquely accessible to lepton colliders is the higgstrahlung reaction: $e^+e^- \rightarrow Zh$. The decay of the Z boson into lepton pairs e^+e^- or $\mu^+\mu^-$ allows high precision kinematic measurements of the process without directly measuring the Higgs boson itself [15]. This allows measurement of the Higgs mass and its branching fractions in a model-independent manner, while also making measurements of missing energy possible. If the Higgs boson has invisible decays – such as dark matter particles or other undiscovered particles that don't couple to the SM – the higgstrahlung process allows their existence to be identified.

An additional benefit of the higgstrahlung process is that the recoiling Z boson can be used to identify all the Higgs decay modes, and thus direct measurement of Higgs couplings with minimal bias. With this understanding of the Higgs couplings and their rates and branching ratios, it is possible to perform a model-independent determination of the total rate of Higgs decay Γ_h . This result then allows calculation of the absolute size of all other Higgs couplings [15].

In addition, the production of top quark pairs in combination with a Higgs boson will allow direct measurement of the top-Higgs Yukawa coupling. This is the strongest Higgs coupling in the SM, and as such is most sensitive to new physics. A study examining the top-Higgs Yukawa coupling in detail can be found in Chapter 5 of this thesis.

1.2.2 Top physics

In addition to the Higgs, the top quark is of high interest to physics programmes at a future lepton collider. Since its discovery at Fermilab in 1995 [16], there have been no lepton colliders operating with sufficient energy to produce top quarks – unlike the charm and bottom quarks, which were studied in further detail in lepton colliders after their discovery. The production threshold for top quarks is 350 GeV, and no lepton colliders capable of this energy have been constructed.

The detailed study of top quarks and their properties that would be made possible by a lepton collider would have many benefits, primarily in the precision of the measurements. Similar to the Higgs, low QCD backgrounds make top quark events easier to reconstruct. The fact that the collision is between elementary particles, rather than a parton-parton collision as in a hadron collider, also permits a more well-defined centre of mass energy, which is not possible in hadron colliders.

Precision measurement of the top quark is also an important test of the SM. The top quark is most massive particle of the SM, and as such provides a good probe into

the mechanism of electroweak symmetry breaking, and provide insight into its mechanics, should they differ from that of the Standard Model [17].

1.2.3 Supersymmetry

Supersymmetry (SUSY) is one of several candidate models for BSM physics, and currently one of the most widely-researched and well-motivated [18]. A large programme of searches for supersymmetric particles or signals at the LHC is ongoing, though as of writing no new particles or signals of supersymmetry have been confirmed [19] [20] [21].

For the same reasons that lepton colliders provide ideal environments for doing precision Higgs and top physics, they also provide ideal conditions for supersymmetry searches. One example [22] is searches for the first- and second-generation sleptons \tilde{e} and $\tilde{\mu}$ via slepton pair production:

$$\begin{aligned} e^+ e^- &\rightarrow \tilde{e}_R^+ \tilde{e}_R^- \rightarrow e^+ e^- \tilde{\chi}_1^0 \tilde{\chi}_1^0 \\ e^+ e^- &\rightarrow \tilde{\mu}_R^+ \tilde{\mu}_R^- \rightarrow \mu^+ \mu^- \tilde{\chi}_0^1 \tilde{\chi}_0^1 \end{aligned}$$

This requires high-efficiency reconstruction of leptons, as well as the usage of Boosted Decision Trees (BDT) to distinguish the process from SM processes and SUSY backgrounds.

A variety of similar processes involving supersymmetric particles would be available to study at a high-energy lepton collider, using the higher-precision detectors and lower backgrounds to improve current limits. Precise measurement of these processes and their cross-sections, as well as the masses of any resulting particles, will help to provide evidence for or put limits on supersymmetric theories.

1.3 The International Linear Collider

The International Linear Collider (ILC) is a proposed high-luminosity linear electron-positron collider based upon 1.3 GHz superconducting radio frequency (SCRF) accelerating technology [24]. The ILC would have a centre of mass energy of 250 GeV in the initial stage, upgradable to 500 GeV and then in principle to 1 TeV at a later date, with a luminosity of $3.6 \times 10^{34} \text{ cm}^{-2} \text{ s}^{-1}$ and using magnets with an accelerating gradient of 31.5 MVm⁻¹ in metre-long superconducting nine-cell niobium cavities operating at 2K. The total footprint of the complex, including both accelerator arms, the storage rings, and the interaction point, would be 31 km in length. Other parameters of the ILC can be seen in Table 1.3.

One of the unique features of the ILC is the “push-pull” detector system. This is a moving platform in the chamber housing the interaction point (IP), upon which two detectors can be mounted. The platform can be moved to exchange which detector is in the interaction point, allowing a linear collider to function with multiple detectors. This allows the two detectors to specialise for different physics studies and goals, much like the various experiments at the LHC at CERN, which would normally not be possible with a linear collider.

There were a number of proposed sites for the ILC, including Fermilab in the United States, CERN in Geneva, DESY in Hamburg, and JINR near Moscow [24]. The most recent possible site, which has had significant attention and planning devoted to it, is the Kitakami Highlands region of Iwate prefecture in Japan. This would be a greenfield site, located on the side of a mountain range and requiring that a significant amount of the facility’s infrastructure be located underground, in tunnels dug within the granite rock of the region.

The ILC project published a Technical Design Report (TDR) in 2013 [24] with extensive details of the technology and ongoing research and development into making the collider a reality. As the location of the collider has yet to be determined, there is currently no estimated dates for the construction of the ILC. However according to a recent report [25], if the Japanese government were to approve hosting the ILC and the project was listed as high priority in the report from the European Strategy Update in May 2020, then a period of at least four years would be needed for detailed planning and international negotiations. Following this, there would be a ten-year period for construction and commissioning of the collider, which would result in first physics in the early- to mid-2030s, around the same time as the HL-LHC will be concluding its own physics programme.

However, a report from the Science Council of Japan (a representative organisation of the Japanese science community) released in early 2019 expressed that they had not reached a consensus as to whether to support hosting the ILC in Japan. Some of the reasons cited were concerns over international cost-sharing in the long-term, as well as whether the expected scientific outcomes would justify the unprecedented human resource requirements and infrastructure necessary to make the ILC a reality [26].

On 7th March 2019, the Japanese government released a statement to say that they would not be making a proposal to host the collider [27]. They however expressed a keen interest in the future of the project, and that they would be continuing to contribute towards the research and development of the ILC.

1.3.1 ILC detectors

Detector design for the ILC is driven by the requirements of the physics programme – many of the physics goals and targeted processes are highly dependent upon hadronic states, so precise jet reconstruction and high jet energy resolution is critical to meeting the expectations placed upon the ILC.

The technique thought to provide the necessary level of accuracy is *particle flow* [28]. This technique determines jet energy by reconstructing the four-vectors of all of the constituent particles of the jet and summing them, rather than measuring the total energy deposited in the calorimeters. By understanding that jets deposit the majority of their energy as charged particles and photons, and a much smaller fraction as neutral hadrons (10%), the individual components can be measured by separate parts of the detector. Charged particles are measured by the trackers, photons and electrons are measured in electromagnetic calorimeters, and neutral hadrons are measured in the hadronic calorimeter. As the hadronic calorimeters are used only to measure a much smaller fraction of the overall jet energy, the effect of lower energy resolution on the overall jet energy resolution is reduced. This allows much higher resolution measurements of jet energy, e.g. $\sigma_E/E \lesssim 3.8\%$. for jet energies in the range 40-400 GeV [28].

The requirements for the use of particle flow methods are a very good separation of charged and neutral particles, translating into a need for high-efficiency trackers, and calorimeters capable of high-efficiency reconstruction of neutral particles. The design of the detectors for the ILC has proceeded from these requirements.

The need for large separations between charged and neutral particles requires that the vertex detector, tracker, and calorimeter systems are all contained within a magnetic field, so that charged particles' path is curved by the field. In general, this separation depends on the physical size of the detector and the strength of the magnetic field. Thus there are essentially two basic approaches to detector design: a large detector with a lower magnetic field, using the size of the detector to separate charged particles from neutral particles; or a more compact detector utilising a much stronger magnetic field to create the same separation.

These two approaches are shown in the two detector concepts for the ILC – the International Large Detector using a 3.5 T magnetic field, and the more compact Silicon Detector using a much stronger 5 T magnetic field. These two detectors will be discussed in detail below.

The International Large Detector (ILD)

The International Large Detector (ILD) is a detector concept for the ILC intended as a multi-purpose detector, with a strong focus on optimising the performance of particle flow algorithms as much as possible [30]. To attain this, it uses several technologies for very high-resolution and high-efficiency tracking, as well as highly-granular calorimeters.

For vertex tracking, the ILD uses three double-layers of pixel detectors using monolithic active pixel sensor (MAPS) technology, with a spatial resolution of $4\text{ }\mu\text{m}$ and a timing resolution of 2-4 μs . For tracking, the ILD uses a hybrid system, combining a gaseous time projection chamber (TPC) with silicon detector layers placed both inside and outside the TPC volume. This combination allows a high tracking efficiency with a low material usage.

The calorimeter system must be highly granular in order to best utilise particle flow. The calorimeters are split into the electromagnetic calorimeter (ECAL) and hadronic calorimeter (HCAL). The ECAL utilises a silicon diode sampling calorimeter with diode pads of $5 \times 5\text{ mm}^2$. An option for an ECAL using thin scintillator strips is also being investigated. The HCAL has two possible options available. The Analogue Hadronic Calorimeter (AHCAL) uses silicon photomultipliers (SiPM) on tiles of plastic scintillator with a resolution of $3 \times 3\text{ cm}^2$ using a fully analogue readout. The Semi-Digital Hadronic Calorimeter (SDHCAL) uses resistive plate chambers (RPC) with a higher granularity of $1 \times 1\text{ cm}^2$, but does not use a fully analogue output, meaning that amplitude information is more limited.

These detectors are placed within a solenoid capable of generating a 3.5 T magnetic field, and then within an iron flux return yoke which is instrumented for muon identification and tail catching, as well as providing structural support for the detector. The finished ILD is expected to weigh 14,000 metric tonnes.

The Silicon Detector (SiD)

The Silicon Detector (SiD) is a detector concept for the ILC that uses primarily silicon-based technology, with the aim to reduce cost while still maintaining high performance and attaining the ILC's physics goals [30]. The SiD is also more compact than the ILD, utilising a stronger magnetic field to compensate.

The vertex and tracker systems are both composed of silicon sensors, using a cylindrical configuration. The vertex detector uses silicon pixel sensors while the tracker uses silicon strip sensors, both designed to be used with power pulsing – the electronics are only powered and active when it is known that bunches will be colliding. This reduces power

and cooling requirements.

The high-granularity calorimeters are both nested within the barrel, inside the magnetic field. The ECAL uses 30 alternating layers of tungsten absorber and silicon active layers, in $3.5 \times 3.5 \text{ mm}^2$ hexagonal pixels. The HCAL uses alternating layers of steel absorber and a glass resistive plate chamber, with cells of $10 \times 10 \text{ mm}^2$

Outside of the calorimeter, the superconducting solenoid generates a 5 T magnetic field, which enables the more compact detector design – a higher magnetic field increases the spatial separation between charged and neutral particles, which is necessary for usage of particle flow algorithms.

Outside of the magnetic field is an iron flux return yoke, which similarly to the ILD concept also acts as a structural support and is instrumented for muon identification and tail catching.

1.4 The Compact Linear Collider

The Compact Linear Collider (CLIC) is a proposed linear electron-positron collider that would be located at CERN in Geneva, Switzerland [31]. The accelerator is a staged design, with the initial stage having a centre of mass energy of 380 GeV, focusing on precision measurements of the top quark and Higgs physics. The further stages would increase the centre of mass energy to 1.5 TeV, then finally 3 TeV. Physics goals in these later stages would involve searches for new physics processes, as well as precision measurements of rare Higgs processes, and of new states discovered at the LHC or earlier stages of CLIC [32].

To attain these extremely high energies, the CLIC accelerators will need to produce accelerating gradients as high as 100 MVm^{-1} . These cannot be achieved with traditional klystrons due to the extremely high peak RF power needed. Klystrons capable of providing this would be inefficient and prohibitively expensive, so the CLIC accelerators plan to use a two-beam acceleration scheme. A drive beam is used, with low energy but high power. RF power is then extracted from the drive beam to power the main accelerator. In this way, the high power, shorter duration pulses can be achieved more economically, allowing the high acceleration gradients that will allow each arm of CLIC to accelerate electrons up to 1.5 TeV in only 21 km. Other parameters of the CLIC can be seen in Table 1.3.

The proposed site for the CLIC experiment would be at CERN, built beneath the existing LHC ring and stretching across the French-Swiss border, running parallel to the Jura mountain range. This placement is determined by the geological features of the region around Geneva and the feet of the Juras, where the tunnels would be dug into the

sedimentary ‘molasse’ rock in the area.

As of writing, the CLIC collaboration released a Conceptual Design Report (CDR) in 2016 detailing the current state of planning for the experiment [31]. It has also submitted input to the European Particle Physics Strategy Update, which will give strategic direction as to which projects the international particle physics community chooses to pursue from 2020 onwards.

If given the go-ahead at the European Strategy Meeting, there would be a five-year preparation phase from 2020-2025 for finalising development of hardware, technical proposals, industrial procurement, site authorisation, etc. Construction would then take place from 2025-2034, with first beams in 2035.

The detector concepts envisioned for CLIC are similar in design to those for the ILC, and are usually referred to as CLIC_ILD and CLIC_SiD. See 1.3.1 for a detailed description of these detector concepts.

1.5 The Future Circular Collider

The Future Circular Collider (FCC) is a series of concepts for a future collider that would be located in the Geneva area near the existing LHC ring [34]. The FCC project as a whole has three different accelerator concepts – the FCC-hh for proton-proton and ion-ion collisions, the FCC-ee for electron-positron collisions, and the FCC-he for electron-proton collisions.

The initial proposal is to construct a circular electron-positron collider – the FCC-ee – with a circumference of 100 km and delivering a maximum centre of mass energy of 400 GeV. The motivation for this is that at this energy range – the electroweak scale – the FCC would be able to access the Z pole, the W- and top-pair production thresholds, as well as producing a large number of Higgs bosons [35]. Other parameters of the FCC can be seen in Table 1.3.

Unlike linear colliders, staged energy increases are not part of the FCC-ee plan. The usage of low-mass particles like electrons in a circular collider results in a high energy loss due to synchrotron radiation, which must be mitigated by the constant addition of energy. Significantly higher energies than those planned by the FCC-ee are not currently practical due to these losses. Instead, the FCC-ee would concentrate on a physics programme in the 90-365 GeV energy range, leveraging the much higher luminosities available to a circular collider compared to linear colliders in the same energy range.

A further part of the proposal for the FCC is that following the conclusion of the physics

programme of the FCC-ee, the tunnels and infrastructure would be re-used for the FCC-hh, a hadron collider. This follows in the footsteps of the LHC, which was constructed in tunnels originally built to house the Large Electron Positron Collider (LEP). It is claimed that the FCC-hh built in these tunnels would be able to reach centre of mass energies of at least 100 TeV.

According to the given timeline, the FCC-ee would begin construction in 2028, and first physics would take place in 2039.

1.6 The Circular Electron Positron Collider

The Circular Electron Positron Collider (CEPC) is a proposal for a circular electron-positron collider with a circumference of 100 km that would be hosted in China, with a centre of mass energy of 240 GeV to operate as a Higgs factory [37]. It is also intended to operate at 91 GeV and 160 GeV to produce large numbers of Z and W bosons⁴. This lower centre of mass energy is due to considerations of energy loss via synchrotron radiation. However, the CEPC collaboration intends to utilise these to produce several synchrotron radiation light sources, including two gamma-ray beamlines. Other parameters of the CEPC can be seen in Table 1.3.

The CEPC project released a Conceptual Design Report (CDR) in 2018 detailing the current state of planning for the experiment [37]. It has also been submitted as input to the European Particle Physics Strategy Update. The current timeline envisions a five-year research and development period from 2018-2022, and construction to start in 2022, completing in 2030. The physics programme is expected to last for ten years, concluding in 2040.

Similarly to the FCC, it is expected that technology for superconducting magnets at high field strengths will have developed sufficiently to allow the tunnels to be used to house a high-energy hadron collider, called the Super Proton Proton Collider (SPPC).

The detectors of the CEPC as outlined in the CDR are very similar in design to the ILD, in the design of using a silicon vertex tracker, a TPC tracker, and similar options for the calorimeters. An additional difference is the optioning of a dual-readout calorimeter to replace the electromagnetic and hadronic calorimeters [38].

There would be two interaction points around the ring, allowing both detectors to operate at the same time, as opposed to the ILC's push-pull system.

⁴The W boson study would be largely concentrated around the pair production threshold to allow measurement of its mass via cross-section dependence

Standard Model of Elementary Particles

	three generations of matter (fermions)			interactions / force carriers (bosons)	
	I	II	III		
QUARKS	mass $\approx 2.2 \text{ MeV}/c^2$ charge $2/3$ spin $1/2$ up	mass $\approx 1.28 \text{ GeV}/c^2$ charge $2/3$ spin $1/2$ charm	mass $\approx 173.1 \text{ GeV}/c^2$ charge $2/3$ spin $1/2$ top	mass 0 charge 0 spin 1 gluon	mass $\approx 124.97 \text{ GeV}/c^2$ charge 0 spin 0 Higgs
	mass $\approx 4.7 \text{ MeV}/c^2$ charge $-1/3$ spin $1/2$ down	mass $\approx 96 \text{ MeV}/c^2$ charge $-1/3$ spin $1/2$ strange	mass $\approx 4.18 \text{ GeV}/c^2$ charge $-1/3$ spin $1/2$ bottom	mass 0 charge 0 spin 1 photon	
	mass $\approx 0.511 \text{ MeV}/c^2$ charge -1 spin $1/2$ electron	mass $\approx 105.66 \text{ MeV}/c^2$ charge -1 spin $1/2$ muon	mass $\approx 1.7768 \text{ GeV}/c^2$ charge -1 spin $1/2$ tau	mass $\approx 91.19 \text{ GeV}/c^2$ charge 0 spin 1 Z boson	
	mass $< 2.2 \text{ eV}/c^2$ charge 0 spin $1/2$ electron neutrino	mass $< 0.17 \text{ MeV}/c^2$ charge 0 spin $1/2$ muon neutrino	mass $< 18.2 \text{ MeV}/c^2$ charge 0 spin $1/2$ tau neutrino	mass $\approx 80.39 \text{ GeV}/c^2$ charge ± 1 spin 1 W boson	
					GAUGE BOSONS VECTOR BOSONS
					SCALAR BOSONS

Figure 1.1: Table of particles in the Standard Model, each with their mass, charge and spin [3]. The quarks are often grouped by their charge, named after the first generation – the top row are “up-type” quarks and the bottom row are “down-type” quarks.

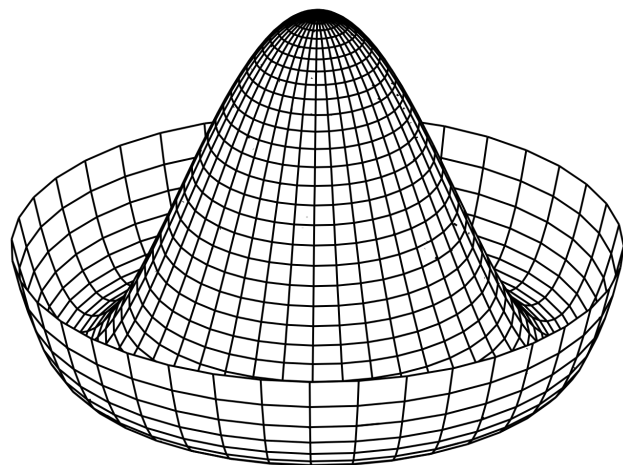


Figure 1.2: Diagram of the Higgs potential, or Mexican hat potential.

Energy (GeV)	Reaction	Physics goal
91	$e^+e^- \rightarrow Z$	ultra-precision electroweak
160	$e^+e^- \rightarrow WW$	ultra-precision W mass
250	$e^+e^- \rightarrow Zh$	precision Higgs couplings
350-500	$e^+e^- \rightarrow t\bar{t}$	top quark mass and coupling
	$e^+e^- \rightarrow WW$	precision W coupling
	$e^+e^- \rightarrow \nu\bar{\nu}h$	precision Higgs couplings
500	$e^+e^- \rightarrow f\bar{f}$	precision search for Z'
	$e^+e^- \rightarrow t\bar{t}h$	top-Higgs Yukawa coupling
	$e^+e^- \rightarrow Zh h$	Higgs self-coupling
	$e^+e^- \rightarrow \tilde{\chi}\tilde{\chi}$	supersymmetry searches
	$e^+e^- \rightarrow AH, H^+, H^-$	extended Higgs states
700-1000	$e^+e^- \rightarrow \nu\bar{\nu}hh$	Higgs self-coupling
	$e^+e^- \rightarrow \nu\bar{\nu}VV$	composite Higgs
	$e^+e^- \rightarrow \nu\bar{\nu}t\bar{t}$	composite Higgs and top
	$e^+e^- \rightarrow \tilde{t}\tilde{t}^*$	supersymmetry searches

Table 1.1: Physics processes of interest at lepton colliders up to 1 TeV.

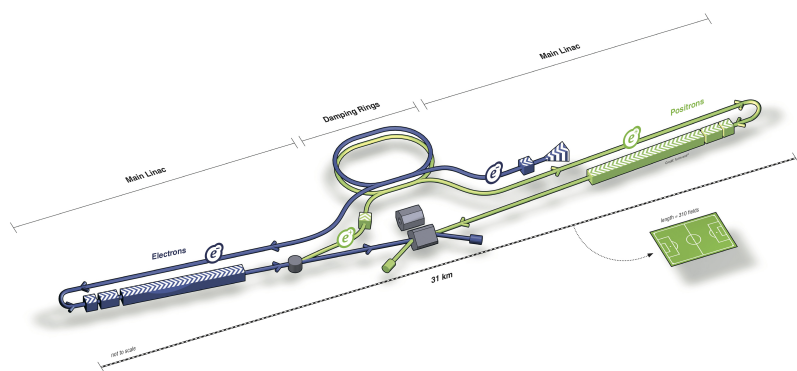


Figure 1.3: View of the accelerator complex for the International Linear Collider, showing the two linacs and storage and damping rings, with football field for scale.

Process	HL-LHC	CLIC
Heavy Higgs scalar mixing angle $\sin^2\gamma$	< 4%	< 0.24%
Higgs self-coupling $\Delta\lambda$	50% at 60% CL	[-7%, +11%] at 68% CL
$\text{BR}(\text{H} \rightarrow \text{invisible})$		< 0.69% at 90% CL
Higgs compositeness scale m_*	$m_* > 3 \text{ TeV}$ ($> 7 \text{ TeV}$ for $g_* \simeq 8$)	Discovery up to $m_* = 10 \text{ TeV}$ (40 TeV for $g_* \simeq 8$)
Top compositeness scale m_*		Discovery up to $m_* = 8 \text{ TeV}$ (20 TeV for small coupling g_*)
Higgsino mass	> 250 GeV	> 1.2 TeV
Slepton mass		Discovery up to 1.5 TeV
RPV wino mass		> 1.5 TeV ($0.03 \text{ m} < c\tau < 30 \text{ m}$)
Z' (SM couplings) mass	Discovery up to 7 TeV	Discovery up to 20 TeV
NMSSM scalar singlet mass	> 650 GeV ($\tan\beta = 4$)	> 1.5 TeV ($\tan\beta = 4$)
Twin Higgs scalar singlet mass	$m_\sigma = f > 1 \text{ TeV}$	$m_\sigma = f > 4.5 \text{ TeV}$
Relaxion mass	< 24 GeV	< 12 GeV (all for vanishing $\sin\theta$)
Relaxion mixing angle $\sin^2\theta$		$\leq 2.3\%$
Neutrino Type-2 see-saw triplet		> 1.5 TeV (for any triplet vev) > 10 TeV (for any triplet Yukawa coupling $\simeq 0.1$)
Inverse see-saw RH neutrino		> 10 TeV (for Yukawa coupling $\simeq 1$)
Scale $V_{LL}^{-1/2}$ for LFV $(\bar{e}e)(\bar{e}\tau)$		> 42 TeV

Table 1.2: Limits on new physics for the Compact Linear Collider, as compared with the High Luminosity Large Hadron Collider (HL-LHC). The given sensitivities assume the full CLIC physic programme covering the three centre of mass energies 380 GeV, 1.4 TeV and 3 TeV, with integrated luminosities of 1^{-1} , 2.5^{-1} and 5 ab^{-1} respectively. All limits are at a 95% confidence level (CL) unless stated otherwise. Values taken from [23].

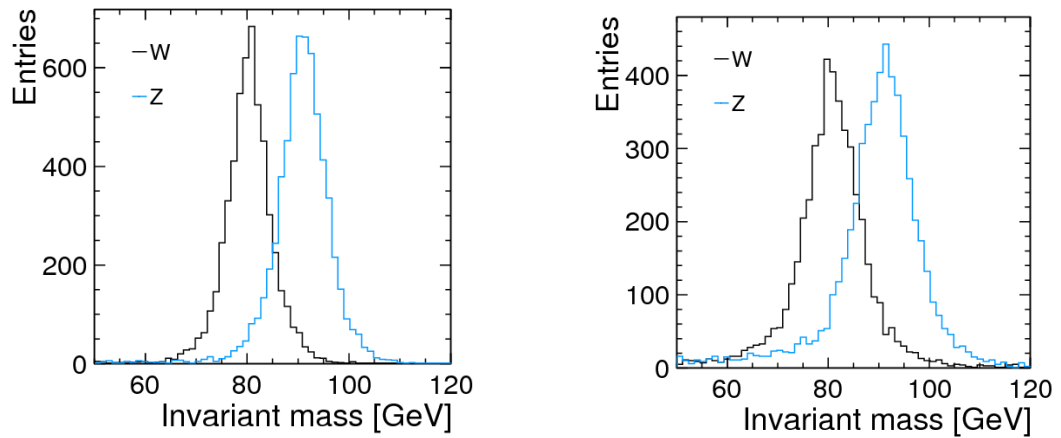


Figure 1.4: Distributions of invariant mass of the W and Z boson from a study into the effects of particle flow algorithms at the Compact Linear Collider, showing a clear separation of the W and Z boson masses both without (left) and with (right) backgrounds [29].

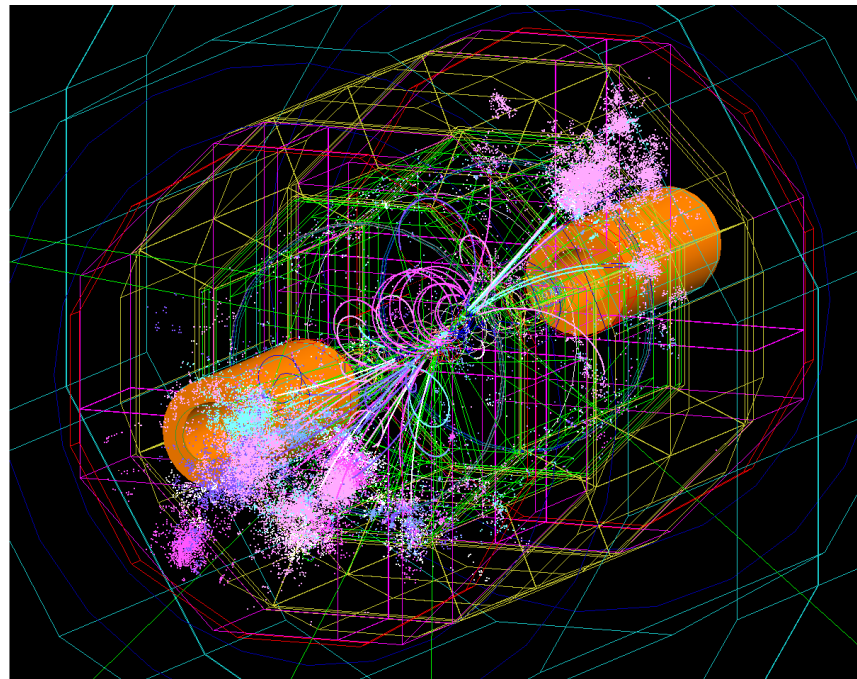


Figure 1.5: Visualisation of a simulated $e^+e^- \rightarrow t\bar{t}h$ event in the ILD. Charged particles can be easily identified by the curved or spiral paths they take within the magnetic field, and the jets are visible as the light pink and purple areas near the beampipes on either side.

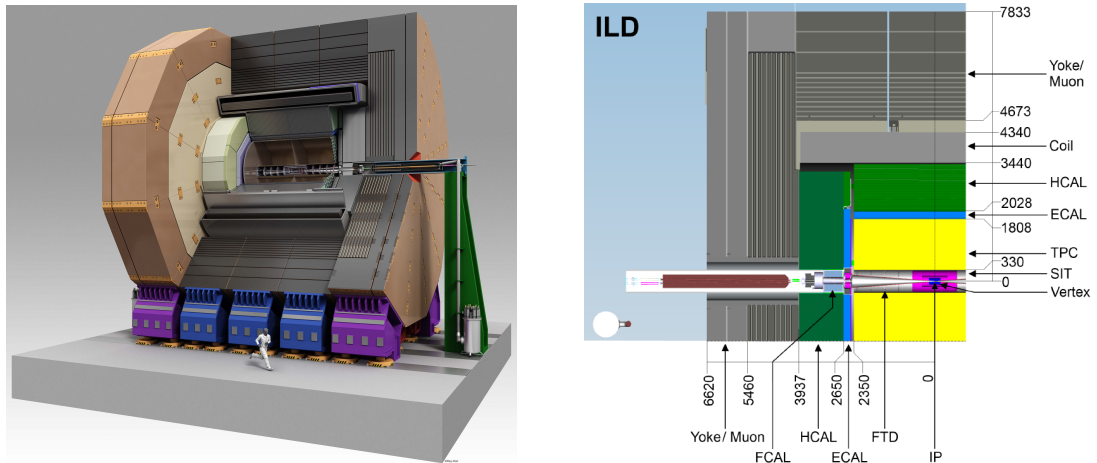


Figure 1.6: Rendering of the finished ILD cutaway to show the internal features (left); and a quadrant view of the ILD components (right) [30].

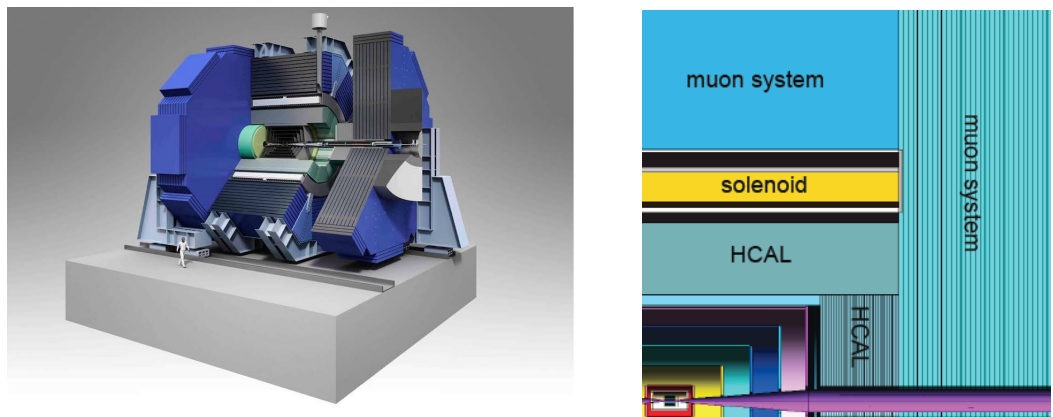


Figure 1.7: Isometric view of the finished SiD cutaway to show the internal features (left); and a quadrant view of the SiD components (right) [30].

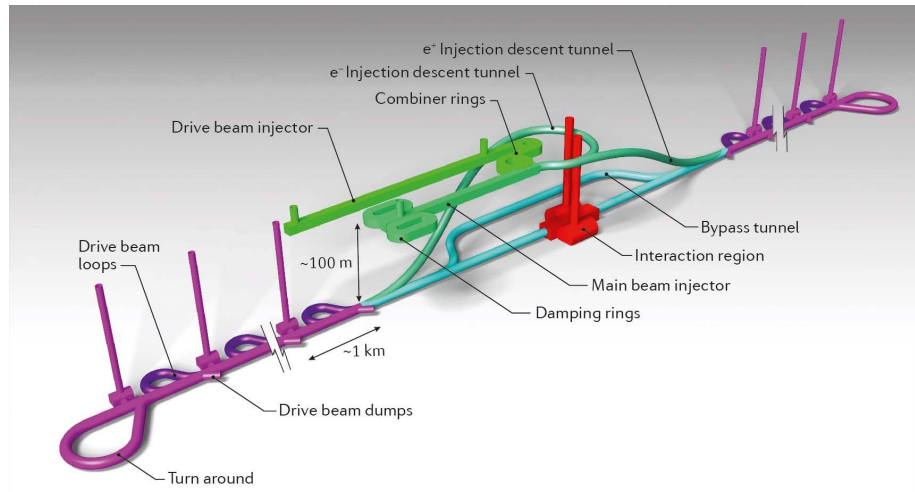


Figure 1.8: View of the accelerator complex for the Compact Linear Collider, showing the main beams and drive beams, and the interaction region [33].

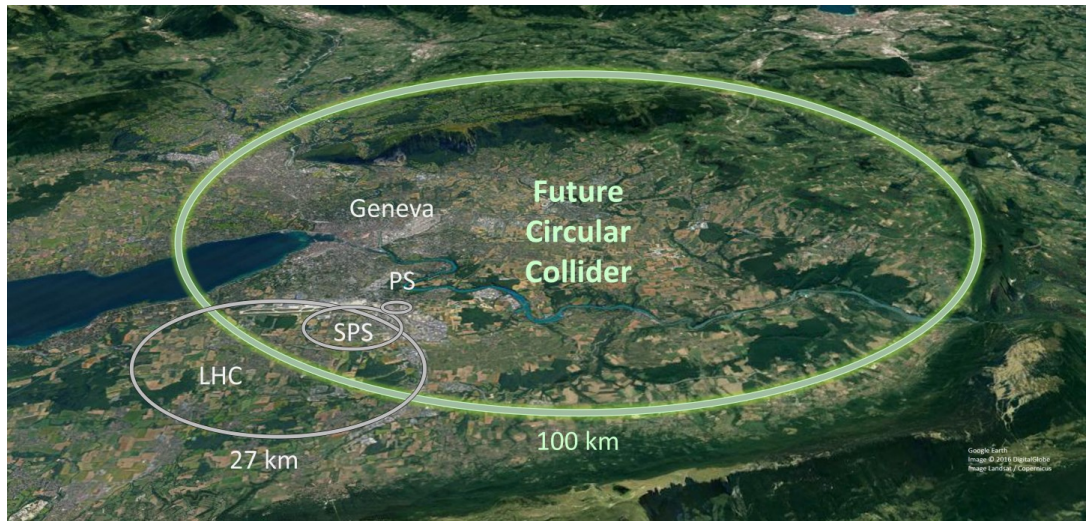


Figure 1.9: The ring of the proposed Future Circular Collider laid over satellite imagery of the region around the French-Swiss border at Geneva. The current accelerators are shown in grey for scale [36].

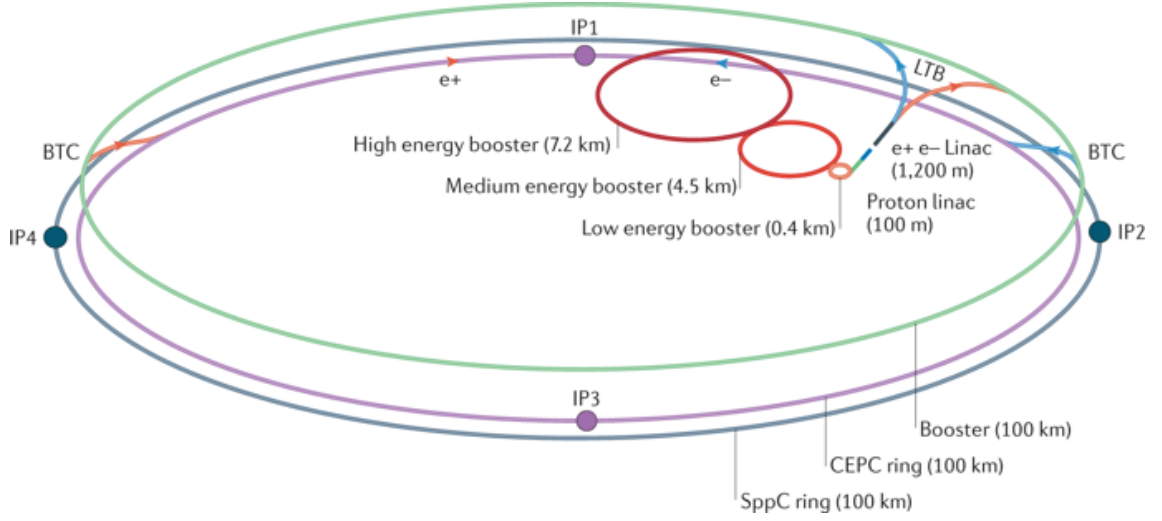


Figure 1.10: Diagram showing the tunnels of the accelerator complex for the proposed Circular Electron Positron Collider, with the multiple booster rings and linacs [39].

Parameter		ILC	CLIC	FCC-ee	CEPC
Maximum centre of mass energy	(GeV)	1400	3000	400	240
Luminosity	($10^{34} \text{cm}^{-2}\text{s}^{-1}$)	3.6	5.9	1.8	2
Power consumption	(MW)	300	589	TBD	TBD
Bunches per train		2450	312	98	50
Bunch separation	(ns)	366	0.5	25	25
Bunch length	(μm)	250	44	1160	2700
Bunch population	(10^{10})	1.74	0.37	14	37.9
Repetition frequency	5 Hz	50 Hz	5	100 Hz	
Accelerating gradient	(MV/m)	31.5	100	N/A	N/A
Bending radius	(km)	N/A	N/A	11	6.1
Energy loss per turn	(GeV)	N/A	N/A	7.55	3.11

Table 1.3: Summary and comparison of future lepton collider concepts

Chapter 2

Data acquisition software

Before software can be reusable
it first has to be usable.

Ralph Johnson

This chapter will discuss the usage of online monitoring and data quality monitoring software for high energy physics testbeams, specifically the Data Quality Monitoring for High-Energy Physics tool (abbreviated as DQM4hep). This tool was initially developed for a specific detector prototype, but was able to be expanded for the use of other detectors. This online monitor was then proposed as an option for Work Package 5 of the AIDA-2020 collaboration, to be used as a generic online monitor and data quality monitor (this will be discussed in depth in Chapter 3).

This chapter describes DQM4hep in detail, including the motivation for the usage of generic software tools as outlined by the AIDA-2020 collaboration. The codebase, structure, networking and implementation of the software framework is described in detail.

Following this, detailed documentation for a user guide describing the structure, usage, running and authoring of the user-specific parts of the framework is presented. This represented the distillation of significant experience using the framework on many testbeams of different kinds and goals.

This work was presented at the Beam Telescopes and Test Beams workshop in 2016, and as a poster and corresponding conference proceedings at both the Topical Workshop for Electronics in Particle Physics [40] and the IEEE Nuclear Science Symposium and Medical Imaging Conference [41] in 2017. In addition, I led a software training session in the use of DQM4hep at the Beam Telescopes and Test Beams workshop in 2017.

2.1 Introduction

Data Acquisition (DAQ) is a critical component of all modern particle physics experiments across all stages of technological readiness, from the very beginning of hardware testing in tabletop experiments to full-scale international experiments like the Large Hadron Collider.

In the modern era of particle physics, the interplay of hardware and software at minuscule timescales drives everything, and almost all results are highly dependent upon the speed and efficiency of the electronics and computer systems that extract data from the detectors. A massive quantity of work goes into creating, testing and optimising the systems that will acquire, process, sort and transport data before it is ever seen by the physicist operating the experiment.

Of particular interest in this thesis is the data acquisition software during the development phase, where individual detector subcomponents are undergoing prototyping and testing. These development and iteration cycles are tied closely to testbeam facilities such as the Super Proton Synchrotron (SPS) at CERN and the DESY II synchrotron at DESY. At this point in the development cycle, the detectors are beginning to take shape and this is where data acquisition (or DAQ) becomes an important consideration.

In addition to this, the data acquisition solutions used during the testbeam phase of detector development are likely to inform the final data acquisition solution; either by evolving directly into the final software, or by identifying and evaluating the particular features or challenges of the subdetector components that the software must take into account or accommodate.

During this stage, each individual detector component – such as a vertex tracker or hadronic calorimeter – will be developed by small teams, and the natural tendency is for each of these groups to set their own standards and develop their own tools, prioritising the features that are important to their specific case. However, in the past this approach has generated a variety of *ad hoc* solutions for testbeam software, many of which cannot be applied outside of their original scope. This results in different teams solving the same problems and implementing the same solutions for each subdetector.

An alternative to this is to develop a suite of tools or frameworks that are generic – capable of being used and deployed for a wide variety of different uses and detector types. In this way, we could greatly reduce the effort used to recreate the same solutions for each new detector, allowing more science to be done faster.

2.1.1 Online monitoring and data quality monitoring

The area of this that we have chosen to contribute to is the development of online monitoring and data quality monitoring tools. Data from testbeams is often not processed fully until well after it has been taken, sometimes after the testbeam has ended, due to constraints on time or processing power. If there were errors, incongruencies, or any other systematic biases with the data, these problems cannot be identified immediately, and as a result may be present in multiple runs, spoiling data and wasting precious time during the already extremely time-sensitive environment of a testbeam.

Online monitoring addresses these issues by allowing the experimenters to see a “preview” of the data being collected. It can provide both a quantitative and qualitative look into how the detectors are responding, and what the data will look like when properly processed, allowing any potential issues to be identified and fixed in a timely manner. This means that good online monitoring can improve the efficiency of a testbeam, increasing the “yield” of data from a given experiment.

Another aspect of this is data quality monitoring (DQM), which assesses the ‘quality’ of the data being taken. The definition of data’s quality will vary depending on the hardware, software, and goals of the experiment, but will usually constitute some form of statistical measure. In this regard, data quality monitoring can be seen as an extension of the concept of online monitoring, focusing more closely on the quantitative aspects. In general, DQM provides the most benefit in more mature experiments, relying on previous experience with the detector and collected data to understand how the data appears when the device is functioning correctly.

In pursuit of all of the above aims, this chapter will discuss the Data Quality Monitoring for High-Energy Physics tool (DQM4hep) developed for online monitoring and data quality monitoring, going into the detail of its properties, principles, applications and development. Deployment and usage of the framework will be discussed in greater detail in Chapters [3](#) and [4](#).

Existing online monitoring and data quality monitoring tools

Online monitoring and data quality monitoring tools already exist, however these are usually designed for a specific application. One example of an online monitoring tool operating primarily at the testbeam stage is EU Data Acquisition (EUDAQ). EUDAQ is currently widely used within the AIDA-2020 collaboration as a data acquisition tool, but also has a set of modules for online monitoring [[42](#)].

However, these modules were intended only for the operation of beam telescopes, and as such the monitoring system has hardcoded features that are highly specific to these detectors, such as a detector being made out of several planes. As a result, using EUDAQ for online monitoring is impossible unless the detector is a beam telescope.

In contrast, the online monitoring systems for the large experiments at the LHC are structured much less rigidly. By way of example, the ATLAS experiment uses a tool called Data Quality Monitoring Framework (DQMF) [43], which is extremely versatile. Given the large number of people present during runs of the detector who will need to access and see the data, this software is designed with scalability as a primary concern, as well as quick and robust checks for the quality of data.

However, the ATLAS experiment has the advantage of being mostly fixed – the structure of the detector itself will not change outside of scheduled upgrades which are signposted years ahead of time. The definitions for the quality of data taken will also not change dramatically, as the design of the detector and the triggering and DAQ systems have been set. DQMF focuses most of its flexibility on the user-facing end, such as histograms, user interfaces and displays, as these are the parts most likely to require change. The DQMF software would not be capable of adapting to another detector – not even a large LHC experiment – without a major rewrite.

These show by way of example the case for a tool like DQM4hep – a framework that is flexible in *all* stages, from the structure of the device taking data, to the ways to process that data for users, to the automated checks to validate it.

2.1.2 The AIDA-2020 project

This work on DQM4hep takes place within the context of the AIDA-2020 project [44], an EU-funded research programme for developing infrastructure and technologies for particle physics detector development and testing, comprising 24 member countries and lead by CERN.

The overarching goal of AIDA-2020 is to develop common tools and infrastructures for physics testbeams. The collaboration is split into work packages focusing on specific areas, and the work detailed in this thesis takes place within Work Package 5 for data acquisition systems for beam tests.

The goal of this work package is to create a suite of tools that are designed with a variety of possible uses in mind, thereby reducing the work and development time necessary to implement data acquisition and monitoring setups, speeding up the planning and

deployment of physics testbeams.

2.2 Overview of DQM4hep

Data Quality Monitoring for High-Energy Physics is an online monitoring and data quality monitoring framework developed for physics testbeams for high-energy and particle physics, developed by Rémi Eté and Antoine Pingault [45]. It is designed to fulfil the requirements of monitoring for physics testbeams in a generic way. The framework is written in the C++11 standard and can run on any Linux distribution. The only requirements for installation are a compiler compliant with the C++11 standard, cmake 3.4 or higher, and ROOT 6. All other dependencies are downloaded and compiled automatically during installation.

The two core principles of DQM4hep are genericness and modularity. The framework is based upon a plugin system that allows shared libraries to be loaded and hook classes for further use. This structure allows for independent components of the framework to be used, not used, or exchanged, by isolating each function of the program into independent processes. The components that are specific to any particular use case are written by the users, and the rest of the framework then handles packaging this information in a useful way and networking to transmit it to where it is needed, meaning that the user does not have to worry about the mechanics of data storage, serialisation or transmission. The network communication is handled by Distributed Information Management System (DIM) [46].

The experiment-specific components have to be written by the user, but these components use standard C++ code with a few DQM4hep-specific functions to handle their integration into the framework, making them easy to understand for users who already have experience coding in C++. This also means that the framework is capable of working with any data format that can be packed into, decoded from, and accessed with normal C++ methods, including those that can be loaded from external libraries. This results in a framework that is able to deal with any kind of data, including user-defined data types, making it more flexible, portable and easily reusable.

2.2.1 Architecture

DQM4hep is designed with genericness as its core paradigm, using processes and algorithms that are independent of data type. The ability to run multiple instances of each process of the framework is also key to its flexibility, allowing users to, for example, sep-

arate sub-detector data from data that has undergone event building, operate in online or offline modes, or distribute the computational load of the analysis over several networked computers.

The generic nature of the framework lies in two core features. Firstly, the abstract Event Data Model (EDM). An event data model is the structure of the events in the data. For instance, a software ‘event’ might in fact be a readout cycle, where the detector writes data to the data acquisition device when its memory is full. Or it might be a physical event, in which case the event is further defined by the trigger – an event that is triggered internally by the detector itself will have a different structure to an event that is externally triggered, such as by a bunch-crossing ID. DQM4hep uses an abstract container for the event itself and allows the user to define its type, structure, and how serialisation should be handled. This means it can handle *any* type of data.

Second, the plugin system. This is a system that allows the inclusion of any user-defined classes or methods via external libraries. These can be used to specify the serialisation method for data, the procedure for online analysis, or many other purposes. The plugin system for end-users consists of four different types of plugins: analysis modules, standalone modules, file reader plugins, and file streamer plugins.

A diagram of the overall structure of the framework can be seen in Fig. 2.1.

Analysis modules

Analysis modules receive events from the data acquisition system, processing the data according to a user-specified procedure to create ROOT TObjects such as histograms, graphs, plots, etc. The analysis module then handles encapsulating these objects as monitor elements, and sending them to the rest of the framework for display and storage.

An analysis module is specific to one use case, and is intended to be written by the user with their data format and processing needs in mind. However, the framework provides both templates and examples for how to write an analysis module.

An example of the structure of the framework utilising an analysis module can be seen in Fig. 2.2.

Standalone modules

Standalone modules are identical in form to analysis modules described above. The distinction is that a standalone module does not operate on data coming from the data acquisition device. One of the intended and most common usages of standalone modules

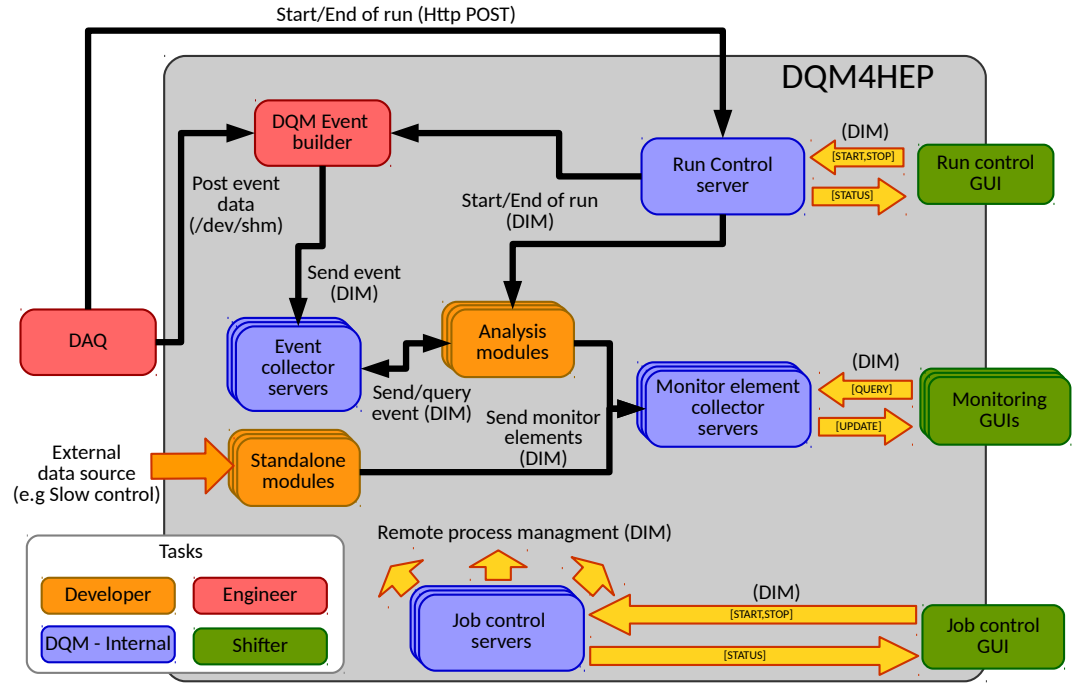


Figure 2.1: The global online architecture of DQM4hep. Each block is colour-coded to show which operator of the testbeam is responsible for the process.

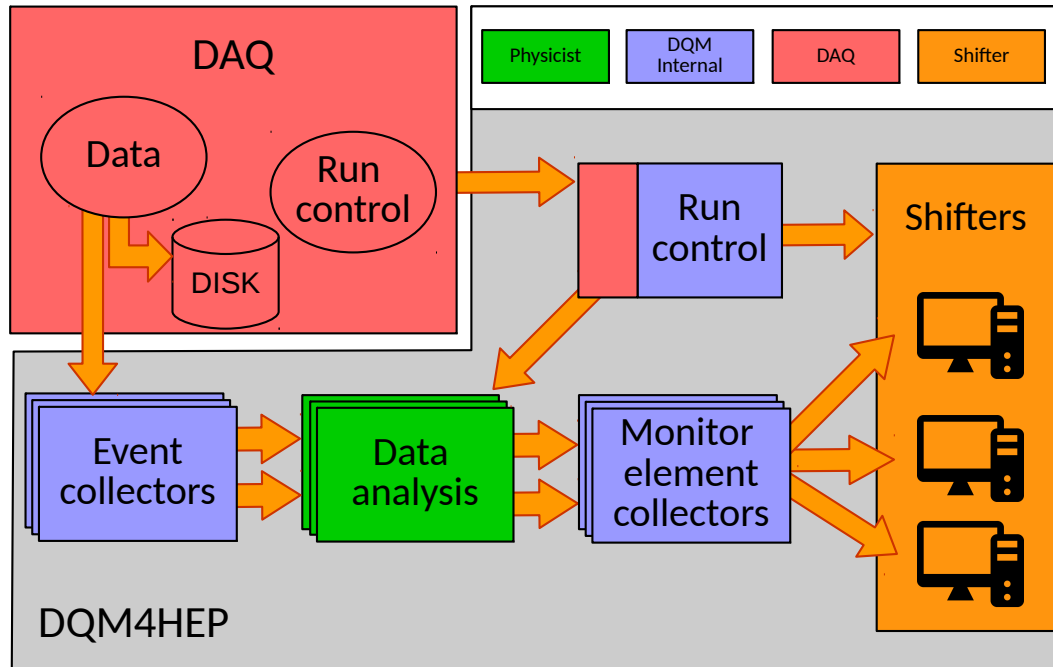


Figure 2.2: The structure of running DQM4hep online using an analysis module.

is as a slow control, taking data from monitoring sensors on the device rather than data, to report on the condition of the hardware. Standalone modules could also be used to *generate* data, if needed, acting as a programmed signal generator or random number generator.

An example of the structure of the framework utilising a standalone module can be seen in Fig. 2.3.

File reader plugins

A file reader is a type of plugin that reads a file from the disk and packs it into a data structure necessary for usage within DQM4hep. They are used primarily for offline monitoring or data processing. File readers can be made for any kind of file, provided the user understands the data structure. There are existing examples of file readers for data stored as binary, plain text, LCIO files, and ROOT TTrees.

An example of the structure of the framework utilising a file reader plugin can be seen in Fig. 2.4.

File streamer plugins

A file streamer is a type of plugin that reads data from a stream and packs it into a data structure necessary for usage within DQM4hep. They are for receiving data from a data acquisition device for online monitoring. File streamers can be made for any kind of data stream, provided the user understands the data structure. File streamers are considered the “default” in DQM4hep.

2.2.2 Visualisation and graphical user interface

As of writing, the graphic user interface (GUI) and visualisation elements of the framework are still under active development for a new version. Therefore this topic will be split into two sections: one to describe the existing GUI, and one to discuss the motivations and goals for the new GUI under development.

Current GUI and visualisation

The current version of the GUI is built with Qt [47] , a free and open-source toolkit and framework for creating graphic user interfaces and widgets that are independent of the operating system. The motivation for choosing Qt was that ROOT provides an option for integration between ROOT and Qt, allowing ROOT classes like `TCanvas` to be

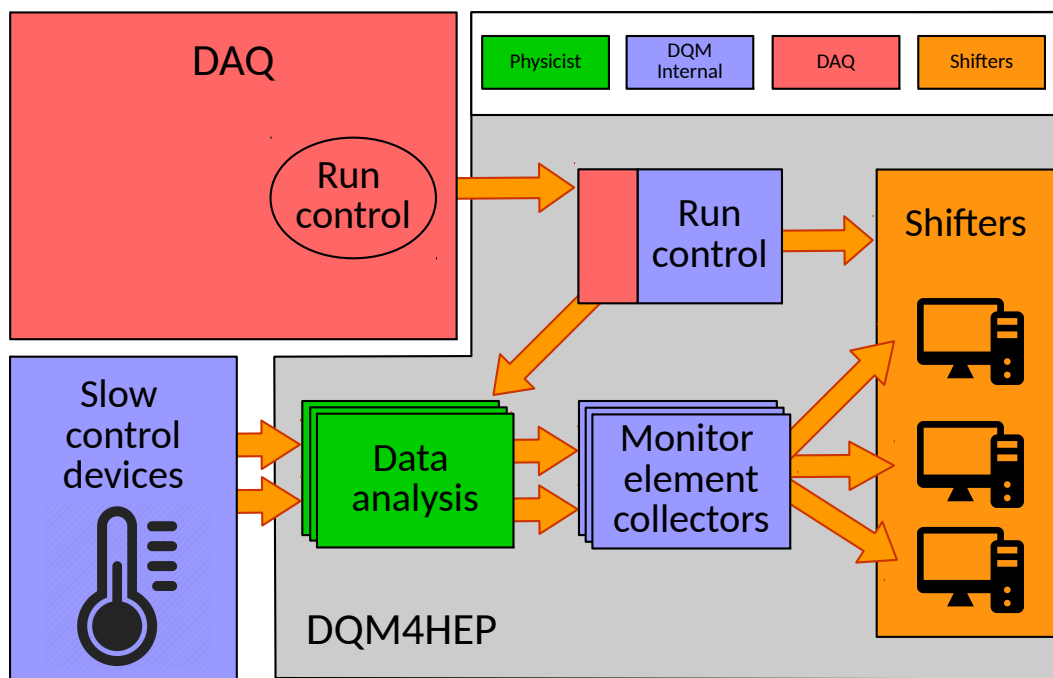


Figure 2.3: The structure of running DQM4hep online using a stand alone module.

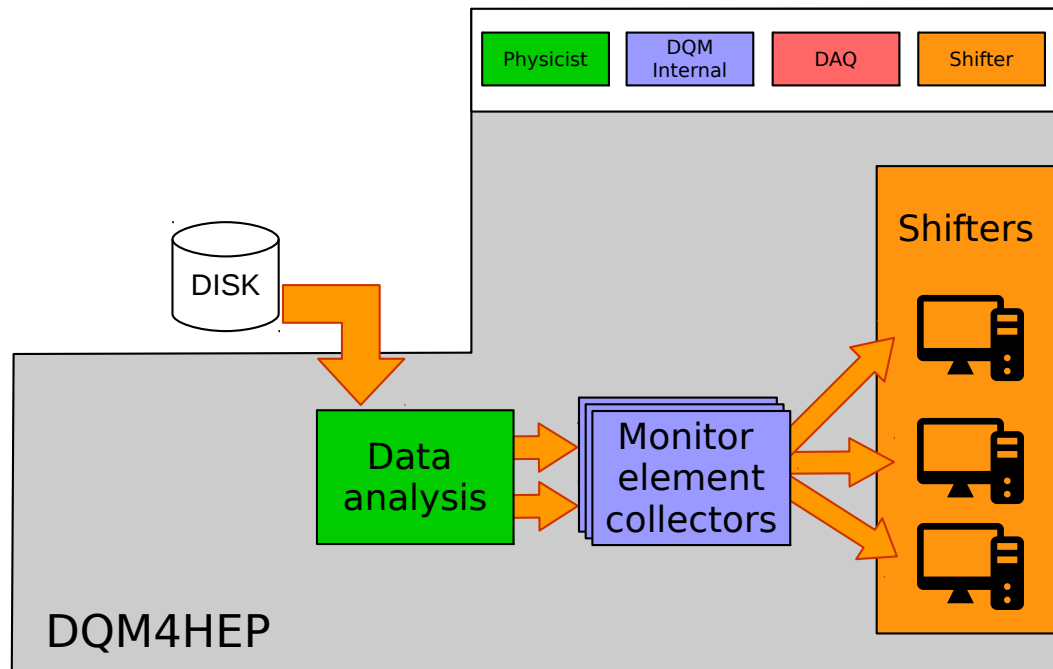


Figure 2.4: The structure of running DQM4hep offline using a file reader module.

“embedded” into Qt widgets. This simplified the implementation of a GUI, allowing a graphical interface based on Qt to be written, then graphics from ROOT simply opened within the existing widgets and windows.

This interface is used in multiple places, including the run control process and the monitoring GUI. The monitoring GUI is built on a system of canvases. Each canvas can have multiple plots open, which can be resized, maximised, minimised, etc. and manipulated as normal for ROOT plots. The user can also create new canvases for more space to arrange plots.

In addition to this, there is an optional provision for a monitoring steering file, which contains presets of canvases, and the plots displayed on them. This is extremely useful when dealing with large datasets or large numbers of plots, as the plots required by the user can be opened automatically when the monitoring interface is run.

An example of the Qt-based monitoring GUI in use can be seen in Fig. 2.5.

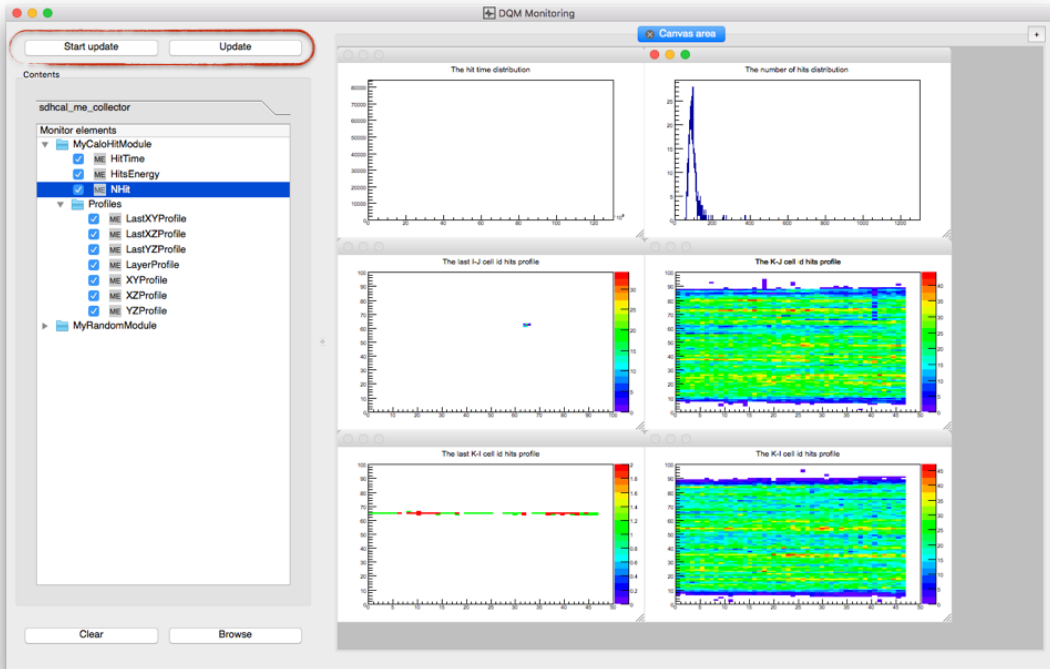


Figure 2.5: An example of the current Qt-based monitoring GUI in use. The panel on the left shows a list of all running analysis modules, and the monitor elements that they contain shown in a folder- or filesystem-like structure. The large right panel is the main canvas, where plots are displayed and can be resized, maximised, or manipulated as normal for ROOT objects. The data used for this demonstration is from an SDHCAL testbeam.

New user interface and visualisation package

For the newer versions of DQM4hep, the decision was made to overhaul the GUI and visualisation packages, removing Qt from the framework and moving to a web-based interface.

The removal of Qt was motivated by two reasons. Firstly, the integration with ROOT provided some complications, since running DQM4hep’s Qt-based GUI requires an installation of ROOT compiled with the `--enable-Qt` flag enabled. The majority of ROOT installations in remotely-accessible file systems based at CERN and DESY (which are heavily used for analysis and testbeams) were not compiled this way. Secondly, Qt was an additional dependency that must be installed prior to use, making the software more dependent upon the operating system, compiler tools, and environment of the machine, and thus less generic and easy to use.

The removal of the Qt GUI allows for greater freedom with development. The intended goal is to have a browser-based GUI, removing dependency on any external GUI libraries and allowing it to function on any device. This will also make it more user-friendly and convenient, as the interfaces for run control, networking, and data monitoring and quality display can be simply run in different tabs of a web browser.

As of writing, the web interface is under active development by Rémi Eté and is not yet complete. However, a mock-up of the web interface can be seen in Fig. 2.6.

2.3 Analysis modules

An analysis module is a plugin that uses data to create monitor elements, which are the core object that drives online monitoring in DQM4hep. Analysis modules are thus a central piece of using DQM4hep as an online monitor.

Mechanically, analysis modules are plugins that read events from a file reader or file streamer plugin, perform some user-defined process to the data to produce a plot, graph, histogram or other ROOT object before emitting it to the rest of the framework as a monitor element.

The most basic analysis module will simply structure information coming from the data acquisition device into a human-readable plot, but analysis modules are able to do anything that can be done in C++ or ROOT, so can contain an arbitrary amount of processing. This means that analysis modules can also be used for online analysis or processing of data, making them very powerful tools for online monitoring.

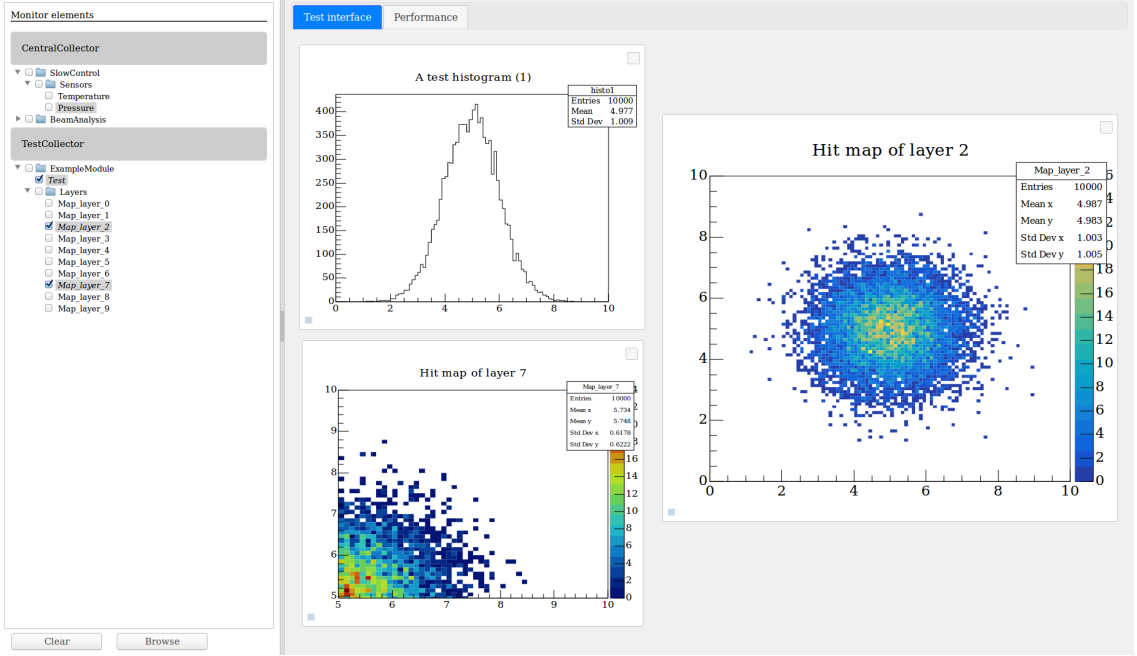


Figure 2.6: A preview of the planned web-based monitoring interface. The structure is similar to the existing interface (see Fig. 2.5), but rendered in a web browser. The plots displayed here are not real data, but “dummy” data for testing purposes.

2.3.1 Running an analysis module

The `dqm4hep-start-module` executable is used to run an analysis module, in combination with an XML steering file. The available arguments are as follows:

```
-h
---help
```

Displays usage information, then exits.

```
-f
---steering-file
```

(Required) Gives the path to the XML steering file that defines what analysis modules to run and their parameters. See the next section for more information on these steering files.

```
-t
---type
```

The type of module to run. This overwrites the module type in the steering file.

```
-n
---name
```

The name for this instance of the module. This overwrites the module name in the steering file.

```
--v
--verbosity
```

The verbosity of the logger. Options are `trace`, `debug`, `info`, `warning`, `error`, `critical`, and `off`. This is `warning` by default.

```
--_
--ignore-rest
```

Ignores any arguments following this flag.

```
--version
```

Displays version information, then exits.

Steering files

An XML steering file is used to pass parameters to the analysis module, including the type of analysis module, the plots to create, and what other processes to connect to.

Steering files are broadly made of four sections: the application settings, the archiver settings, the analysis module, and the monitor elements.

The application settings specify how to run the application itself, including which other file readers or streamers to connect to, which run control is being used, etc.

The archiver setting specify whether the results of running the analysis module are written to an archive, which is a ROOT file containing the monitor elements that the analysis module created.

The analysis module section sets the type of analysis module to run, and gives it a unique name to distinguish it from other instances of the same module. Both of these parameters can be set at the command line (see above).

The monitor element section specifies the monitor elements used in the file. “Monitor element” is a generic name for any kind of ROOT object, which may be a histogram, graph, plot, drawing, etc. The name, directory, and properties of monitor elements are set here, depending on what type of object the monitor element is.

2.3.2 Creating analysis modules

This sections describes the process of writing new analysis modules.

In addition to writing the analysis module code, a compiled analysis module needs to be declared as a plugin for DQM4hep to be able to use it. The absolute path to the library file for new analysis modules needs to be appended to the `DQM4hep_PLUGIN_DLL` environment variable.

Writing analysis modules

Analysis modules must be written specifically for the type of data they receive and for a certain analysis or set of analyses to perform. This means that the ideal person to write an analysis module is someone familiar with both the experiment’s event structure and the goals of the monitoring.

Each analysis module is a single .cc file. E.g. `ExampleModule.cc` would define an analysis module called `ExampleModule` that would be found in the `dqm4hep-exampleproject/source/src/plugins` directory.

The .cc file then has several sections that must be written, described in separate sections below.

Variable declaration

In this section of the file, the variables that must be persistent over the entire running of the module are declared. These variables will not go out of scope, so are usually reserved for the monitor elements themselves, or counters that must persist over the entire module. Monitor elements must be declared as the `online::OnlineElementPtr` type. None of the declared variables are initialised here; initialision is done in later functions.

`readsettings`

This function reads the settings from the XML steering file, meaning that anything that needs to be initialised from the steering file is done here. This notably includes all monitor elements. Typically the `core::OnlineElementPtr` will have been declared during the preamble, then is assigned here based on the steering file using the `online::ModuleApi::getMonitorElement()` function.

`initModule`

This process is run once, when the analysis module is initialised. Anything that needs to be done only once at the beginning should be done here. The use of this function is

limited, as most tasks that need to be reset are reset at the beginning of a run using `startOfRun()` below.

startOfRun

The `startOfRun` function handles code that should be executed only once per run, at the beginning. This is commonly used for counters that must persist over the entire run, for instance if a detector can give an error signal, a counter to store the number of error signals is initialised here so that it is persistent over the entire run, and the number of error signals can be totalled at the end of the run.

endOfRun

This is the end-of-run counterpart to `startOfRun()`. In general, this function will encapsulate logic that must deal with counters or procedures that were initialised or begun in `startOfRun()`.

endModule

This function is called when the module ends, and is usually used for deleting or cleaning up any objects created during the `initModule()` function. Most normal use cases will not need this function, as cleanup of objects such as variables or monitor elements is handled by the framework.

process

This is the function where the analysis module performs the main processing of data. In this function, events are loaded into memory from the event stream or file reader, and made available for use. Data can then be processed using normal C++ methods, then filled into monitor elements to be sent to the monitor element collectors so they can be presented in the user interface, or stored by the archiver.

Plugin declaration

Analysis modules are DQM4hep plugins, so must be declared as a plugin using DQM4hep's facility for this so that the main executables can access them. At the end of the module, the following code must be included to declare the analysis module as a plugin:

```
DQM_PLUGIN_DECL(ModuleName, "ModuleName");
```

This should take place at the very end of the file but within the `dqm4hep` and `example` namespaces.

When an analysis module is declared as a plugin, the main DQM4hep executable must be given the directory of the library to load the plugin at runtime. This is done by ensuring that the directory of the library is within the search path defined by the `DQM4hep_PLUGIN_DLL` environment variable:

```
export DQM4hep_PLUGIN_DLL=$DQM4hep_PLUGIN_DLL:/path/to/module/lib/
libDQMExample.so
```

Once this is added, DQM4hep can access the libraries and run the analysis module.

2.3.3 SimpleModule – a worked example

To explain the process of creating and writing analysis modules in more detail, a worked example is presented. For this we imagine a simplified particle physics detector, and write an analysis module called `SimpleModule.cc` to monitor data from it. We also write a steering file called `simple-test.xml` to run the analysis module. Each function of the analysis module will be described in depth, explaining in detail what the code is doing.

In this example, the built-in `GenericEvent` event type is used. For more information on the `GenericEvent` type, see [48]. We will not be using the `startOfCycle` and `endOfCycle` functions.

Detector

We can imagine a simplified particle physics detector as a square plane split into 36 tiles (6 on each side). When a hit occurs the detector reads out the location, ADC, and time of the hit. Each event will correspond to a single hit.

The data acquisition device sends us an event made of four integer values:

- `xPos` – the position of a hit on the x-axis of the detector, from 0 to 5
- `yPos` – the position of a hit on the y-axis of the detector, from 0 to 5
- `ADC` – the ADC of the hit, in arbitrary units, between 0 and 1500
- `timeHit` – the time the hit occurred, in arbitrary units

Goals

Before writing the module, the variables and properties to monitor must be determined. For this detector and its analysis module, there are three goals:

- Spectrum histogram – a single histogram containing the ADC of each hit for the entire run, producing an energy spectrum.
- Hitmap – a hitmap showing the distribution of hits across the detector.
- Radiation damage – if we imagine that ADCs higher than 1000 are likely to cause radiation damage to the detector, then monitoring the number of hits in the entire run exceeding this threshold allows an estimation of how damaged the detector may be.

Preamble

Here the pointers for all monitor elements are initialised. One is required for the ADC spectrum, and one for the hitmap. They don't need to have their type declared here – this is done later. The convention adopted for DQM4hep is to prefix all monitor element pointers with `m_p` to distinguish them, as they are an important type.

Variables for handling the information about radiation damage are also created here, as they need to persist between events. These are declared here and will be initialised later.

```
private :
    online::OnlineElementPtr m_pSpectrum;
    online::OnlineElementPtr m_pHitmap;
    int radiationDamageADCThreshold;
    int damageHitsCounter;
```

readSettings

Here the monitor elements are assigned, reading in their information from the XML steering file. To do this the `online::ModuleApi::getMonitorElement()` function is used, which searches in the XML steering file for the corresponding information. This function has three arguments: the first is always `this`, the second is the directory the monitor element is in, and the third is a string of the name given to the monitor element in the steering file. These monitor elements are placed at the top directory, so the second argument is `/`.

```
void SimpleModule::initModule() {
    m_pSpectrum = online:ModuleApi::getMonitorElement(this, "/", "ADC_Spectrum");
    m_pHitmap = online:ModuleApi::getMonitorElement(this, "/", "Hitmap");
}
```

Any other variables that need to be initialised only when the module starts should be placed here. This is a good place to define the threshold for radiation damage:

```
radiationDamageADCThreshold = 1000;
```

startOfRun

The only thing necessary to do at the start of each new run is to ensure that the counter for hits above the threshold for radiation damage is reset to zero:

```
void SimpleModule::startOfRun(core::Run & /*run*/) {
    damageHitsCounter = 0;
}
```

This ensures that even with multiple runs in the same file, the counter resets correctly.

endOfRun

Once a run has finished, the number of hits that might have caused radiation damage should be read out. There are many ways to do this, but the simplest is to send a message to the logger:

```
void SimpleModule::endOfRun(const core::Run & /*run*/) {
    dqm_info("Number of hits above radiation damage threshold: {0}",
             damageHitsCounter);
}
```

For more information on the `dqm_info()` function and its syntax, see the section on the logging tools here [\[49\]](#).

process

The first thing to do is make sure that the `process()` function has access to the `GenericEvent`. This is done by making it an argument of the function, calling it `pEvent` to make it clear that this is a pointer to an event and not an event object. Basic error-checking is then done, to ensure that the current event exists:

```
void SimpleModule::process(core::EventPtr pEvent) {

    if (nullptr == pEvent) {
        dqm_warning("Event pointer is invalid - skipping this event");
        return;
    }
}
```

The `dqm_warning()` function publishes a message to the logger, with the `warning` level. See the section on the logging tools for more information.

Forcing this function to `return` ensures that the analysis module doesn't attempt to access an event that does not exist. Otherwise, this would cause a segmentation fault and crash the analysis module. Since the `process()` function runs separately for each event, this has the effect of skipping to the next event.

Now the pointer of the event needs to be assigned so that the object itself can be accessed. A new variable of type `core::GenericEvent` is created, then the `getEvent()` function is used to assign it.

```
core::GenericEvent *pGenericEvent = pEvent->getEvent<core::GenericEvent>()
;
```

A variable is needed to store the information pulled from the event, then the information can be extracted using the `getValues()` function:

```
int xPos;
int yPos;
int ADC;
int timeHit;

pGenericEvent->getValues("xPos", xPos);
pGenericEvent->getValues("yPos", yPos);
pGenericEvent->getValues("ADC", ADC);
pGenericEvent->getValues("timeHit", timeHit);
```

The `getValues()` function takes two arguments: the first is a key in the form of a string, which identifies a piece of data within the `GenericEvent`. The second is the object to place the retrieved data into. In this case, the same names are used for simplicity. This works because the first variable is a string, used as a key to find information within the `GenericEvent`.

Now all the data is loaded into memory and available for use.

First the ADC is added to the `ADC_Spectrum` plot. To do this, the monitor element

`m_pSpectrum` must be cast to the correct ROOT object type, using the `objectTo()` function, then use ROOT's `Fill()` function:

```
m_pSpectrum->objectTo<TH1I>()->Fill(ADC);
```

Then the same must be done for the bitmap. This time it needs to be cast to a `TH2I` object and filled with the x- and y-positions as well as the ADC:

```
m_pBitmap->objectTo<TH2I>()->Fill(xPos, yPos, ADC);
```

And lastly, a check is performed for whether the ADC was high enough to cause radiation damage, and if so increment the counter:

```
if (ADC >= radiationDamageADCThreshold) {
    damageHitsCounter++;
}
```

Steering file

Now the analysis module is complete, there needs to be a steering file to run it. This is started by making a file called `simple-test.xml`. Then the `<dqm4hep>` environment is opened, as this will contain everything else:

```
<dqm4hep>

    <!-- everything else will be in here -->

</dqm4hep>
```

There are then four sections to write: the application settings, the archiver settings, the analysis module, and the monitor elements.

Application settings

This section of the steering file controls the parameters that are needed to run the module itself. This part of the file is where the module is specified to be running online (receiving events from an event collector) or offline (receiving events from a file reader).

This analysis module will be run offline, so the important fields here are `EventReader`, which is which type of file reader to use to read events, and `EventFileName`, which specifies the path to the file to read.

If this were running online, the `RunControl`, `EventCollector`, `EventSource` and `MonitorElementCollector` would have to give the names of those processes. When running offline, these names can be set to anything, so they are given dummy names.

```
<settings mode="EventReader">
  <parameter name="EnableStatistics"> true </parameter>
  <parameter name="EventReader"> SimpleEventReader </parameter>
  <parameter name="EventFileName"> /foo/bar/simpleEventDatafile.root </
    parameter>
  <parameter name="CyclePeriod"> 1 </parameter>
  <parameter name="CycleCounter"> 0 </parameter>
  <parameter name="CycleTimeout"> 0 </parameter>
  <parameter name="RunControl"> DummyRunControl </parameter>
  <parameter name="EventCollector"> DummyEventCollector </parameter>
  <parameter name="EventSource"> DummyEventSource </parameter>
  <parameter name="MonitorElementCollector"> DummyMECollector </parameter>
</settings>
```

Archiver settings

This section controls the archiver, which creates an archive of all monitor elements in the form of a ROOT file when the analysis module exits. If the archiver isn't needed, it can be set to `enable="false"` and ignored.

In this case the archiver is needed, so it is set to `true`. A filename for the archive needs to be given, e.g. `archive-run42.root`. The OpenMode is chosen to be `RECREATE` as the archive should be re-written every time the module is run, although `APPEND` would add events onto an existing file. `AllowOverwrite` is set to `true` so that old archives can be overwritten easily. As run numbers are not used in the analysis module, `AppendRunNumber` is set to `false`.

```
<archiver enable="true">
  <parameter name="FileName" value="archive-run42.root"/>
  <parameter name="OpenMode" value="RECREATE"/>
  <parameter name="AllowOverwrite" value="true"/>
  <parameter name="AppendRunNumber" value="false"/>
  <selectors>
    <selector regex=".*" select="true"/>
  </selectors>
</archiver>
```

Analysis module

This section contains a declaration of which analysis module to execute, and the name to give it. A running analysis module needs a unique name to distinguish it from other

modules of the same type running in the same environment.

This steering file has to run SimpleModule. Only one instance is needed at a time, but the name has to be different than the module's base name, so:

```
<module type="SimpleModule" name="mySimpleModule"/>
```

Monitor elements

This section is where the monitor elements to use and the parameters of the ROOT objects are declared. This entire section will be within the `<storage>` and `<monitorElements>` environments:

```
<storage>
  <monitorElements>

    <!-- monitor elements will go here -->

  </monitorElements>
</storage>
```

To create a ROOT object, the `<bookElement>` environment is used to declare its type, path, name, title, and any other parameters the ROOT object requires. For example, to create a histogram for the ADC spectrum, a TH1I is needed as the ADCs are integers. The range of the ADCs is from 0 to 1500, so the range can be set accordingly.

```
<bookElement type="TH1I" path="/" name="ADC_Spectrum" title="Spectrum of all
ADCs" nBinsX="150" minX="0" maxX="1500">
</bookElement>
```

Similarly, the monitor element for the bitmap is defined:

```
<bookElement type="TH2D" path="/" name="Bitmap" title="Bitmap of the example
detector" nBinsX="6" minX="0" maxX="5" nBinsY="6" minY="0" maxY="5">
</bookElement>
```

XML loops

In this example, loops aren't necessary, but defining monitor elements using a for-loop in XML is a useful feature, so it is discussed here. For example, if one of the goals were to create a histogram for each of the 36 tiles in the detector, a for-loop would allow this to be created with a smaller amount of code

To do this, the `<for>` environment is used, using `tileNumber` as the id. Then a template monitor element definition is written out using `$ FORtileNumber` whenever the tile number should be inserted:

```
<for id="tileNumber" begin="0" end="35" increment="1">
    <bookElement type="TH1D" path="/" name="Tile$FOR{channelNum}" title=""
        Spectrum for tile $FOR{channelNum} nBinsX="150" minX="0" maxX="1500">
    </bookElement>
</for>
```

This would then create a series of monitor elements called `Tile0`, `Tile1`, `Tile2`, etc.

Building and running

To compile the analysis file, the normal build commands are issued from the build directory, found in `dqm4hep-example/build`:

```
cmake ..
make install
```

Running `cmake` is only needed for the first compilation after creating a new module – it isn't necessary when recompiling a module that has been compiled before.

Once the analysis module has compiled successfully, DQM4hep must be given the path to its libraries so that the main installation of DQM4hep can utilise it. This is done by appending the path to the libraries to the `DQM4hep_PLUGIN_DLL` environment variable:

```
export DQM4hep_PLUGIN_DLL=$DQM4hep_PLUGIN_DLL:/path/to/dqm4hep-example/lib/
libDQMExample.so
```

In order to run, DIM must also be running, but for offline use this is simple. In a new terminal window:

```
export DIM_DNS_NODE=localhost
dns
```

Then to run the analysis module, the `dqm4hep-start-module` executable is run, pointing it to the steering file using the `-f` argument. Since a logging output at the ‘info’ level was implemented, the argument `-v` must be given to manually set the logging level to `info` so that it can be seen in the output.

```
dqm4hep-start-module -f simple-test.xml -v info
```

The analysis module will then run. Once it has finished, the archiver will create the archive in the directory it was run in.

2.4 Data quality monitoring

Data quality monitoring (DQM) is a type of data monitoring where the data is tested using some form of statistical or mathematical process to produce a value corresponding to the “quality” of the dataset. This can take many forms, such as comparing an experimental dataset to reference data acquired from previous experiments, or requiring that the χ^2 or p-value of a dataset may need to pass a certain threshold to be considered valid.

The definition of the “quality” statistic will differ according to a variety of factors such as the type of data, the aim of an experiment, etc. Common examples are p-values, or binary pass-fail tests where data that passes has a quality of 1, and 0 otherwise.

One of the benefits of data quality monitoring is that it provides a more reproducible and robust set of checks on data-taking, allowing quantitative analysis of the performance of a detector prototype. It can also be used as a way for shifters without detailed knowledge of the hardware, software, or physics to determine whether the detector is performing as intended during a testbeam when experts are not available, by using the quality statistics as a guide.

Previous versions of DQM4hep did not have infrastructure to support data quality monitoring, but this was added during refactoring in preparation for the next release version. Once this was in place, this permitted an array of quality tests to be developed, implemented, and tested.

A quality test (or qtest) processes a series of monitor elements (ROOT TObjects) according to a set of criteria defined in the test’s code. This test produces a numerical result between 0 and 1, referred to as the “quality”. Within the framework, quality tests are self-contained C++ code files, which hook into the framework’s system for execution. Quality tests are run by using the executable `dqm4hep-run-qtests` and a steering file to define parameters, such as which files to load, which quality tests to execute, and what the passing and failing boundaries are for each quality test.

2.4.1 Quality tests

The quality tests that were implemented in DQM4hep are described in detail below. Each test requires a certain type of object as an input and has its own definition of what the “quality” statistic represents. Some quality tests also require a reference to compare against the input data, which is also described.

A summary of the quality tests can be found in Table 2.1.

Property within expected test

This is a quality test that takes either a TH1 or TGraph object, and finds some user-defined parameter. The parameter must be one of: mean, mean90, root mean square (RMS), root mean square 90 (RMS90), or median. It then checks whether either: that this parameter is within a user-specified range; or that it is above or below the user-specified threshold. If a range is being used, the result is the p-value of the property being within the specified range. If a threshold is being used, then the result is 1 if the property passes the threshold, 0 otherwise.

Exact reference comparison test

This is a quality test that takes any TObject, and compares it to a user-specified reference object (which must be of the same type). The result is 1 if the two objects are exactly identical, 0 otherwise.

Fit parameter in range test

This is a quality test that takes either a TH1, TGraph, or TGraph2D object and plots a user-defined function onto it, solving for one of the parameters of the function, then checks it against a user-defined range. The result is the p-value of the parameter being within the specified range.

Kolmogorov-Smirnov test

This is a quality test that takes either a TH1 or a TGraph object, and performs the Kolmogorov-Smirnov test between that object and a specified reference. The result is the p-value of the Kolmogorov-Smirnov test. The Kolmogorov-Smirnov test is intended for unbinned data, not histograms, but ROOT provides a function for performing the Kolmogorov-Smirnov test on histograms, so this functionality is also included for the sake of completeness.

Pearson χ^2 test

This is a quality test that takes a TH1 object and performs the Pearson χ^2 test between that object and a specified reference. This test is analogous to the Kolmogorov-Smirnov test, but is designed specifically to work for binned histogram data. The result is the p-value output by the χ^2 test.

Quality Test	TObjects	Required	Optional
PropertyWithinExpectedTest	TH1 TGraph	Property Method (see 2.4.1)	
ExactRefCompareTest	Any TObject	None	CompareUnderflow CompareOverflow
FitParamInRangeTest	TH1 TGraph TGraph2D	FitFormula, TestParameter DeviationLower DeviationUpper	GuessParameters FunctionRange UseLogLikelihood UsePearsonChi2 ImproveFitResult
KolmogorovTest	TH1 TGraph	None	UseUnderflow UseOverflow
Chi2Test	TH1	None	ComparisonType UseUnderflow UseOverflow

Table 2.1: Table summarising all quality tests implemented in DQM4hep and their properties.

2.4.2 Running quality tests

Quality tests can be run using the `dqm4hep-run-qtests` executable, found in `dqm4hep-core/bin/`. This executable handles the running of the actual binaries for each qtest, as well as obtaining monitor elements from the ROOT file and the setting of parameters. This executable has one required arguments and several optional ones, detailed below.

Arguments

```
-h
--help
```

Displays usage information, then exits.

```
-i <string>
--input-qtest-file <string>
```

(Required) Gives the path to the XML steering file that defines what quality tests to run, their parameters, and what monitor elements to run them on. See the section below for more information on these steering files.

```
-c
--compress-json
```

Turns on compression for the JSON qtest report output file. Off by default.

```
-w
--write-monitor-elements
```

Turns on writing of monitor elements in the qtest report. Off by default.

```
-p <string>
--print-only <string>
```

Prints only the quality reports of the given flag. Options are `undefined`, `invalid`, `insuf_stat`, `success`, `warning`, `error`.

```
-e <string>
--exit-on <string>
```

Forces the program to exit if any qtest results in the given code. or greater. Options are `ignore`, `failure`, `warning`, `error`. This is `failure` by default.

```
-v <string>
--verbosity <string>
```

The verbosity of the logger. Options are `trace`, `debug`, `info`, `warning`, `error`, `critical`, and `off`. This is `warning` by default.

```
-q <string>
--report-file <string>
```

Gives the path of the qtest report output file (in JSON) format.

```
-o <string>
--root-output <string>
```

Gives the path of a ROOT output file to save the processed monitor elements.

```
--ignore_rest
```

Ignores any arguments following this flag.

```
--version
```

Displays version information, then exits.

Steering file

Steering files use XML to store all the information needed to execute a qtest. There are two main sections: the `<qtests>` block and the `<monitorElements>` block, both of which must be within the `<dqm4hep>` XML tag.

The `<qtests>` block defines the qtests to execute along with their settings or parameters, without reference to what they will be run on. The structure and parameters of these is highly dependent upon the qtest being used – see the section for each qtest above.

The `<monitorElements>` block opens a file using the `<file>` tag, within which each monitor element is opened with `<fileElement>`. Inside this tag, all of the qtests to execute on this monitor element are given. In this example below, the qtests `ExampleTest1` and `ExampleTest2` are both performed on the monitor element `TestHistogram`:

```
<monitorElements>

    <file name="test_samples.root">
        <fileElement path="\TestDirectory" name="TestHistogram">
            <qtest name="ExampleTest1" />
            <qtest name="ExampleTest2" />
        </fileElement>
    </file>

</monitorElements>
```

Some kinds of qtests require reference objects to compare against, which must be declared in the `<references>` block. References have a `name` parameter which gives the path to the file used as a reference, and an `id` which is a short tag for referring to them later in the XML file. For example:

```
<references>
  <file id="mc-ref" name="montecarlo_reference_samples.root"/>
  <file id="ex-ref" name="experiment_reference_samples.root"/>
</references>
```

When a qtest that requires a reference is declared, the reference is given within the `<fileElement>` tag:

```
<fileElement path="\TestDirectory" name="TestHistogram">
  <reference id="MyReference"/>
  <qtest name="ExampleTest1"/>
</fileElement>
```

This performs the qtest `ExampleTest1` on the monitor element `TestHistogram`, looking for another ROOT object of the same name within the file `MyReference` points to. It is also possible to use a specific object in a file as the reference:

```
<fileElement path="\TestDirectory" name="TestHistogram">
  <reference id="MyReference" path="/path/to/the/reference/file" name="ReferenceHistogram"/>
  <qtest name="ExampleTest2"/>
</fileElement>
```

In this case, this performs `ExampleTest2` on the monitor element `TestHistogram`, using the object `ReferenceHistogram` as the reference.

2.4.3 Writing quality tests

Users can create their own quality tests if the included tests do not satisfy their requirements. Quality tests are a type of plugin – see the *plugin system* section of the DQM4hep documentation [50] for more information on plugins, including how to write and compile them.

The code for the built-in quality tests can be found in `dqm4hep-core/source/src/plugins/` and can be used as references or templates. Files for quality tests should be given a descriptive name in CamelCase, and end with `Test`, e.g. `ExactRefCompareTest.cc`.

The code for a quality test requires only a single .cc file, which has four functions: the constructor, the destructor, `readSettings`, and `userRun`. Each is discussed in a separate

subsection below. If required, further functions can be implemented as needed. This is left for the user to decide.

Code should be written to catch common errors and throw appropriate exceptions, especially for errors that cause segmentation faults. This will help to avoid a QTest preventing other QTests from running should an error occur. Errors are reported using the `reportMessage()` function, and the error message will appear in the summary of the QTest after it has run.

Constructor and destructor

For the constructor and destructor, it's enough to copy existing code, changing the name of the QTest and the variables to be initialised. The program that runs QTests handles everything else. Care should be taken to initialise variables properly and to give the QTest a good description:

```
ExampleTest :: ExampleTest(const std :: string &qname)
    : QualityTest("ExampleTest", qname),
      m_someFloatParameter(0. f),
      m_someIntParameter(0)
{
    m_description = "A description of the test's functionality, as well as the
                     meaning of the quality statistic it outputs.";
}
```

readSettings

The `readSettings` function initialises the variables of the QTest from the XML steering file, which is loaded into memory via `xmlHandle`. This function should be used to read in information from the XML file and validate it to make sure the test can be run. Variables are read in using a combination of pre-processor macros and `XmlHelper`. For example:

```
RETURN_RESULT_IF(STATUS_CODE_SUCCESS, !=, XmlHelper :: readParameter(xmlHandle
    , "PropertyName", m_property))
```

Note that the above example will fail if the parameter is not present in the XML file, so should only be used for parameters that are required. If a parameter is optional, use the `RETURN_RESULT_IF_AND_IF` macro instead. This allows the parameter to be returned if it is found, or does nothing if it is not. For example:

```
RETURN_RESULT_IF_AND_IF(STATUS_CODE_SUCCESS, STATUS_CODE_NOT_FOUND, !=
    XmlHelper :: readParameter(xmlHandle, "PropertyName", m_property))
```

For more information on status codes, pre-processor macros, and XML parsing with `XmlHelper`, see the core tools section of the documentation.

Parameters should be checked to make sure that the qtest can be run and that the result is meaningful. While `XmlHelper::readParameter` and similar functions can take an optional fourth argument for a validator delta function, users should make code clear and readable by using `if-else` statements. This is especially important when checking against more complicated criteria.

userRun

The `userRun` function defines the process of the qtest itself, using the monitor element. The result *must* be a float between 0.0 and 1.0 that represents the “quality” or “goodness” of the test. The meaning of this quality statistic depends on the test but is often a p-value. At absolute minimum, it should represent a pass-fail case, so that a passing qtest gives a quality of 1 and a failing qtest gives a quality of 0.

The monitor element must first be cast to an appropriate class. This should be done using the `objectTo` function. For example, if the monitor element is a TH1:

```
TH1* myHistogram = pMonitorElement->objectTo<TH1>();
```

After this, the object can be accessed using its normal methods, and the qtest can be written using normal C++ code for ROOT objects.

It is useful to include a check for whether the monitor element exists and is the correct type, to prevent segmentation faults, using a comparison to `nullptr` and throwing an appropriate status code if the check fails. For example:

```
if ( nullptr == pMonitorElement->objectTo<TH1>() )
{
    report.m_message("Object does not exist or is of unrecognised type!");
    throw StatusCodeException(STATUS_CODE_INVALID_PTR);
}
```

The meaning of these status codes is documented under *Status codes and useful pre-processor macros* in the core tools section of the documentation.

Once the quality statistic of the test is known, it is output using `report.m_quality`. Any other information can be output using `report.m_message` – this is useful for including comments on the result.

2.5 Documentation and user manual

One of the biggest hurdles for the promotion and uptake of a new framework is the lack of understanding or familiarity with its use. Many research teams will continue to use existing software solutions, which may be suboptimal or difficult to use, according to the principle of “better the devil you know than the devil you don’t”. The first step to overcoming this is to produce clear, readable and complete documentation across the entire range of features the framework has and then to ensure the package exists before testbeam campaigns begin, and represent a clear advantage to the end user.

The DQM4hep framework has two sets of documentation with different intended readers and different aims, so these will be discussed separately.

2.5.1 Doxygen documentation

Doxygen is a tool for automatically generating documentation resources for C++ code, relying on marked sections of documentation written within the actual code itself. Doxygen is able to directly obtain the structure of code, objects, functions, etc. from the code, allowing it to automatically generate a complex and rich set of documentation that categorises and indexes objects based on their inheritance, namespace, etc.

Doxygen can also generate an HTML- or L^AT_EX-based document that can be used as a local reference guide or hosted online. This makes Doxygen a powerful tool for documenting the technical aspects of code, demonstrating hierarchies of functions and objects, and an extremely useful reference guide for large programs or frameworks.

While Doxygen documentation is extremely useful, it does have some limitations. Doxygen functions more as a technical reference for code, lacking any overviews or instructions due to its automatic generation. This kind of documentation lacks a holistic element, and has no way for new users or those less familiar with the codebase to understand the overarching concepts. This can make it inaccessible for new users. The way this was addressed will be discussed in the next section.

DQM4hep has a Doxygen website hosted on the internet, which is available here [\[51\]](#).

2.5.2 User manual

The existing documentation featured the common elements of the framework – such as the plugin system, event interface, logger, and XML parser – explained in detail, with clear examples and straightforward advice on their use.

My contribution to this was to write in-depth explanations on the structure, usage, and creation of analysis modules and quality tests, the two parts that are most specific to end-users. The experience acquired using the framework and deploying it on testbeams for the first time, as well as integrating it with different detectors, provided a strong knowledge base to write the user manual intended for a user approaching the framework for the first time. These testbeams are described in more detail in Chapters 3 and 4.

The user manual can be found online here [52].

Analysis module guide

There is an in-depth explanation of each of the component functions of an analysis module, discussing which actions or data processing should be done in each, and their intended purposes. There is also an explanation of the XML steering files that are necessary to run an analysis module, and instructions on how the executable is run, along with its arguments.

In addition to this there is a worked example of an analysis module from start to finish. A simplified particle physics detector and its data format is defined, and then the reader is lead through the process of writing an analysis module step-by-step and function-by-function to obtain certain plots and results from the data. This is intended to give a more concrete demonstration of usage, as an easier to follow example.

Quality testing guide

There is extensive documentation of quality testing; each quality test is described in detail, including their purpose, output, required parameters, and optional parameters. In addition to this, there is a guide for how to run quality tests, including an explanation of running from the command line and an in-depth look at the structure of the XML steering files required.

Finally there is a section explaining how to write new quality tests. This includes a detailed explanation of the purpose of each function within a quality test file, what the required outputs are and how to utilise them, error testing, and advice on maintaining a style consistent with the rest of the framework.

2.6 Adaptation to other detectors

Due to the modularity and genericness of DQM4hep, the process of deploying it for a new detector is simple – the only parts of DQM4hep that need to be made for any specific

use case are the analysis modules, standalone modules, streamer plugin, and file reader plugin. For all of these plugins, there are templates available in the codebase, as well as examples of in-use plugins for other detectors. A few special DQM4hep-specific functions are necessary for these plugins to hook into the framework properly, but apart from these all user-provided plugins are written in normal C++ code that also integrates ROOT, so should be familiar to most users.

A file streamer or file reader must be written by the user given a specific data structure. This requires knowledge of both the event data model of the data acquisition setup, as well as the structure of the data files. The ideal person to write this code is someone with detailed knowledge of the data acquisition software being used, and the data storage or streaming.

In general, only one of the file streamer or file reader plugins will be needed. Both of these plugins are similar in structure and differ only on where they get the data from – a file reader loads a file from disk, whereas a streamer loads it from the data acquisition system. If the data will be monitored offline or “nearly-online” by loading files from disk, then a file reader plugin must be written. If the data is to be monitored online, then a streamer plugin must be written.

Once the information is accessible from either the file reader or streamer, the framework handles passing this data to the analysis modules. Analysis modules are a type of plugin which take data that has been packaged into events by a file reader or streamer plugin and performs some analysis on it. The main action an analysis module must do is create a monitor element (a ROOT TObject) then emit it to the rest of the framework. Before this step an arbitrary amount of processing can be done, e.g. checking validation bits, thresholds, error-checking, and so on. Monitoring the data quality can be done from within analysis modules but this is not recommended as dedicated quality tests (see section above) are available.

For each analysis module that is being run, an XML steering file is required to provide the parameters and networking information to all the processes needed. A single steering file can call only a single analysis or standalone module, but multiple steering files can be run in parallel by the framework.

Examples of using DQM4hep with testbeams both within the AIDA-2020 community and outside of it can be found in Chapters [3](#) and [4](#), respectively.

Chapter 3

AIDA-2020 testbeams

I love fools' experiments.

I am always making them.

Charles Darwin

This chapter discusses the DQM4hep framework, specifically focusing on the deployment, testing, and usage of the framework on testbeams within the AIDA-2020 collaboration [44]. Three testbeams are described in detail, as they are representative of the overall progression of the usage of DQM4hep as a data monitoring tool – the first implementation and deployment, further developments from lessons learnt in the initial usages, and finally a mature tool that has been integrated into the workflow of a testbeam and is familiar to the physicists running the experiment.

For the early testbeams, the detector prototypes being tested are described, along with the data format being used, in order to explain the particular needs of the detector. The results of the testbeam are discussed, in the form of what analysis modules are developed and their uses. In later testbeams, only the elements that changed are discussed, to demonstrate the ongoing refinement of the framework and its expanded use.

The work presented here formed part of several papers, journal articles, and presentations, including presentations at the Beam Telescopes and Testbeam workshop over the years 2016-2018 [40] [41].

3.1 Introduction

One of the most important aspects of testing and developing DQM4hep was to ensure that it was as generic as it was intended to be, and this meant deploying and using the framework on physics testbeams. DQM4hep was originally developed during testbeams

of the Silicon Tungsten Electronic Calorimeter (SiWECAL) [53], and its early testing phases were predominantly based on this detector. However, in trying to develop it as a generic monitor, and to satisfy the requirements of a generic data monitoring and quality monitoring tool for AIDA-2020, it was essential that it was tested on other detectors of different types to demonstrate its generic nature.

The CALICE-AHCAL prototype

The Analogue Hadronic Calorimeter (or CALICE-AHCAL) is a sampling calorimeter formed of steel absorber plates and plastic scintillator tiles, read out by silicon photomultipliers (SiPMs) as active material [54]. One of the important features of the AHCAL is that the prototypes were designed using techniques suitable for mass production, such as injection-moulding and automated foil-wrapping of the scintillator tiles, and pick-and-place assembly of the layers and their electronics. It also uses power pulsing – rapidly cycling power so that the electronics are active only when the beam is present, according to a known beam structure (see Table 1.3). This helps to reduce power consumption and heat production, making cooling the layers easier. Some assembled layers of the AHCAL prototype can be seen in Fig. 3.1.



Figure 3.1: Two varieties of AHCAL layers.

CALICE testbeams

The CALICE testbeams were done with the *Forschung mit Lepton Collidern* (FLC)¹ group based at DESY in Hamburg, working on the AHCAL prototype. Regular testbeams were held at the DESY II synchrotron at DESY in Hamburg, Germany and at the Super Proton Synchrotron (SPS) at CERN in Geneva, Switzerland. The goals for these testbeams varied over time but common focuses for the hardware were power-pulsing tests, and commissioning and calibration of new detector boards to test variations and changes to

¹EN: Research with Lepton Colliders

the manufacturing process. The testbeams were often used as testbeds for data acquisition electronics and software, such as the EUDAQ data acquisition software, the AIDA-2020 Beam Interface (BIF), and DQM4hep.

DQM4hep was used as an online monitoring and data quality monitoring tool for AHCAL testbeams beginning in May 2016, and in further testbeams between 2016 and 2018. The majority of these testbeams occurred at the DESY II facility, but two took place at the CERN SPS in May 2017 and June 2018.

3.2 The beamline facilities

3.2.1 DESY II

Testbeams at DESY utilise the DESY II synchrotron to generate particle beams for testing. These particle beams are electron/positron beams generated via bremsstrahlung. A carbon fibre target within the path of the electrons in the synchrotron itself generates bremsstrahlung photons, which then strike a secondary metal target to produce electron/- positron pairs. These electrons and positrons are spread out into a fan shape using a dipole magnet, and a set of collimators select a portion of this beam to be used for the testbeam. These electron/positron beams have an energy range of 1-6 GeV [55].

3.2.2 CERN-SPS

The Super Proton Synchrotron (SPS) at CERN provides two areas for testbeams and irradiation testing – the North Area and the East Area. The testbeam described in this chapter took place in the North Area of the SPS.

The primary beam available at the North Area is a 450 GeV proton beam, extracted from the SPS. This primary beam can then be converted into secondary or tertiary beams via the use of targets placed in the beampipe. With these options, the SPS can generate beams of electrons, muons, pions, or hadrons [56] [57].

The SPS is also used for filling of the Large Hadron Collider during operation, so the number of spills per second is dependent upon whether the LHC is being filled.

3.3 May 2016 testbeam at DESY II

The first deployment of DQM4hep on an AHCAL testbeam was at DESY II during May 2016. The testbeam was to be two weeks in duration, following a one-week setup and preparation period. Besides testing the deployment and usage of DQM4hep, the goals of

this testbeam where to test MIP calibration of a new AHCAL base unit (HBU), to test the power pulsing feature, and to perform TDC calibrations. In addition to these goals for the AHCAL, a device called a Beam Interface (BIF), another part of the ongoing work of AIDA-2020 Work Package 5, was being tested [58].

Before and during the testbeam, the majority of the development for AHCAL-specific analysis modules was undertaken. Prior to this, DQM4hep had only been used on Si-WECAL beams, and was untested for other detectors.

File reader and streamer plugins for the LCIO data format were already available in a DQM4hep package called `dqm4ilc`². This meant that the plugins necessary for the framework to open, access and serialise the LCIO data format were already available.

3.3.1 Data format

The data for the AHCAL is in the Linear Collider Input/Output (LCIO) format, using an object type called LCGenericObject, which is a generic format for use when the existing data formats are not suitable. It comprises two parts: the block of data itself, held in 14-bit numbers; and a header containing user-defined parameters, in this case a timestamp, a typename for the object, and a description of the data contained in the object.

The structure of a single event in LCGenericObject format can be seen below, which is the result of using the `dumpEvent` tool to dump the contents of an LCIO event to the command line:

```
----- print out of LCGenericObject collection -----  
  
flag: 0x0  
parameter DAQquality [int]: 1,  
parameter DataDescription [string]: i:CycleNr:i:BunchXID;i:EvtNr;i:  
    ChipID;i:NChannels:i:TDC14bit[NC];i:ADC14bit[NC],  
parameter Timestamp [string]: Tue, 09 Feb 2016 18:20:43 +0100,  
parameter TypeName [string]: CaliceObject,  
  
[ id ] i:Type,i:EventCnt,i:TS_Low,i:TS_High - isFixedSize: false  
-----  
[00000004] i:0; i:15; i:15; i:0; i:36; i:12423; i:12422; i:12421;  
    i:12420; i:12419; i:12418; i:12417; i:12416; i:12415; i:12414;
```

²This package is now deprecated.

```
i:12413; i:12412; i:12411; i:12410; i:12409; i:12408; i:12407;
i:12406; i:12405; i:12404; i:12403; i:12402; i:12401; i:12400;
i:12399; i:12398; i:12397; i:12396; i:12395; i:12394; i:12393;
i:12392; i:12391; i:12390; i:12389; i:12388; i:12459; i:12458;
i:12457; i:12456; i:12455; i:12454; i:12453; i:12452; i:12451;
i:12450; i:12449; i:12448; i:12447; i:12446; i:12445; i:12444;
i:12443; i:12442; i:12441; i:12440; i:12439; i:12438; i:12437;
i:12436; i:12435; i:12434; i:12433; i:12432; i:12431; i:12430;
i:12429; i:12428; i:12427; i:12426; i:12425; i:12424;
```

In this case, the `TDC14bit[NC]` and `ADC14bit[NC]` are arrays, each holding a number of elements equal to the `NChannels` variable, in this case 36. Each element of these arrays corresponds to a single physical scintillator tile within the detector, and identifies which chip it belongs to using `ChipID`. The `ADC14bit` and `TDC14bit` arrays contain binary data, which is represented above converted directly to decimal. An additional conversion from this format to specific information such as validation bits, hit bits, etc. was also needed.

3.3.2 Results

Over the course of the preparation week, the foundations were laid for the analysis module. This involved gaining a familiarity with the data structure, loading data from previous testbeams into DQM4hep offline, and attempting to read it in basic ways. The first module was not ready for the beginning of the testbeam proper, but a few days afterward plots were being produced in DQM4hep from “nearly-online” testbeam data.

The first analysis module developed was the `AHCALRawModule`. The majority of the processing in this module was decoding of the data from the binary format and extracting the information from it. After this, validation bits and hit bits in the data were checked to classify data as ‘good’ or ‘bad’ hits. Then the actual ADCs and TDCs were filled into their respective histograms.

The first module acted as a proof-of-concept, and once this was done further work started on creating more modules with a wider variety of features and plots to provide better coverage for online monitoring. Two separate modules were created and refined during this testbeam – `AHCALRawModuleChannel` and `AHCALRawModuleGlobal`.

The channel module created a per-spectrum channel of all ADCs, integrated over the whole run. It was able to load a number of individual channels, though due to the



Figure 3.2: The T22 beam area at the DESY II synchrotron, looking towards the beam aperture.

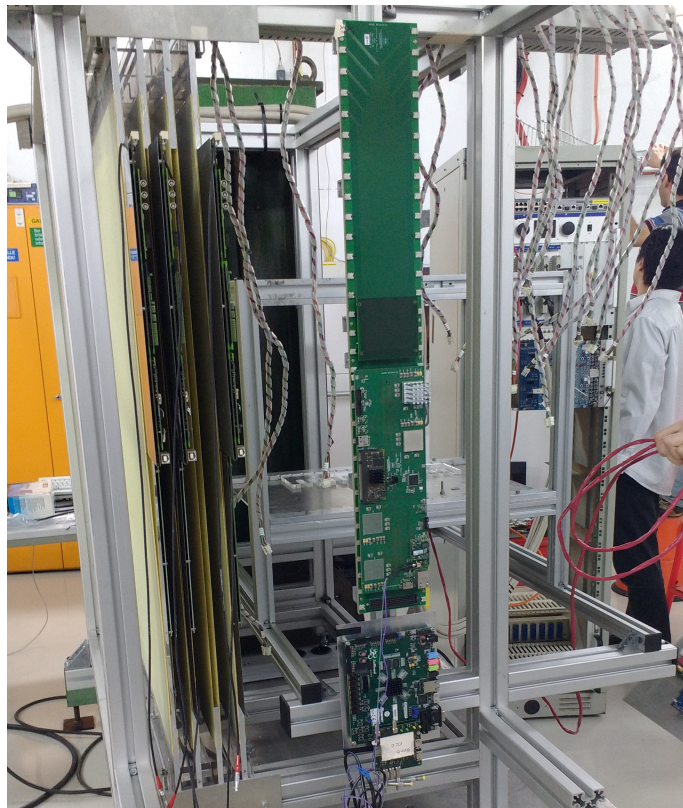


Figure 3.3: Close-up of the layers and electronics assembled in the support structure in the beam area. During operation, the detectors were covered with black fabric to block ambient light from impinging upon the SiPMs.

memory requirement, it could not track all channels simultaneously. To work around this, we implemented a facility for the module to read which channels to monitor from the XML steering file, so that these could be defined at runtime. An example of some of the per-channel spectra created using this module can be seen in Fig. 3.4

The global module produced a 2D histogram containing cells for each channel, coloured for the ADC in that channel. This didn't produce a heatmap as the geometry information was not available in this plot, but did allow easy identification of dead channels and channels that were in the beamspot. An example of this can be seen in Fig. 3.5.

Overall, once the monitoring had been set up and initial bugs and problems fixed, it became a routine tool of the testbeam. This was made easier by the usage of XML steering files for the monitoring interface canvases, allowing groups of plots and histograms to be automatically opened when the monitoring interface was started. This meant that with little effort, all information necessary for monitoring was easily available.

An example of the monitoring interface in use can be seen in Fig. 3.6.

3.4 July 2016 testbeam at DESY II

The next usage of DQM4hep was a testbeam during July 2016, also at the DESY II facility. The testbeam was to be one week long, with a one-week preparation period. The primary goal for DQM4hep in this testbeam was to establish heatmaps of the calorimeter. This would give a visual representation of the layers, allowing identification of the beamspot, allowing dead or miscalibrated channels to be identified visually.

Creating a heatmap for the AHCAL was nontrivial, as the information coming from the data acquisition device and stored in LCIO format did not encode location, as repeating this information for every channel for every event would increase the size of the data, and this information can be stored once in a map or configuration database. Each channel was instead identified by its “electronics number” – a combination of the ChipID of the board the channel was located on, and the number of the channel on that board.

Each layer was formed of four boards (each one with a ChipID), each of which contained sixteen layers. The orientation of the boards, which boards were in a layer, and the order of the layers in the stack were all changeable, so an additional requirement for the heatmap function was that it could take an external geometry file that could be changed or automatically generated.

DQM4hep has internal functions for parsing XML data, so an XML file was chosen as the format to store the geometry data. By making this an XML file, it avoided hard-

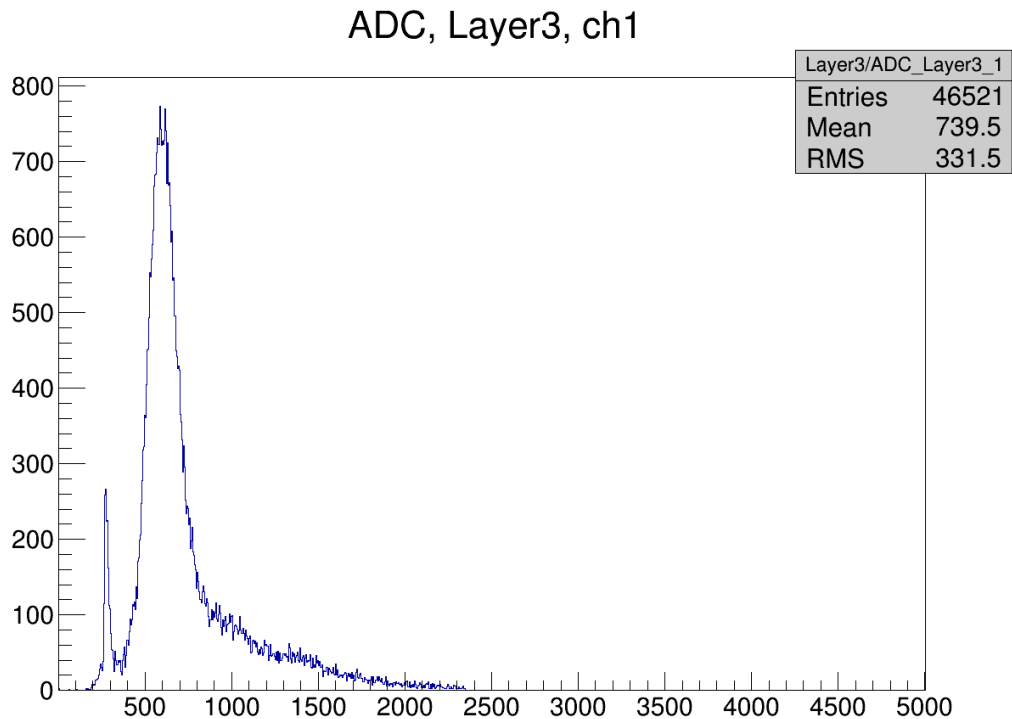


Figure 3.4: Histogram produced by `AHCALRawModuleChannel` showing an ADC spectrum of a single channel for one run. The pedestal can be seen at approximately 300 and the MIP peak at around 650.

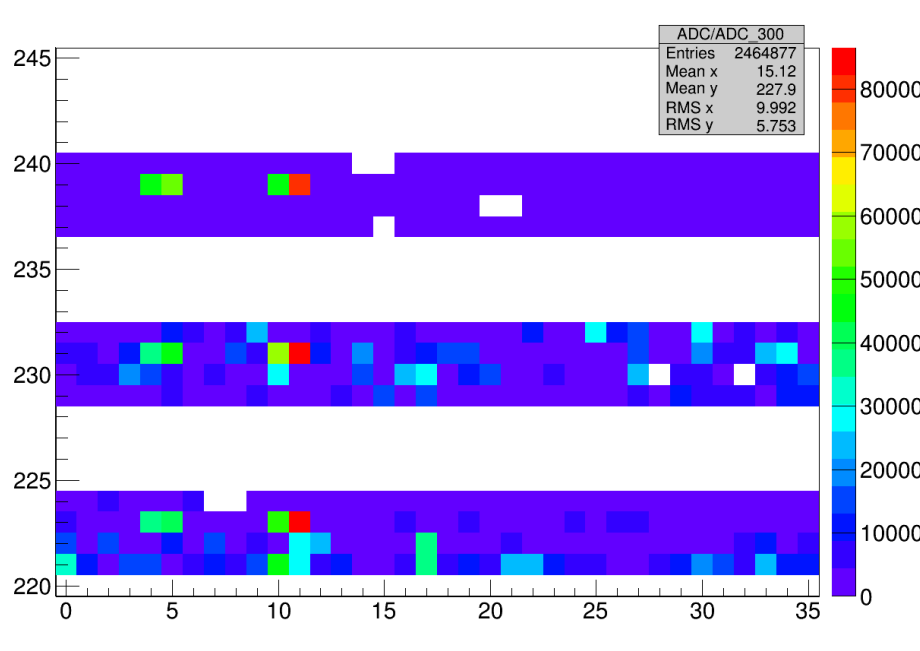


Figure 3.5: Histogram produced by `AHCALRawModuleGlobal` showing all ADCs exceeding 300 over a single run. Dead or nonresponsive channels are seen as white squares. The horizontal gaps are due to the fact that some ChipIDs were not present.

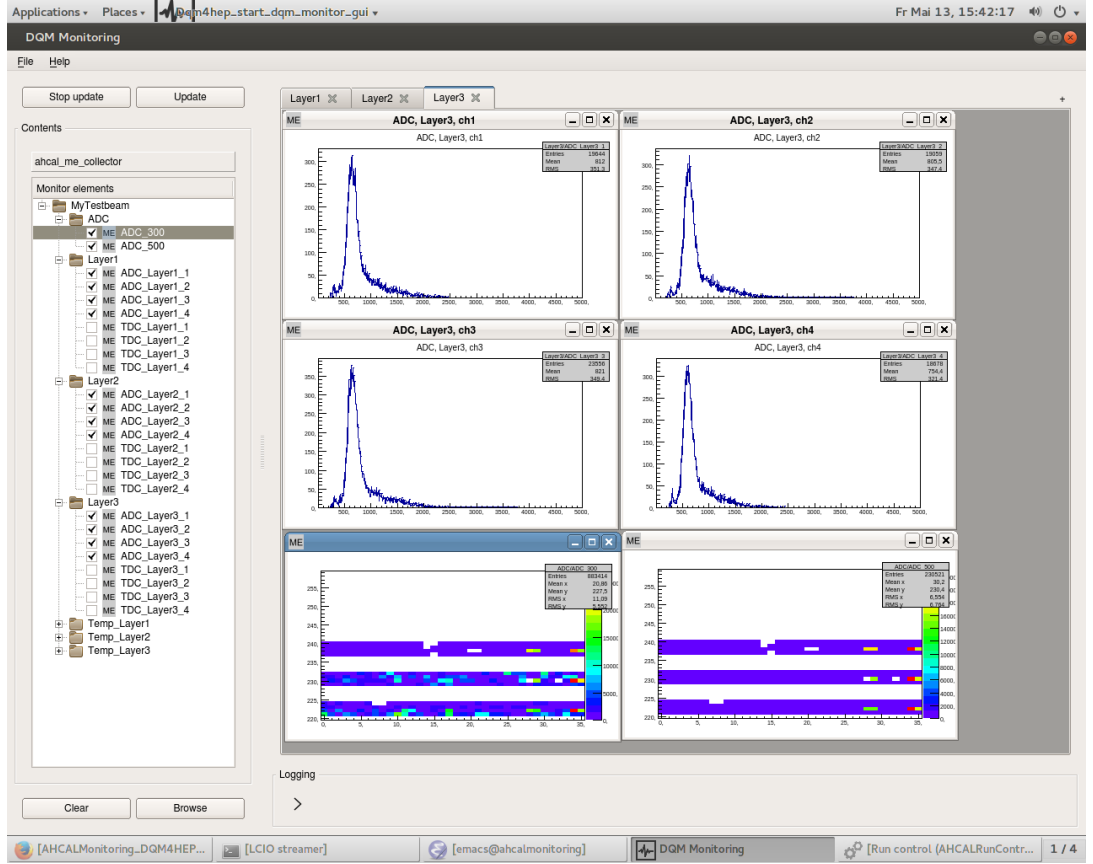


Figure 3.6: A full screencapture from the May 2016 testbeam showing the monitoring interface in use during power pulsing tests, displaying a MIP scan. The top four histograms are spectra of individual channels in the calorimeter, while the bottom two are primitive “hitmaps”, similar to Fig. 3.5.

coding the geometry into the framework itself, allowing the geometry data to be changed at runtime. XML also has the benefit of being human-readable. The AH CAL team already used an internal format for the geometry file for offline processing after testbeams, which was constructed and converted into different formats via a shell script, so this could be replicated for the DQM4hep XML file.

For analysis modules needing geometry, the XML file was given as a required parameter for the steering file, which then built a C++ map of the correspondence between electronics number and (i, j, k) co-ordinates of each channel in memory during initialisation. Then a function called `electronicsToIJK` was written that took the electronics number as the argument and returned the position of the channel in geometric co-ordinates. A further function was written, called `IJKToElectronics`, that performed the opposite operation, but this was not used.

Using these new functions, another analysis module called `AHCALHitmap` was written

that created a two dimensional histogram, with each bin representing a channel on the x and y axes for a single layer. This histogram was then filled with the ADCs of that channel for the whole event, producing a heatmap.

The analysis modules for creating heatmaps were prepared ahead of the testbeam, and used extensively. They were used to identify channels that were dead or nonresponsive, as well as to confirm already-known nonresponsive channels.

3.5 May 2017 testbeam at CERN SPS

During May 2017, testbeam time at the CERN Super Proton Synchrotron (SPS) facility was used for further tests for the AHCAL. One of the goals for this testbeam was to evaluate the performance of the power pulsing feature in magnetic fields up to 1.5 T. The process of manufacturing the detector layers and boards was being automated, and a larger number of layers were available for this testbeam, so it also presented a way to test using a larger number of channels than before.

Part of the programme for the testbeam was to use the electron and muon beams available at the SPS for calibrating the newly-produced layers, as well as doing an energy scan with a pion beam.

The monitoring with DQM4hep in this testbeam included analysis modules that monitored the individual channels of all 40 large layers, as well as producing heatmaps of several types, such as unweighted, ADC-weighted, and near-pedestal. Standalone modules monitoring the temperature of the detector hardware were also used.

At this point in the testbeam process, the online monitoring system with DQM4hep had matured, partially due to the data format of the detector having been fixed for some time. Experience with running, using, and modifying the analysis modules had been disseminated throughout the team, and team members wrote their own analysis modules for producing plots.

Because of this, during the testbeam DQM4hep was used as intended – as a tool for shifters to use to diagnose and troubleshoot problems with the beams or detectors. A specific expert on DQM4hep was not necessary, as enough people operating the testbeam understood DQM4hep to be able to modify analysis modules on the fly according to their needs.

For example, when a beam telescope was in use, DQM4hep modules were developed to produce correlation plots, determining whether hits in the AHCAL corresponded to hits in the telescope, allowing quicker debugging of the detectors. See Fig. 3.13.

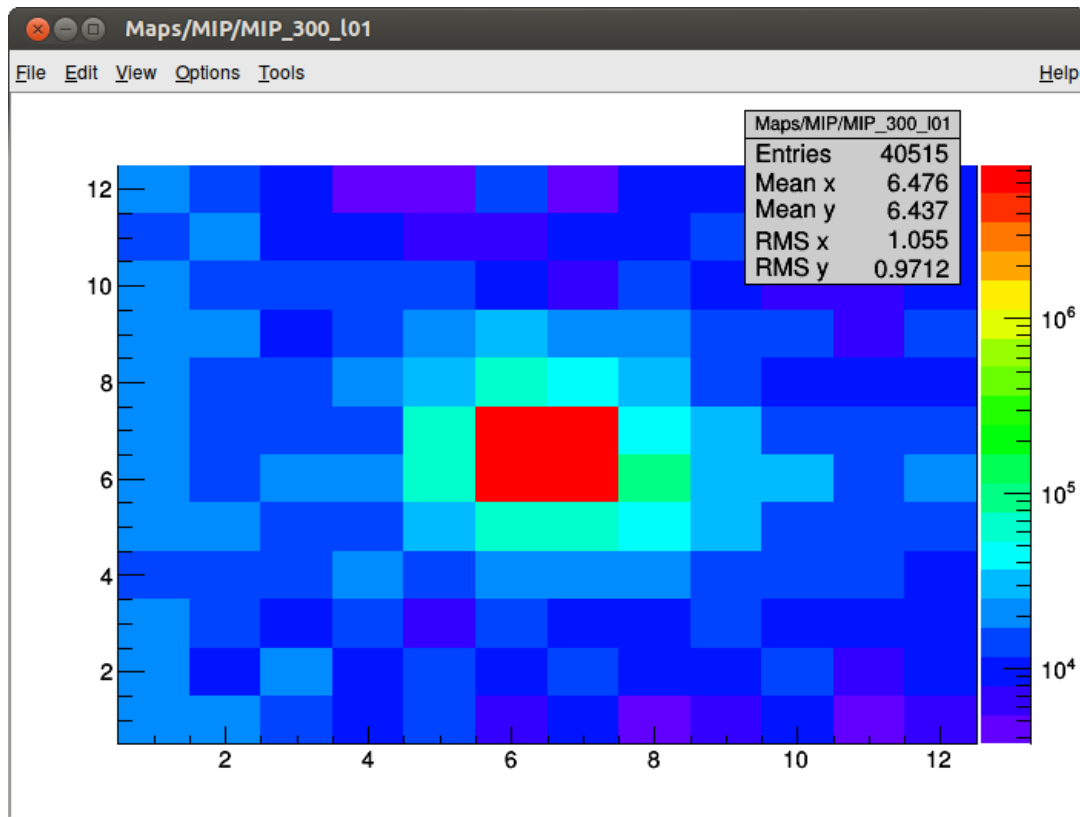


Figure 3.7: A heatmap for a single layer during the July 2016 testbeam, showing all channels with ADCs higher than 300. The beamspot is clearly visible in the centre.

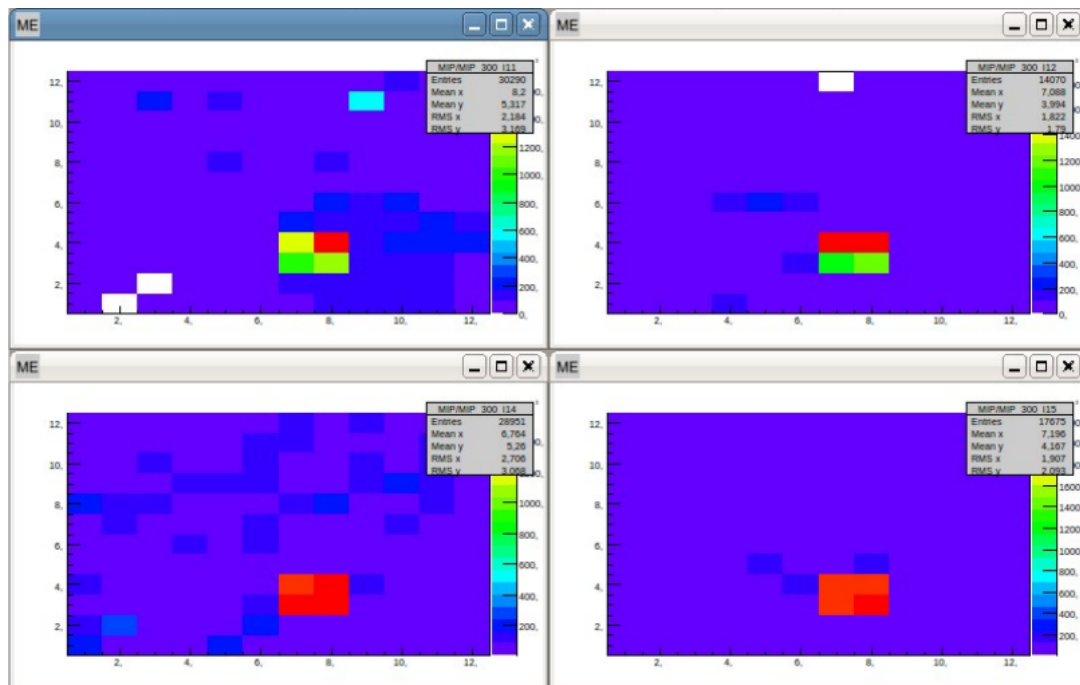


Figure 3.8: A collection of heatmaps for four layers in the stack during the July 2016 testbeam. The beamspot is visible, as are several dead or unresponsive channels in the top-left and top-right heatmaps.



Figure 3.9: The CALICE-AHCAL being unloaded during installation at the CERN SPS during the May 2017 testbeam.



Figure 3.10: The CALICE-AHCAL being moved into position by the cranes in the CERN SPS testbeam area.



Figure 3.11: An overview of the beam hall at the CERN SPS, with the solenoid the CALICE-AHCAL was placed within visible in the centre-right of frame.

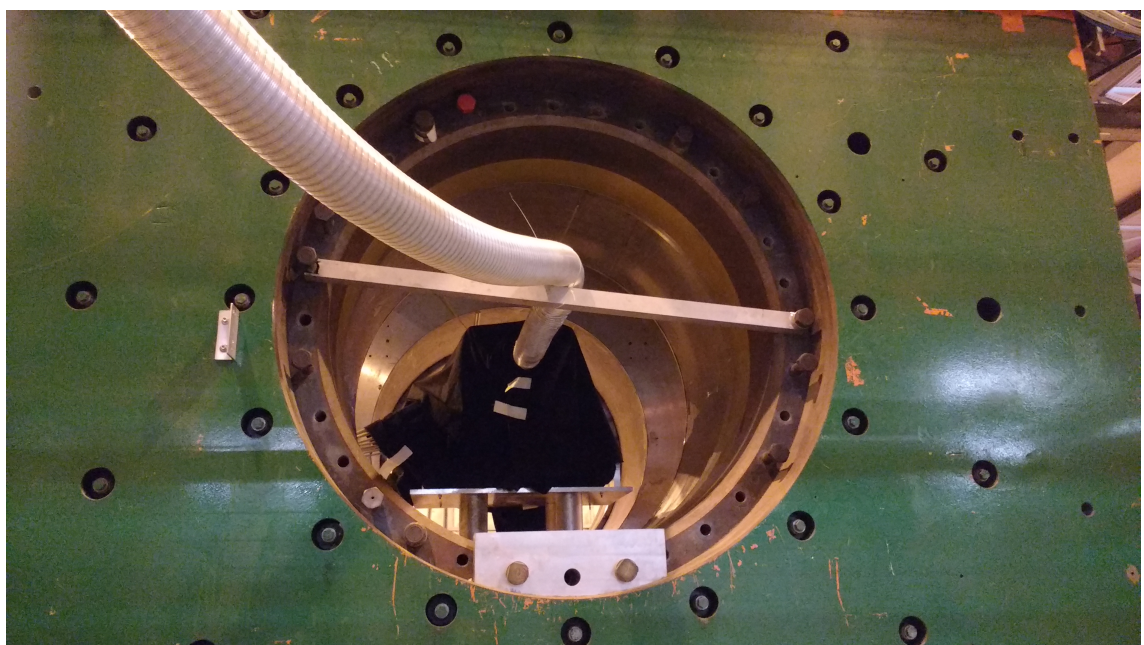


Figure 3.12: The CALICE-AHCAL placed inside the solenoid, covered with black fabric to block ambient light from the SiPMs.

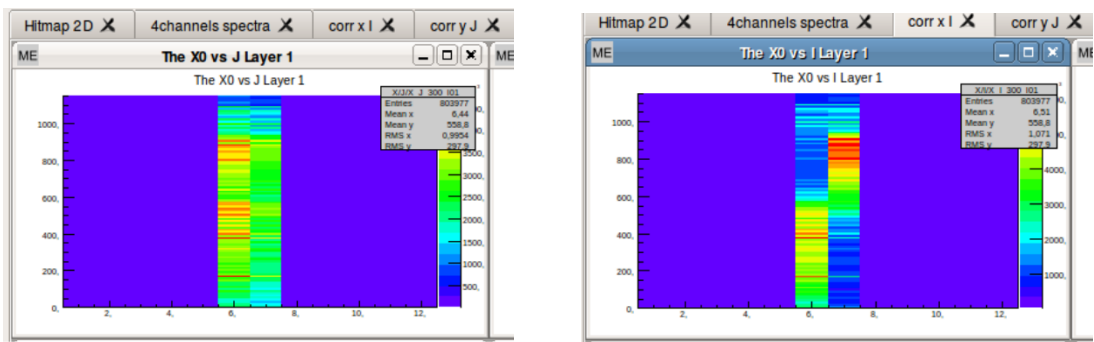


Figure 3.13: Correlation plots showing the correlation between hits in the AHCAL and the beam telescope. Left is an uncorrelated hit, right is a correlated hit.

Chapter 4

IDEA testbeam

Ideas won't keep. Something
must be done about them.

Alfred North Whitehead

In this chapter, the usage of DQM4hep outside of the AIDA-2020 collaboration is discussed. This testbeam was the Innovative Detector for Electron-positron Accelerators (IDEA) combined testbeam. This was a complex testbeam environment, using five separate detector prototypes on the same testbeam, operating as a ‘vertical slice’ of the detector concept for a future lepton collider.

The IDEA testbeam environment and the detectors present are described. Following this, the development of the file readers for all of the datatypes used by the data acquisition systems is described, paying attention to the different needs of the different types of files. Then the development of the analysis modules that took the read raw data and converted it into monitor elements and human-readable plots is discussed. For this testbeam, the aim was first to recreate the existing monitoring solutions, but using the simpler and more systemic approach of DQM4hep to combine them all on one machine and in one program.

Following this, later work in using DQM4hep’s analysis modules as a form of online data processing is described. Again, the usage of this aimed to recreate existing offline analysis that was done using ROOT. This was shown to be possible, and to be computationally lightweight enough to be done online during a testbeam.

4.1 Introduction

While DQM4hep was intended from the beginning as a generic tool, it was developed largely within the AIDA-2020 collaboration, which also promoted a variety of standards

and guidelines for data acquisition devices, data formats, etc. In addition to this, it was also only tested on calorimeter-type detectors within the CALICE collaboration. To be sure that DQM4hep was truly generic – capable of adapting to *any* detector – it was necessary to test it on a wider variety of detectors outside of the AIDA-2020 and CALICE collaborations.

An ideal opportunity arose for this in the form of the IDEA testbeam. The IDEA concept is a proposal for a detector for future lepton colliders such as the FCC-ee or CEPC, using a combination of a silicon vertex detector, large volume drift wire chamber with silicon micro-strips for tracking, a dual-readout calorimeter, and muon chambers. All of these subdetectors are contained within a low-mass superconducting solenoid and an iron flux return yoke. See Fig. 4.1.

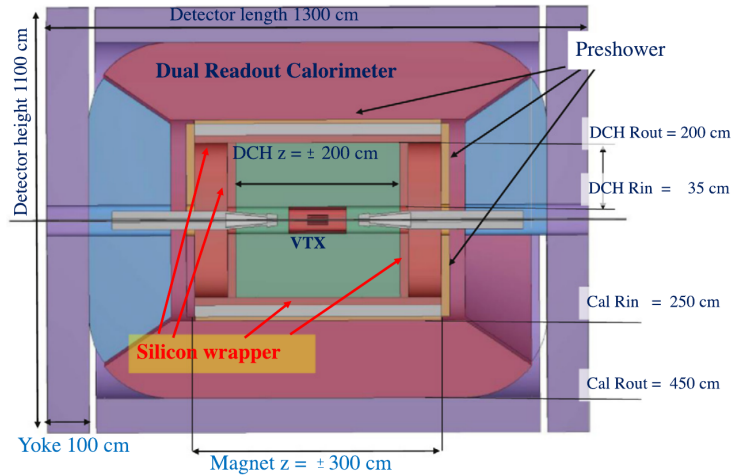


Figure 4.1: Schematic layout of the proposed IDEA detector concept.

The IDEA testbeam was to take place in the H8 beamline area at the CERN SPS, including five separate prototypes, each representative of one subdetector of the IDEA detector concept. This testbeam formed a ‘vertical slice’ of the detector, operating each of the components in one testbeam to test not only each individual component, but how they interacted and could be used together to generate richer information about the beam.

DQM4hep was offered as a possible unified monitoring solution that could integrate information from all of the detectors into a single tool. This provided convenience for the teams operating the testbeam and detectors, and an extremely valuable opportunity to test DQM4hep out of its established operating range, using a wide variety of different detectors. The testbeam took place from the 5th-12th September, with a preparation period of one week before this for installation, setup and calibration.



Figure 4.2: Schematic of the position of the different detectors in the IDEA combined testbeam.



Figure 4.3: Photograph of the testbeam area, looking east across the North Area of the CERN SPS facility.

4.2 Detector components

4.2.1 RD52 dual-readout calorimeter

The Dual Readout Method (DREAM) calorimeter, also called the RD52 calorimeter, is a dual-readout calorimeter built, developed and tested by the RD52 collaboration by researchers based in universities at Gagliari, Cosenza, Pavia, Pisa, Rome, Iowa State and Texas Tech.

The aim of the calorimeter is to use both the Čerenkov and scintillator techniques simultaneously (hence “dual-readout”) to improve calorimetry, especially using calorimeters to measure four-vectors of jets and single hadrons, which suffer a reduced precision compared to electrons and photons. By comparing signals from Čerenkov light and scintillator light, the electromagnetic shower fraction can be measured on an event-by-event basis, eliminating the effects of fluctuations. Unlike many other detectors for future lepton colliders, the DREAM calorimeter is not based around the design requirements of particle flow algorithms.

The prototype of the calorimeter used in the testbeam consists of 9 lead modules, each $9.3 \times 9.3 \times 250 \text{ cm}^3$ in size, with a sampling fraction of 9% and using a photomultiplier tube readout. From simulation studies, the hadronic energy resolution is expected to be approximately $30\%/\sqrt{E}$ [59] [60].

4.2.2 Preshower

The preshower uses two triple-GEM detectors with a surface area of $10 \times 10 \text{ cm}^2$, using a strip readout with a $650 \mu\text{m}$ pitch. The preshower also has a lead absorber layer of variable thickness, using a fixed layer of 5 mm plus additional interchangeable layers. The layers allow the absorber thickness to be varied between 1 and $2.5 X_0$. The gas mixture used during the testbeam was Ar/CO₂/CF₄, and the efficiency expected from previous tests was 97%. The spatial resolution is on the order of $100 \mu\text{m}$ [61].

4.2.3 Muon chamber

The muon chamber comprises one triple-GEM detector (similar to the preshower) with an additional two μ -RWELL prototypes of size $10 \times 10 \text{ cm}^2$. The μ -RWELL detectors have a spatial resolution of $40 \mu\text{m}$, and a rate capability of $10 \text{ MHz}/\text{cm}^2$ [62].

4.2.4 Drift chamber

The prototype of the drift chamber used for the testbeam consisted of 12 layers, each with 12 drift cells of size $1 \times 1 \text{ cm}^2$, giving a total of 144 channels. According to a study of a similar detector prototype, this should give it a resolution of 100 μm in the x- and y-plane, and 1 mm in the z-plane [63].

4.2.5 Ancillary detectors

The ancillary detectors are used to provide information about the position of the beam, the leakage of particles and showers from the detector volumes, and particle identification. They consist of two Delay Wire Chambers (DWC) in front of and behind the drift chamber; leakage counters surrounding the calorimeter; and a preshower detector and muon counter.

4.3 Monitoring

Existing monitoring within the collaboration was capable of producing histograms from the raw file formats, predominantly using C++ code directly to produce ROOT objects. Initially, the goal of the testbeam was to make the same plots used for the existing monitoring systems within DQM4hep. The advantage of this would be that all of the plots were available in one place, making investigating any correlations between them easier.

The necessary components within DQM4hep for monitoring were the creation of file readers for each device to make the data available to DQM4hep, and analysis modules to use this data to create monitor elements.

4.3.1 File readers

Writing file readers for the different detectors meant first understanding the structure of their data and file types. Once data has arrived from the data acquisition device, each of the detectors wrote to a different ‘raw’ format. However, the RD52 calorimeter, drift chamber, and muon and preshower all produced ROOT ntuple files as part of their data acquisition process, in addition to different file formats. It was decided to use these ROOT ntuples as the file format to read into DQM4hep, as due to support for ROOT within the framework, reading data from ROOT ntuples is simpler.

For each of these three instruments a file reader was developed that walked through the ROOT trees, extracting data from the leaves event-by-event, then converted it to

DQM4hep’s inbuilt `GenericEvent` format. Choosing to make them into `GenericEvents` meant that there was no need to implement an additional event type, simplifying the connection between the file readers and analysis modules. The `GenericEvent` type was also easily suited to the type of data, as the majority of the data were series of numbers, which were easily converted into C++ vectors to store in the `GenericEvent`.

An additional motivation for using the ROOT ntuple as the data source was that some of the file types, notably the drift chamber, had not finalised their data structure at the beginning of the testbeam. Using the higher-level structure provided by a ROOT file would be easier to change in the future than reading in data in a binary, hex, text or CSV format.

For the silicon photomultiplier GEM data, the “raw” data format was a text file, containing an XML header followed by a large amount of data in Comma-Separated Values (CSV). This file could be loaded directly into DQM4hep, the XML header separated and parsed with DQM4hep’s internal XML parsing libraries, and the remaining data parsed. The comma-separated values could be easily parsed using the `dqm4hep::core::tokenize` function, which takes a string, a delimiter, and a vector, and parses the string into values separated by the delimiter, loading them into the vector. This made extracting the GEM data extremely simple, even in this format. It also allowed the parameters in the XML header, which included run numbers and physical information of the detector, to be passed into DQM4hep and the analysis module, using the `core::Run` object type.

4.3.2 Analysis modules

During the course of the testbeam, four analysis modules were developed, one for each detector. To begin with, these were ‘dummy’ modules – analysis modules that receive events then do nothing. Dummy modules like this are required to run file readers offline, but are simple to create as they can be produced from a template with minimal changes.

Once the file reader for the RD52 calorimeter was complete, the dummy analysis module for this detector was then changed into a functional module, `RD52MainModule`, to produce plots from the data. The RD52 was chosen as it was the most data-rich of the detectors in the testbeam, and also contained the ancillary detectors, which allow particle selection efficiencies to be studied.

During the course of the testbeam, the `RD52MainModule` was developed to read in and arrange data from the ROOT ntuples and arrange them into distinct vectors for the ADCs, TDCs, pedestals, and ancillaries. Following this, pedestal subtraction of all ADC

and TDC channels was completed. Then the malfunctioning tiles and electronics that meant data had to be re-routed through other available channels was integrated so that the ADC information in the analysis module represented the full state of the detector was completed.

There was insufficient time at the testbeam to develop more complex monitoring than this, but development continued offline with saved data from the testbeam to continue the proof-of-concept. This will be discussed in more detail in the following section.

4.4 Results

Monitoring within DQM4hep was able to replicate all the existing monitoring solutions, combining the monitoring tools for all four detector systems into one framework, with the exception of the drift chamber whose data type was not set during the testbeam, so file readers could not be implemented in time.

Due to time constraints, more complex monitoring such as online processing was not implemented during the testbeam. However, following the testbeam it was decided that DQM4hep could be used to perform some offline analysis functions in addition to the work at the testbeam, as a further proof of its ability to do this at testbeams. In this case, it performs in a similar role to ROOT, with the exception that it uses the existing analysis module infrastructure rather than scripts written specifically for ROOT, and can be run as soon as data is available for monitoring.

The analysis goals outlined to attempt to implement in DQM4hep were performing the ADC to energy calibration and the tower ADC equalisation.

4.4.1 ADC to energy calibration

An important result for calibrating the RD52 detectors was to calibrate the ADC response of the detector to the actual energy of the incident beam. It was known from prior testbeams that the ADC response of the calorimeter is linear over the regimes used in the beam [64]. Therefore, the calibration from ADC to deposited energy can be extrapolated from a single run. This was done using a calibration run using a 20 GeV electron beam incident on Tower 15, the centre of the calorimeter. The nature of the CERN SPS beamline means that electron beams are extremely pure, meaning that this run presents the most well-defined beam, making it ideal for energy calibration. This also means that particle selection to exclude other particles is not necessary.

To calibrate for energy, the total ADC for each event was found by summing the

individual ADC of each channel in the event after the pedestal subtraction. This produced a spectrum of the total ADC count for all channels (Fig. 4.4).

The data was then fitted with a gaussian using ROOT to determine the mean and standard deviation, and the value of the mean ADC taken to be the ADC value for a 20 GeV event. This means that for a 20 GeV event, the total ADC count will be 296.3 ± 0.9 . The energy of any given ADC can then be found using:

$$E_{GeV} = \frac{E_{ADC}}{14.815} \quad (4.1)$$

where E_{GeV} is the energy in GeV, and E_{ADC} is the energy in terms of ADC.

This can then be checked by examining Run 12512, which is an 80 GeV run using a secondary beam of predominantly pions, with some muons. According to Equation 4.1, an energy of 80 GeV should translate to an ADC of 1185.2. The total ADC histogram for the 80 GeV run can be seen in Fig. 4.5, showing that the mean is 1191, which corresponds to an energy of 80.39 GeV.

4.4.2 Tower ADC calibration

Due to a large number of tasks for setting up the testbeam, performing a calibration of the high voltages of the individual towers was not possible in time, so the calorimeter ADCs were not calibrated to have a uniform response. To account for this, calibration runs were taken, where the beam was incident on each individual tower for the whole run, repeated for each tower in the calorimeter. These runs allow the calibration to be done after the testbeam with the data. The layout of the towers in the calorimeter for the testbeam can be seen in Fig. 4.6.

Two sets of calibration runs were performed. The first set covered Towers 1-29 with an 80 GeV secondary beam (primarily pions with some muons)¹. The second set used a 20 GeV pure electron beam, covering Towers 30-36 plus Tower 15. Tower 15 received runs in both sets in order to calibrate the two sets to each other. The run numbers corresponding to each tower is given in Table 4.2.

The initial approach to calibrate the towers was to make a histogram of the ADCs of the scintillators of all events in the tower under the beamspot, for each of the 29 pion runs (see Fig. 4.7). From these, a gaussian fit is used to determine the mean of each channel, shown in Fig. 4.9. The calibration coefficient is then calculated:

¹Due to the nature of the SPS testbeam facility, the composition of secondary beams is not well-defined. Normally it is determined using detectors in the beamline.

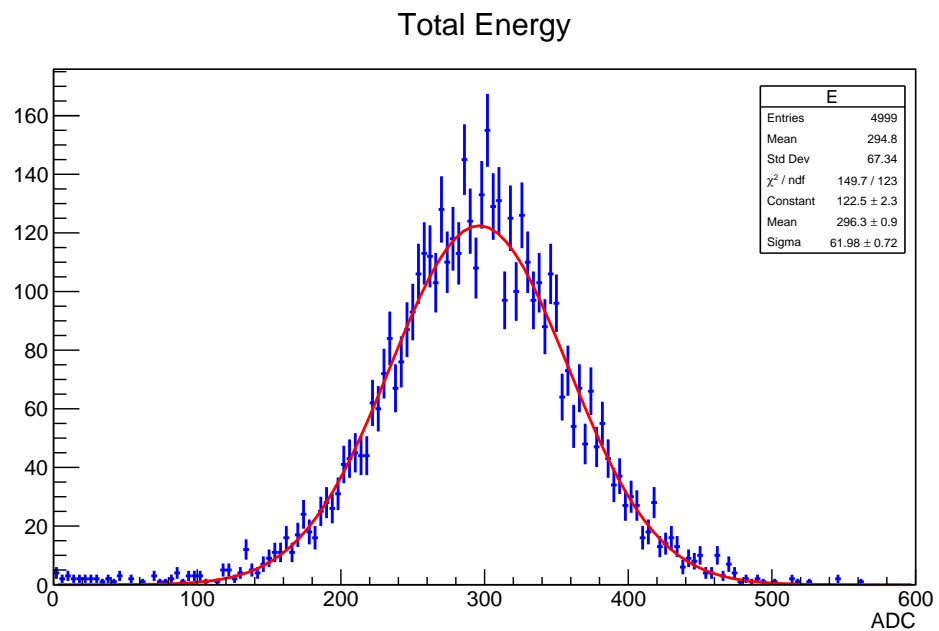


Figure 4.4: Histogram of total ADC in the calorimeter in Run 12659 (20 GeV electrons, Tower 15).

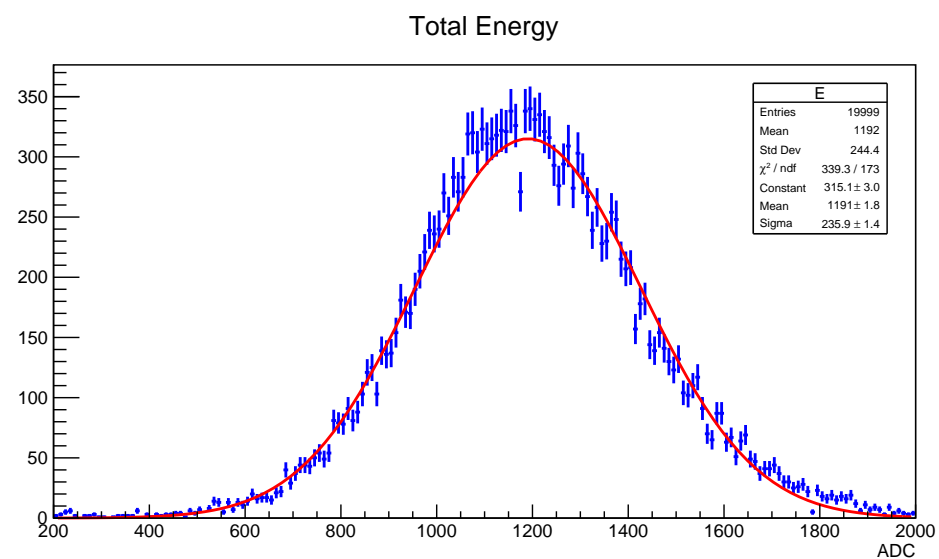


Figure 4.5: Histogram of total ADC in the calorimeter in Run 12512 (80 GeV pions and muons, Tower 15).

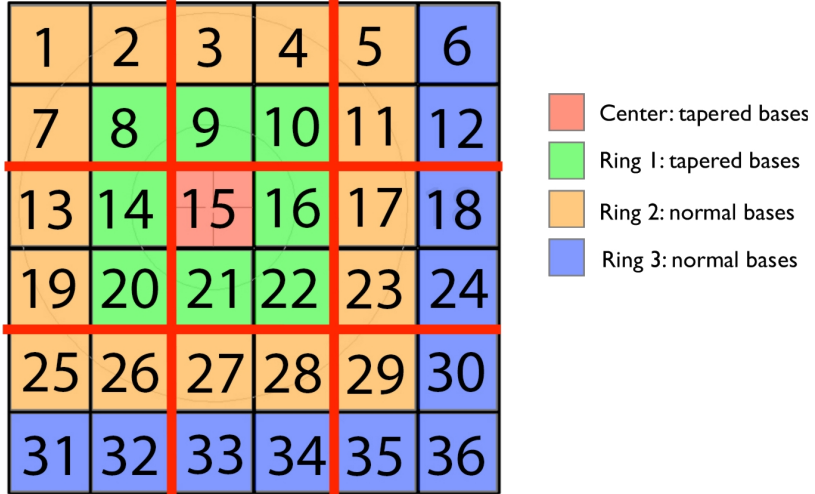


Figure 4.6: The layout of the calorimeter modules (“towers”) in the layers of the RD52 calorimeter used in the IDEA testbeam.

$$C_i = \frac{\mu_{15}}{\mu_i} \quad (4.2)$$

where C_i is the calibration coefficient for the i^{th} tower, μ_{15} is the mean ADC for tower 15, μ_i is the mean ADC of the i^{th} tower. Tower 15 was used as the reference.

The process needed to obtain the calibration coefficients was the use of a bash script that automated the generation of XML steering files for the 29 runs and another bash script that automated the execution of the DQM4hep analysis modules and merging the information into one file.

The analysis module was then re-run, multiplying all ADC values by the calibration coefficient for each tower. The results of the calibration are shown in Figs. 4.8 and 4.10. This did not result in a uniform calibration of all ADCs. This is possibly due to the composition of the beam, as this calibration procedure was done without any particle selection.

Also, discuss how the beam purity can vary within the beam spot and what the beam energy spread is for electrons at 20 GeV vs. the pion beam at 80 GeV.

A pattern of increasing mean ADCs can be seen from Towers 14-19, which repeats in Towers 20-25. These align with the rows on the calorimeter, and this periodic pattern is likely due to some form of leakage or other geometric effect in the calorimeter.

Because particles were not selected, the calibration here does not account for the different ways pions and muons deposit energy in the calorimeter. Pions will produce

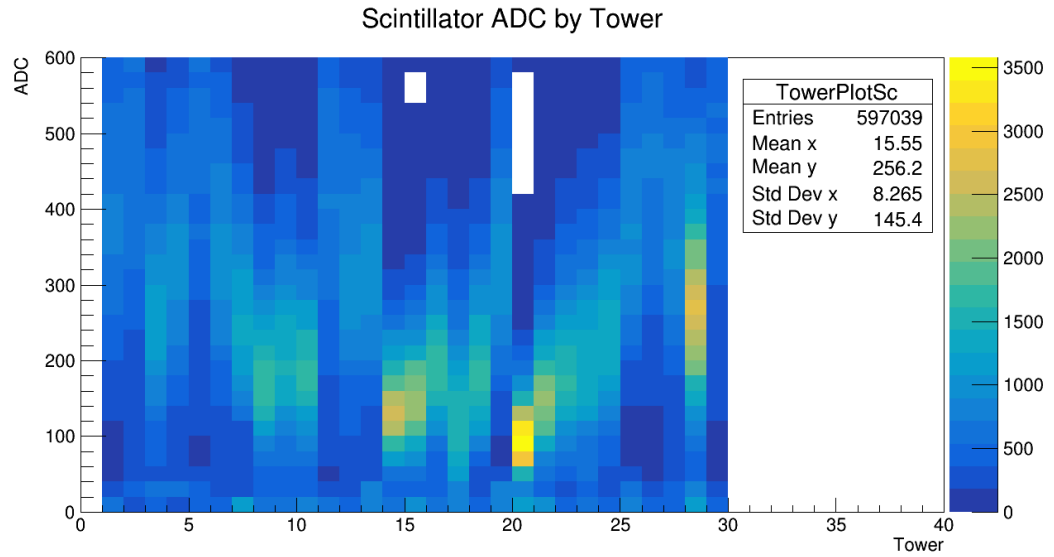


Figure 4.7: Histogram of scintillator ADCs for Towers 1-29 before calibration.

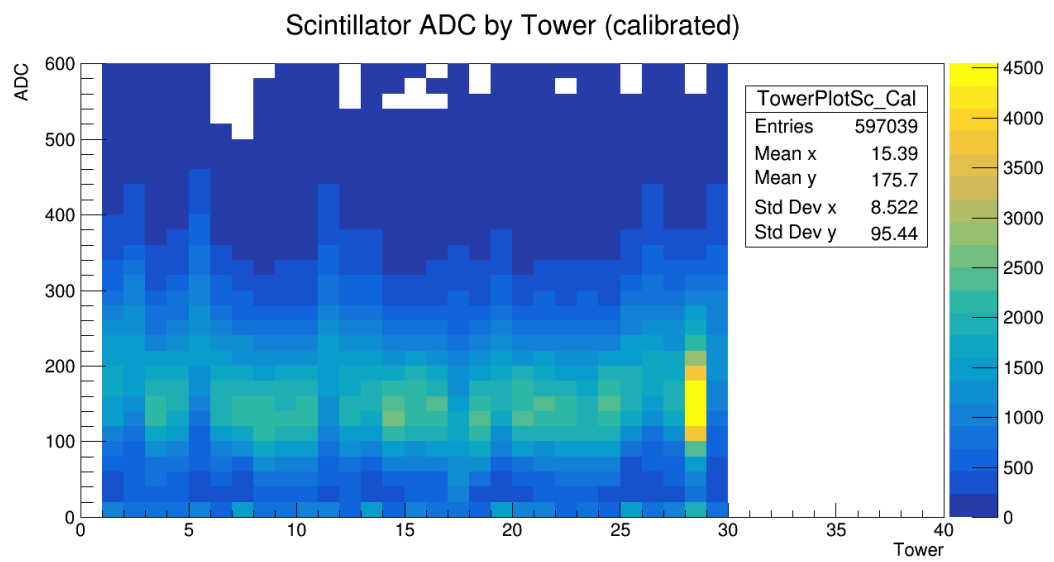


Figure 4.8: Histogram of scintillator ADCs for Towers 1-29 after applying the calibration using all particles.

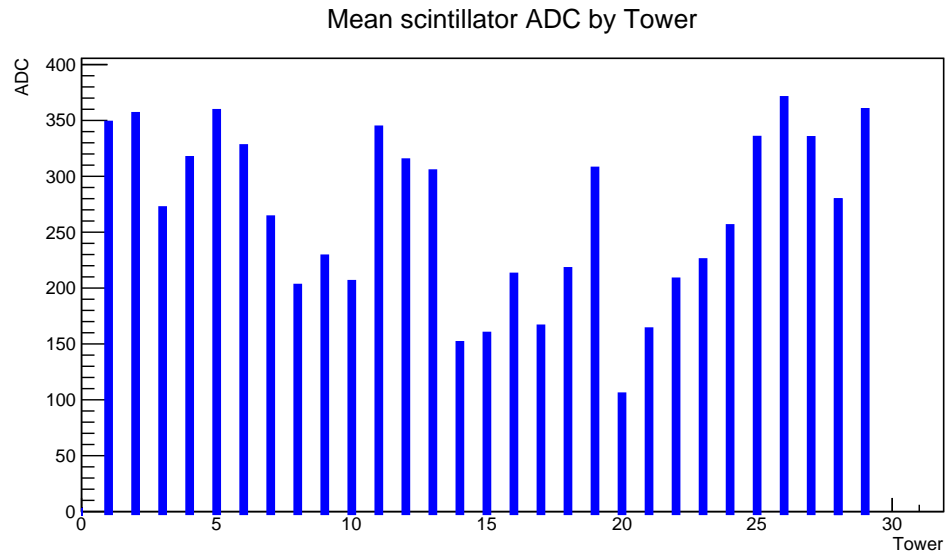


Figure 4.9: Histogram of mean scintillator ADCs for Towers 1-29 before calibration.

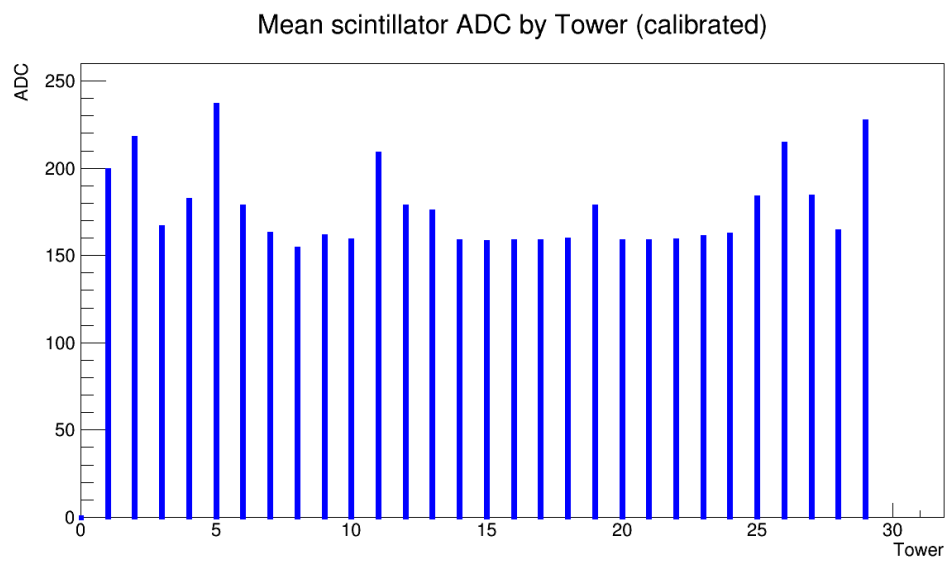


Figure 4.10: Histogram of mean scintillator ADCs for Towers 1-29 after applying the calibration using all particles.

Tower	Run No.	Tower	Run No.
1	12545	16	12526
2	12556	17	12567
3	12558	18	12633
4	12560	19	12591
5	12601	20	12612
6	12638	21	12530
7	12598	22	12528
8	12514	23	12569
9	12518	24	12639
10	12521	25	12610
11	12600	26	12609
12	12636	27	12607
13	12539	28	12604
14	12628	29	12602
15	12512		

Table 4.1: Table of the run numbers and corresponding tower numbers for the calibration runs. All runs are 20,000 events using an 80 GeV secondary beam.

hadronic showers, spreading their energy within a certain radius and depth dependent upon the pion's energy and the nuclear interaction length of the calorimeter. Muons instead act as minimum ionising particles (MIPs), depositing energy along their path through the calorimeter via ionisation losses.

In order to address this, calibration was done twice more, using particle selection criteria determined by another member of the collaboration [65].

Calibration with muons

Given that muons in the calorimeter will leave a MIP-like signal, muons were chosen to be used for calibrating the calorimeter. Muons were selected using two cuts:

- ADC of the muon counter > 10
- ADC of the preshower detector < 20

The same procedure as in Section 4.4.2 was then used, using only muons. The average

ADCs of all towers using muons before calibration can be seen in Fig. 4.11, showing that the response to muons is overall much more uniform across the calorimeter.

The same calibration coefficients were then applied to all particles (Fig. 4.14) and pions only (4.14).

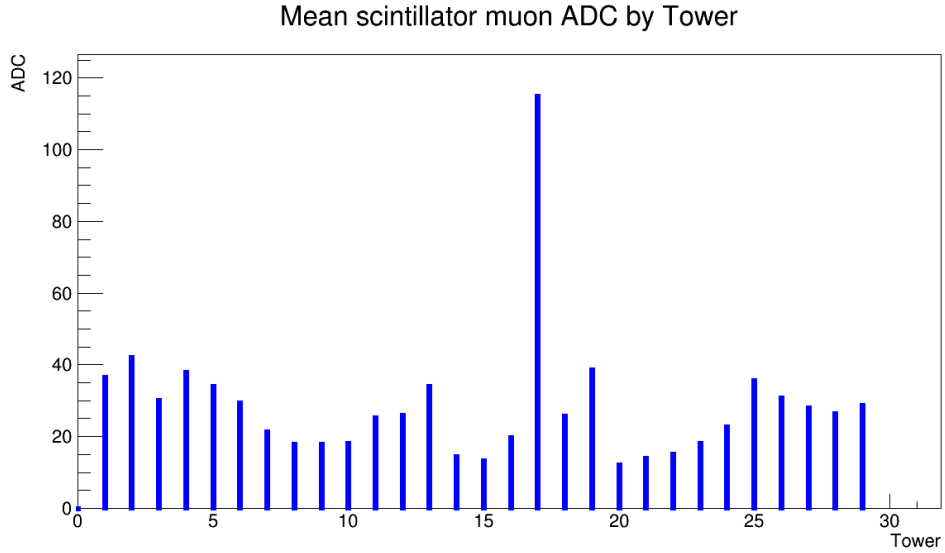


Figure 4.11: Histogram of mean scintillator ADCs for Towers 1-29 using only muons, before calibration.

While the equalisation of pions using the muon response is not as uniform as that for equalising all towers using all particles, it does perform some equalisation, and removes the geometric pattern in the towers. It highlights that Tower 17 appears to have had an unusually high muon response, and as a result of the extremely low equalisation coefficient used to remedy this, produces very low ADC responses in that Tower to other particles. This may be due to a technical fault with that tower, or some geometric effect.

To investigate this further, a section of code was added to the analysis module to create a “heatmap” of ADC means across the detector. The code for creating this was simple, added to the `endOfRun` method of the analysis module:

```

int towerX;
int towerY;
if ((towerNumber % 6) == 0) {
    towerX = 5;
    towerY = -1*(int(towerNumber / 6.0) - 1);
}
else {
    towerX = (towerNumber % 6) - 1;
    towerY = -1*(int(towerNumber / 6.0));
}

```

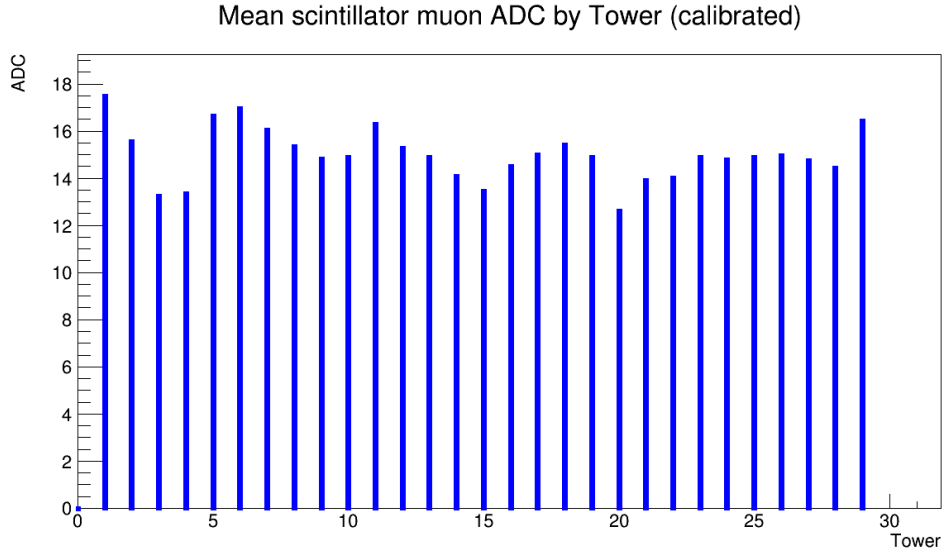


Figure 4.12: Histogram of mean scintillator ADCs for Towers 1-29 using only muons, after applying the calibration using only muons.

```
}
m_pTowerPlotHeatmapMean->objectTo<TH2D>()->Fill(towerX, towerY,
towerMeanSc);
```

The produced histogram can be seen in Fig. 4.16. This histogram shows no clear visual pattern across the detector, instead showing higher mean ADCs on the edges of the detector. While this does not identify the exact cause of this pattern, it does demonstrate that DQM4hep can be used to quickly create *ad hoc* visualisations for irregularities or unexpected behaviours that arise during an experiment, to aid identifying the cause.

The usage of DQM4hep to perform this calibration, similar to that completed by another member of the RD52 collaboration [66] demonstrates that DQM4hep can be used not only for online monitoring and data quality monitoring, but also online or nearly-online analysis of testbeam data.

Tower	C_{all}	C_π
1	0.4551	0.3665
2	0.4450	0.3184
3	0.5842	0.4455
4	0.5008	0.3534
5	0.4417	0.3957
6	0.4845	0.4564
7	0.6026	0.6262
8	0.7617	0.7470
9	0.6953	0.7522
10	0.7729	0.7400
11	0.4607	0.5302
12	0.5040	0.5172
13	0.5203	0.3943
14	1.0561	0.9303
15	1.0000	1.0
16	0.7488	0.6825
17	0.9609	0.1170
18	0.7315	0.5217
19	0.5163	0.3486
20	1.5273	1.1079
21	0.9764	0.9527
22	0.7652	0.8903
23	0.7056	0.7376
24	0.6210	0.5899
25	0.4735	0.3769
26	0.4278	0.4379
27	0.4738	0.4778
28	0.5690	0.5078
29	0.4405	0.4671

Table 4.2: Table of towers in the RD52 calorimeter and their calibration coefficients for all particles (C_{all}) and muons (C_μ).

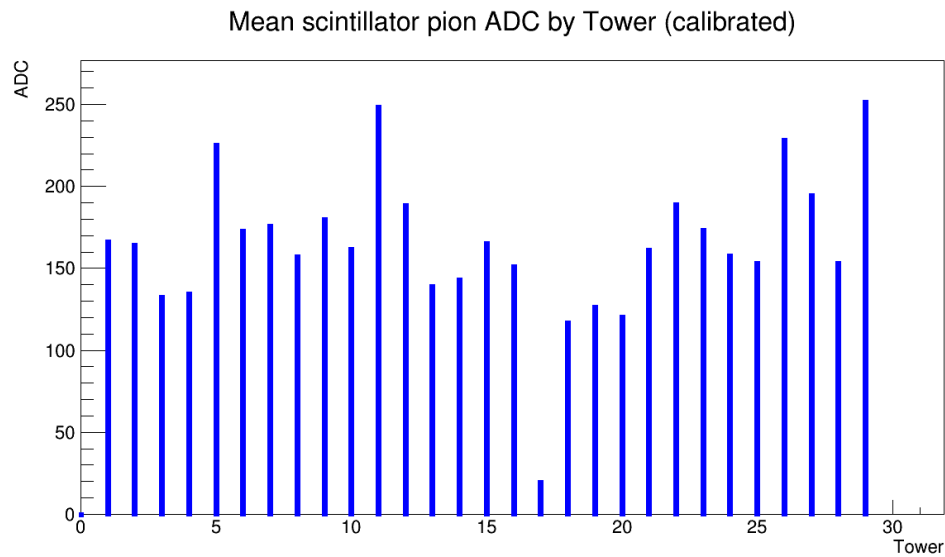


Figure 4.13: Histogram of mean scintillator ADCs for Towers 1-29 using only pions, after applying the calibration using only muons.

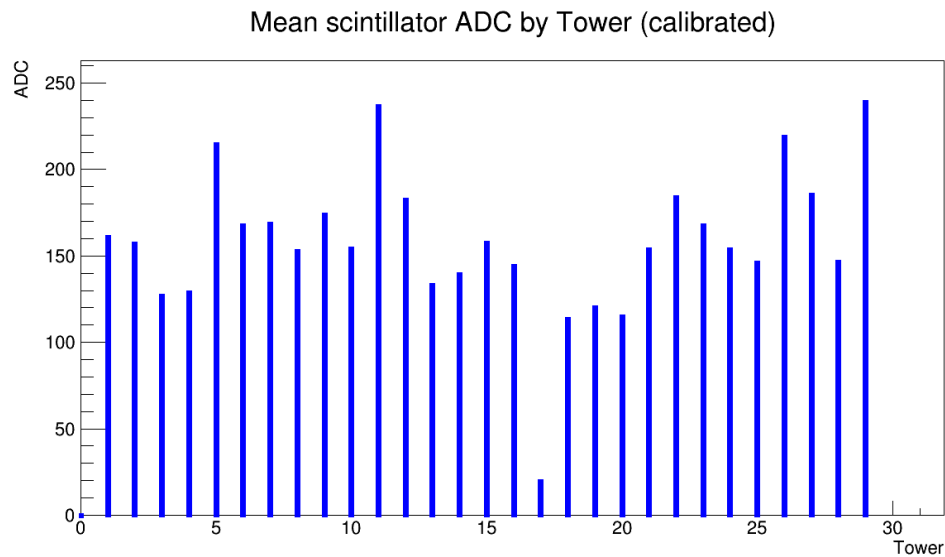


Figure 4.14: Histogram of mean scintillator ADCs for Towers 1-29 using all particles, after applying the calibration using only muons.

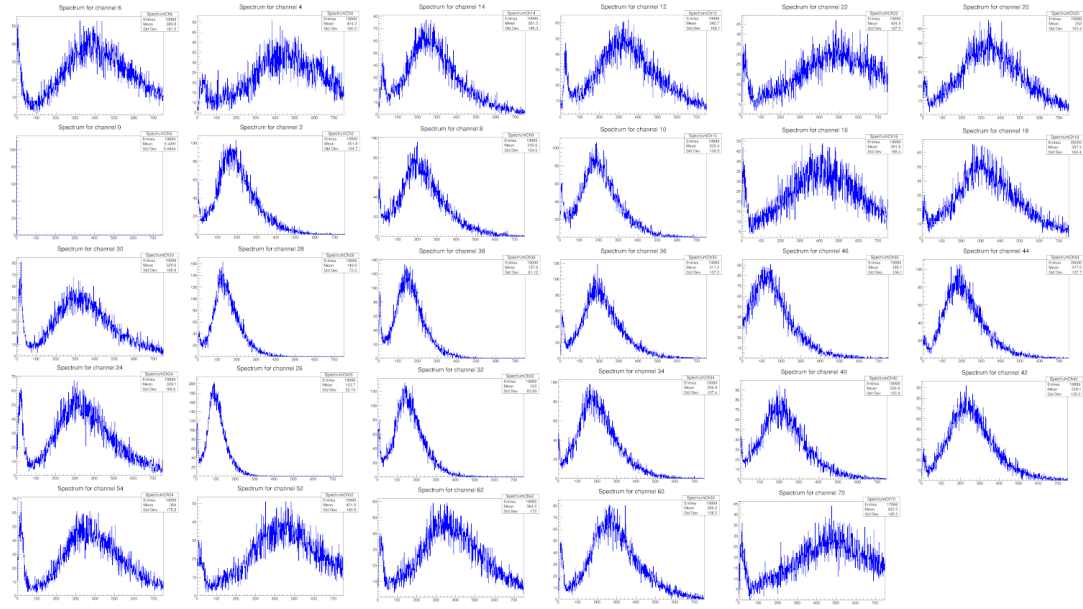


Figure 4.15: Histograms of raw ADCs for each tower, each on the run when the beam was centred in that tower. The empty graph for Tower 7 (channel 0) is due to a hardware failure.

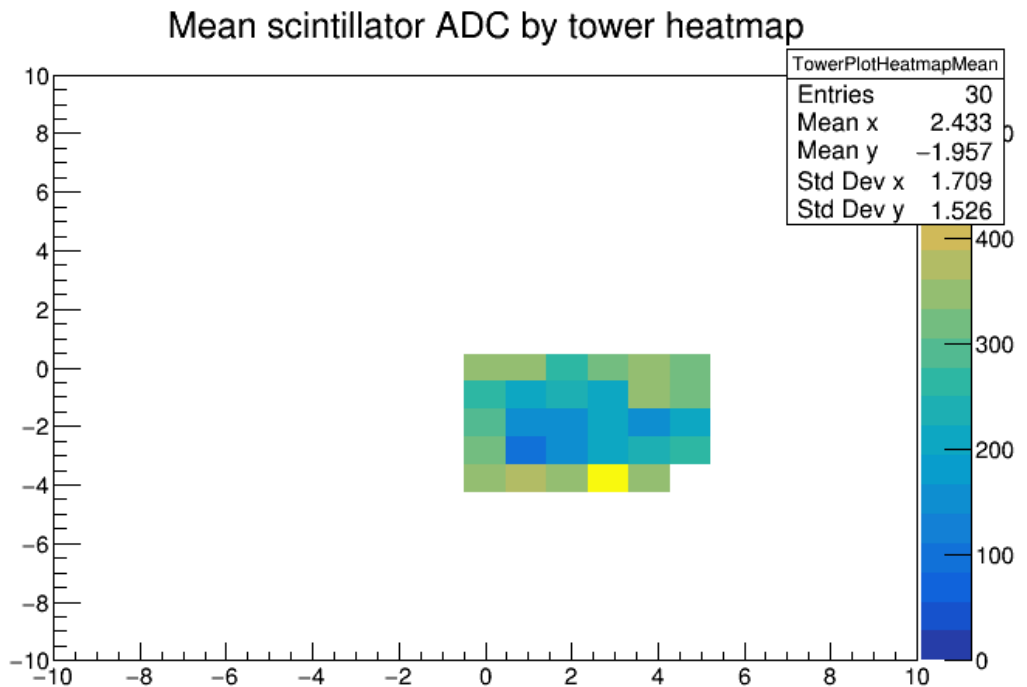


Figure 4.16: Heatmap of the whole detector, with each bin showing the uncalibrated mean ADC for that tower.

Chapter 5

Physics studies for the Compact Linear Collider

Somewhere, something incredible is
waiting to be known.

Carl Sagan

This chapter will discuss the usage of full-scale detector simulations to assess the performance of the proposed CLIC-SiD detector at the Compact Linear Collider machine, during the later stages where centre of mass energies in the tera-scale are possible.

This work was done with the CLIC detector and physics (CLICdp) collaboration to determine the uncertainty on the measurement of the top-Higgs Yukawa coupling in the $e^+e^- \rightarrow t\bar{t}H$ process at a centre of mass energy of $\sqrt{s} = 1.4$ TeV, using the CLIC-SiD detector concept. The analysis as discussed here focuses specifically on the hadronic decay channel, where both top quarks decay to a W boson and bottom quark, and both W bosons decay hadronically. When taken in combination with a similar analysis of the semi-leptonic channel performed by Yixuan Zhang, this allows the expected uncertainty on the top-Higgs Yukawa coupling to be calculated.

This analysis was an update of an earlier study into the sensitivity of the SiD to the top-Higgs Yukawa coupling [67]. The analysis presented here used an updated version of the flavour-tagging software, and a better determination of the contributions of the higgstrahlung diagram.

These results were then contributed to a paper that summarised the top physics potential for CLIC at $\sqrt{s} = 1.4$ TeV, which was submitted to CERN’s European Strategy Update in 2019 [68] [69].

5.1 Introduction

One of the primary goals of all the future lepton colliders discussed in Chapter 1 is to become “Higgs factories” – machines that can produce large numbers of Higgs bosons in a variety of final states, allowing the Higgs sector of the Standard Model to be probed with unprecedented accuracy and coverage.

One of the best ways to examine the Higgs sector is via the production of Higgs bosons in association with top quarks. The coupling between these two particles is the strongest Higgs coupling in the SM, making it one of the easiest ways to examine the properties of the Higgs boson and the Higgs sector. This is the top-Higgs Yukawa coupling y_t . The Standard Model predicts the value of the top-Higgs Yukawa coupling to be:

$$y_t^{SM} = \frac{\sqrt{2m_t}}{v} \quad (5.1)$$

where m_t is the mass of the top quark and v is the vacuum expectation value of the Higgs potential. Many models for new physics predict a deviation from the SM value or new Higgs boson states with different masses, such as two Higgs-doublet models [70], the Minimal Supersymmetric Standard Model (MSSM) [71], composite Higgs [72] and Little Higgs models [73]. Determining the top-Higgs Yukawa coupling will provide an important test of both the Standard Model and a multitude of these new physics models. The various detector models for future lepton colliders will enable this coupling to be measured at the percent level, making this a strong physics motivation for these machines.

The process used for studying the top-Higgs Yukawa coupling is the $e^+e^- \rightarrow t\bar{t}H$ process, also referred to as the ttH process. This allows measurement of the coupling due to the direct interaction between the top quark and Higgs boson at the vertex.

In order to calculate the uncertainty on the coupling, the uncertainty of the cross-section of the ttH process must first be calculated, and this can then be converted into the coupling:

$$\frac{\Delta y_t}{y_t} = \kappa \frac{\Delta \sigma}{\sigma} \quad (5.2)$$

where σ is the cross-section of the process, and κ is a prefactor with its origin in theory, normally assumed to be 0.5. In the previous analysis, this figure was calculated as 0.53. This means that by determining the uncertainty on the cross-section of the ttH process $\frac{\Delta \sigma}{\sigma}$, the uncertainty on the coupling can be determined directly in a model-independent manner.

5.2 The $e^+e^- \rightarrow t\bar{t}H$ process

The $t\bar{t}H$ process offers one of the best ways to examine the interaction of the Higgs boson and the top quark, due to the direct interaction between the two at the vertex where the Higgs boson is radiated from the top quark. This process is also uniquely accessible to the linear lepton colliders, as the production threshold is on the order of 500 GeV, above the maximum design energy of both the FCC-ee and the CEPC.

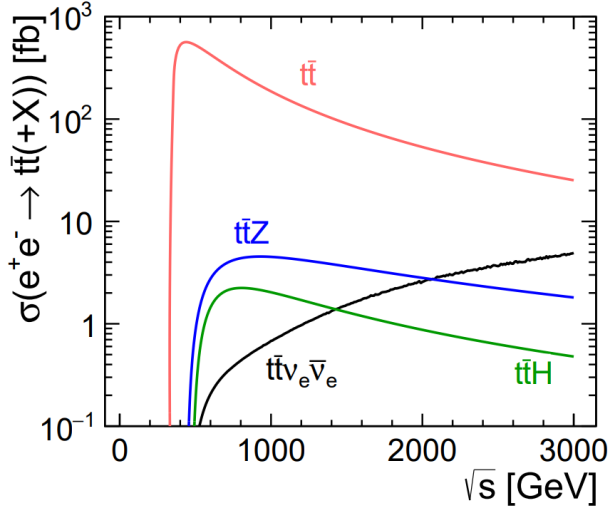


Figure 5.1: The cross-section of various top-quark pair production processes at a lepton collider. This plot assumes a top quark mass of $m_t = 174$ GeV and a Higgs boson mass of $m_H = 125$ GeV, as well as unpolarised beams. The $t\bar{t}$ and $t\bar{t}Z$ processes are important backgrounds for this analysis [23].

The final states of the $t\bar{t}H$ process are complicated due to the variety of decay modes of the particles. In the analysis considered here, the two top quarks are permitted to decay only via the $t \rightarrow W^+ b$ process. The bottom quark forms a jet, while the W boson has all possible decay processes. W bosons can decay *hadronically* into a pair of one up-type quark and one down-type quark (e.g. $u\bar{d}$ or $c\bar{s}$). Or they can decay *leptonically* into a charged lepton and a neutrino of the same flavour (e.g. $e^-\bar{\nu}_e$ or $\mu^+\nu_\mu$). The total branching ratio of all hadronic decays is 68%, and the total branching ratio of all leptonic decays is 32% [74]. We denote a quark-antiquark pair as $q\bar{q}$, and a lepton-neutrino pair as $\ell\nu$.

Given that we focus only on events where the Higgs decays via the process $H \rightarrow b\bar{b}$, there are then three possible final states:

$$e^+e^- \rightarrow t\bar{t}H \rightarrow q\bar{q}q\bar{q}b\bar{b}$$

$$e^+ e^- \rightarrow t\bar{t}H \rightarrow \ell\nu q\bar{q}b\bar{b}$$

$$e^+ e^- \rightarrow t\bar{t}H \rightarrow \ell\nu\ell\nu b\bar{b}$$

Due to the branching ratios, the hadronic and semi-leptonic final states are the most common, and the leptonic final state occurs less than ten percent of the time. This means that the most common final states all heavily rely upon jets, meaning that in order to perform accurate analysis of this process, jet energy resolution and jet reconstruction is of primary importance. As discussed in Chapter 1, the detector concepts for future lepton colliders are designed to focus on jet energy resolution and jet reconstruction, and utilise particle flow to augment this.

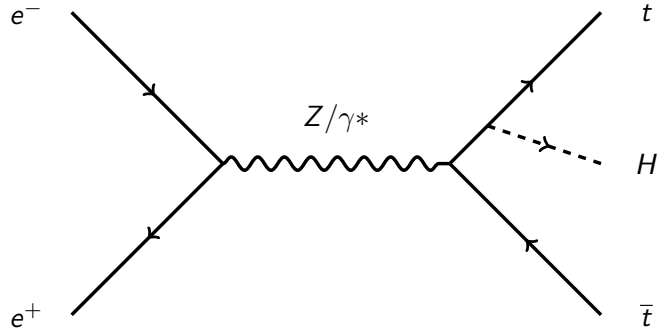


Figure 5.2: Feynman diagram of the ttH event.

There are significant irreducible backgrounds in the form of the $t\bar{t}Z$ and $t\bar{t}b\bar{b}$ processes, both of which are able to produce similar decays with 2, 4 or 6 leptons in the final state. These processes form a large contribution to the background due to their large cross-sections. The $t\bar{t}$ process is also a huge contribution to background because of its extremely high cross-section.

5.2.1 Higgstrahlung

There is also another contribution to the ttH final state in the form of *higgstrahlung*. This process is actually an $e^+ e^- \rightarrow t\bar{t}$ event where the intermediate Z/γ^* radiates a Higgs boson *before* producing the $t\bar{t}$ pair (see Fig. 5.3). This means the final state is ttH but there is no vertex between the top quark and Higgs, meaning this process is not sensitive to the coupling.

If these events are not accounted for when calculating the cross-section of the ttH process, the precision of the coupling measurement will be overestimated, as it is counting

the higgstrahlung events that are not sensitive to the coupling and do not contribute to it.

The effects of higgstrahlung are accounted for by the value of the prefactor κ from Equation 5.2. If the contribution from higgstrahlung is negligible, then $\kappa = 0.5$. When the effect is significant, the value of κ will become greater than 0.5.

This contribution is energy-dependent and at lower energies ($\sqrt{s} \lesssim 500$ GeV) it is assumed to be negligible. However, for energies above 1 TeV, higgstrahlung contributes a non-negligible number of tt̄h events and must be accounted for.

For this analysis, new work using next-to-leading-order (NLO) corrections to QCD, initial state radiation, and beamstrahlung effects [75], determined that $\kappa = 0.503$ [76].

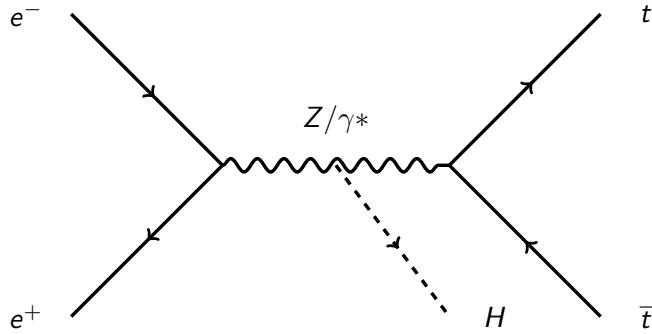


Figure 5.3: Feynman diagram of the higgstrahlung process.

5.3 Generation of Monte Carlo samples

The samples used for the study had been generated using ILCDIRAC [77]. The physics generation was done predominantly in WHIZARD 1.95 [78], using PYTHIA 6.422 [79] for the simulation of hadronisation and fragmentation. Due to constraints of WHIZARD, samples with final states with eight fermions were generated in PHYSSIM [80], also using PYTHIA. The mass of the Higgs boson was set at 125.0 GeV, and the mass of the top quark at 174.0 GeV.

All samples were simulated at $\sqrt{s} = 1.4$ TeV using unpolarised beams, assuming an integrated luminosity of 1.5 ab^{-1} . All samples include an overlay of beam-related backgrounds. See Table 5.1 for a summary of all of the samples used.

Following the generation of the underlying physics events, the interactions of the particles with the detector must be simulated. This was done using the GEANT4 toolkit [81], specifically using the MOKKA tool. Simulation of the signals that result from the

interactions in the detector was done in MARLIN [82].

At the end of this process, the Monte Carlo dataset is in a format identical to how information from the constructed detector would look. At this stage, the analysis can proceed as if the data were real. However, in addition to the simulated detector response, there is also the Monte Carlo truth information, which allows correlation of the simulated detector response data with the “true” particles in the simulation itself. However, the Monte Carlo truth information is only used to determine selection and rejection efficiencies.

The samples were then given weights associated with their expected cross-sections in femtobarns (fb), assuming an integrated luminosity of 1.5 ab^{-1} . See Table 5.1 for a summary of all the generated samples, their cross-sections, sample weights, and expected number of events.

ProdID	Process	Cross-section (fb)	Sample weight	Events in 1.5 ab^{-1}
2435	$t\bar{t}h$, 6 jets, $h \rightarrow b\bar{b}$	0.431	0.03	647
2441	$t\bar{t}h$, 4 jets, $h \rightarrow b\bar{b}$	0.415	0.03	623
2429	$t\bar{t}h$, 2 jets, $h \rightarrow b\bar{b}$	0.100	0.006	150
2438	$t\bar{t}h$, 6 jets, $h \not\rightarrow b\bar{b}$	0.315	0.02	473
2444	$t\bar{t}h$, 4 jets, $h \not\rightarrow b\bar{b}$	0.303	0.02	455
2432	$t\bar{t}h$, 2 jets, $h \not\rightarrow b\bar{b}$	0.073	0.004	110
2450	$t\bar{t}Z$, 6 jets	1.895	0.1	2843
2453	$t\bar{t}Z$, 4 jets	1.825	0.1	2738
2447	$t\bar{t}Z$, 2 jets	0.439	0.03	659
2423	$t\bar{t}b\bar{b}$, 6 jets	0.549	0.03	824
2426	$t\bar{t}b\bar{b}$, 4 jets	0.529	0.03	794
2420	$t\bar{t}b\bar{b}$, 2 jets	0.127	0.008	191
2417	$t\bar{t}$	125.8	1.5	203700

Table 5.1: Table of all signal and background samples used for this analysis. The first two rows are the signal samples, the others are backgrounds.

5.4 Event reconstruction

The $t\bar{t}h$ event has three possible final states, defined by the decay channels of the W bosons produced by the top quarks. The decay of a top quark will always produce a W

boson and a bottom quark. Ignoring the decay of the Higgs boson, there are three possible combinations of final states that can be seen in Table 5.2.

Decay Channel	Final State	No. of leptons	No. of jets	Branching Ratio
Fully hadronic	$q\bar{q}q\bar{q}b\bar{b}$	0	6	46%
Semi-leptonic	$\ell\nu q\bar{q}b\bar{b}$	1	4	45%
Fully leptonic	$\ell\nu\ell\nu b\bar{b}$	2	2	9%

Table 5.2

Given the low branching ratio compared to the other channels, the fully leptonic state is not used in this analysis. Feynman diagrams of the fully hadronic and semi-leptonic final states are shown in Figs. 5.4 and 5.5

5.4.1 Lepton identification

The first step of the analysis procedure is to distinguish between the hadronic and semi-leptonic final states. This is done by finding isolated leptons in the final state. If there are no final-state leptons, the event is classified as hadronic; if there is a single lepton in the final state, the event is classified as semi-leptonic. If there are two leptons in the final state, the event is classified as fully leptonic and discarded.

Finding the leptons that have been produced by the decay of the W boson is relatively simple, as leptons produced in this decay have a much higher energy than leptons produced in jets. In general, leptons produced from W decays have energies in the 50-350 GeV range, which can be found from the reconstructed track energy.

As can be seen in Fig. 5.6, performing a cut on track energies below 15 GeV removes the majority of tau decay products and other particles. This single criterion alone accepts 96.5% of the reconstructed electrons and muons, while accepting only 9.6% of other particles.

However there are additional properties of these leptons that can be used to improve their selection.

Leptons produced within jets will be detected within the same region as the other particles from the same jet, in a high-occupancy region of the detector. Therefore, an isolated lepton detected away from the core of an identified jet is more likely to have originated from the decay of a W boson, rather than from a jet.

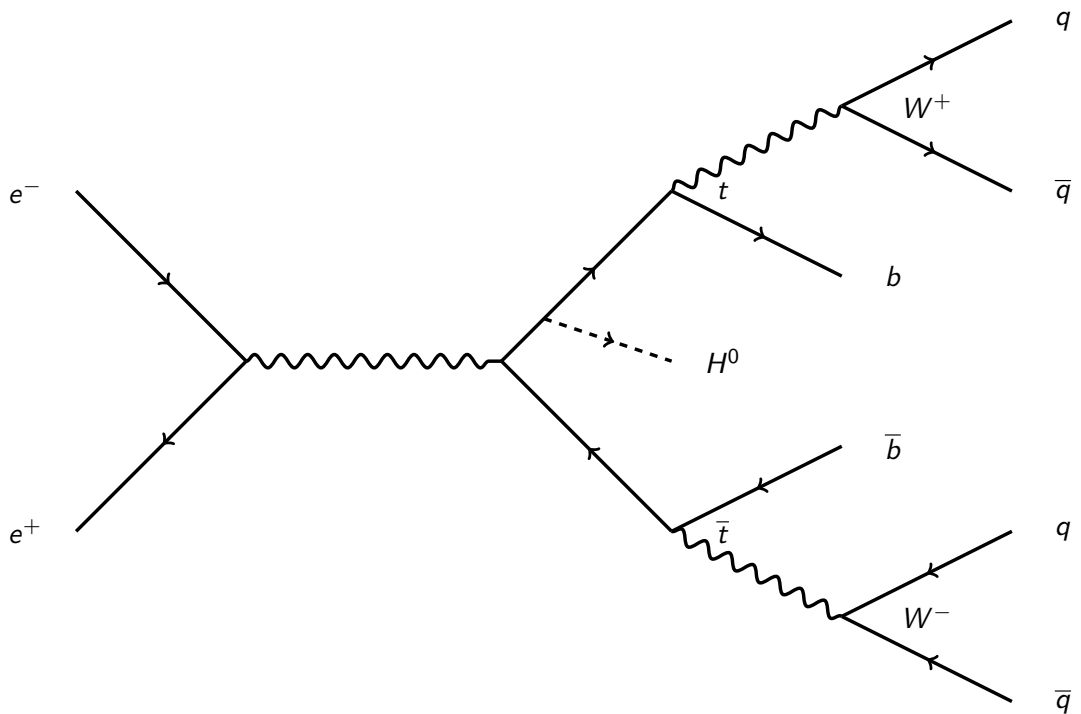


Figure 5.4: Feynman diagram of the $t\bar{t}$ event, showing the fully-hadronic decay channel with the final state $q\bar{q}q\bar{q}b\bar{b}$.

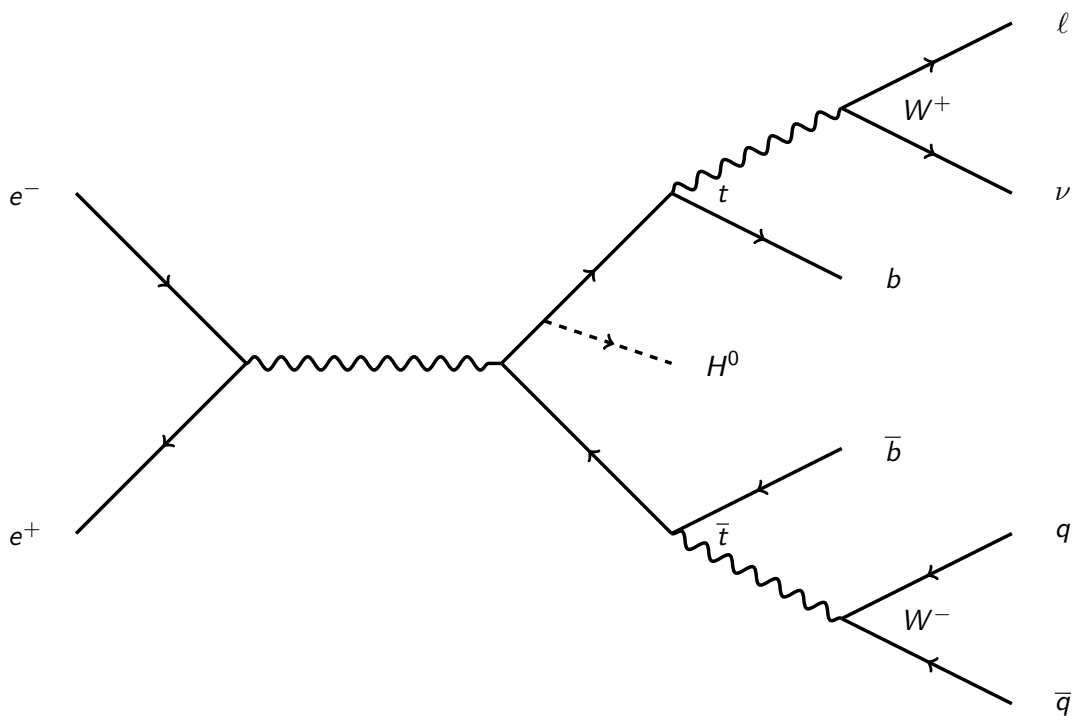


Figure 5.5: Feynman diagram of the $t\bar{t}$ event, showing the semi-leptonic decay channel with the final state $\ell\nu q\bar{q}b\bar{b}$.

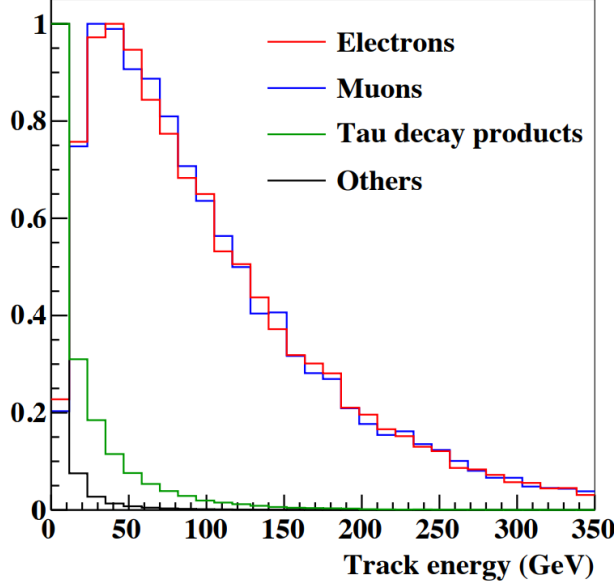


Figure 5.6: Plots of the track energy for truth-matched reconstructed electrons, muons and tau decay products, and all other reconstructed particles that were not truth-matched to a lepton.

The impact parameter (IP) is the distance between the primary vertex that produced a particle, and the closest approach of the particle's track. Electrons and muons produced from W boson decays have much lower IPs than other particles or tau decay products. The impact parameter can be considered in either the longitudinal (Z_0) or radial (d_0) ¹ components, which can be combined for a 3D IP:

$$R_0 = \sqrt{Z_0^2 + d_0^2} \quad (5.3)$$

Figure 5.7 shows the distribution of the three impact parameter variables for truth-matched electrons and muons.

Another property useful for distinguishing electrons and muons decaying from W bosons is the profile of their energy deposition in the calorimeters. We can define a ratio of the energy deposited in the electromagnetic calorimeter to the total energy deposited in the calorimeters:

$$R_{CAL} = \frac{E_{CAL}}{E_{ECAL} + E_{HCAL}} \quad (5.4)$$

Since electrons are contained within the ECAL, their value of R_{CAL} will peak at 1. Muons deposit their energy throughout both calorimeters, so will peak at approximately

¹This is in a cylindrical co-ordinate system, with the central axis of the cylinder along the interaction point of the detector.

0.2 (see Fig. 5.8). Taus cannot be identified this way, as their decay products do not deposit predictable amounts of energy in the calorimeters. Fig. 5.8 shows the separation of electrons and muons from other particles using R_{CAL} .

IsolatedLeptonFinder

To perform the selections to find isolated leptons, the `IsolatedLeptonFinder` processor within MARLIN was used. This lepton finder processor uses criteria based on the properties described above to identify isolated leptons:

- Track energy greater than 15 GeV (Fig. 5.6)
- Each of d_0 , Z_0 and R_0 less than 0.05 mm (Fig. 5.7)
- R_{CAL} greater than 0.5, or in the range 0.05-0.3 (Fig. 5.8)

With these criteria, the isolated lepton finder retains 87.3% of reconstructed isolated electrons and muons, while accepting only 0.4% other particles.

5.4.2 Tau identification

Taus cannot be identified directly due their extremely short lifetime (2.9×10^{-13} s), and must instead be identified from their decay products, which can vary significantly. Taus most commonly decay hadronically into an odd number number of charged or neutral pions, or leptonically into a lepton-neutrino pair; in each case always also producing at least one undetectable tau neutrino.

Identification of taus was done using the `TauFinder` processor [83] within MARLIN, which was adapted for this analysis. The criteria were determined using truth-matching the simulation data to find the best strategy to identify taus.

The processor looks at particles that may have decayed from taus, and forms a tau candidate based on their properties. First it creates a seed track with a p_T greater than 10 GeV, adding all particles within a 0.04 rad cone of the seed track to the tau candidate if every particle has $p_T > 2$ GeV and R_0 within the range 0.01-0.05mm. The reconstructed tau candidate must then be formed of an odd number of charged tracks, with an invariant mass of less than 1.5 GeV. This mass is slightly lower than the true tau invariant mass to account for missing energy in the form of the tau neutrinos. Then an isolation ring is defined in the region 0.04-0.24 rad around the tau candidate seed track. In order to be considered a tau, there must be fewer than five particles in the isolation ring, with a total energy of less than 5 GeV `TauFinder`.

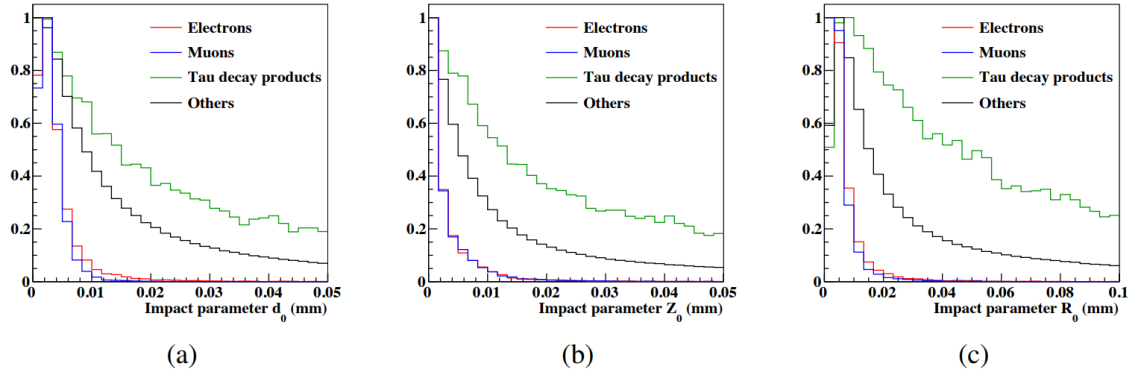


Figure 5.7: Plots of the impact parameters d_0 , Z_0 , and R_0 for truth-matched reconstructed electrons, muons and tau decay products, and all other reconstructed particles that were not truth-matched to a lepton.

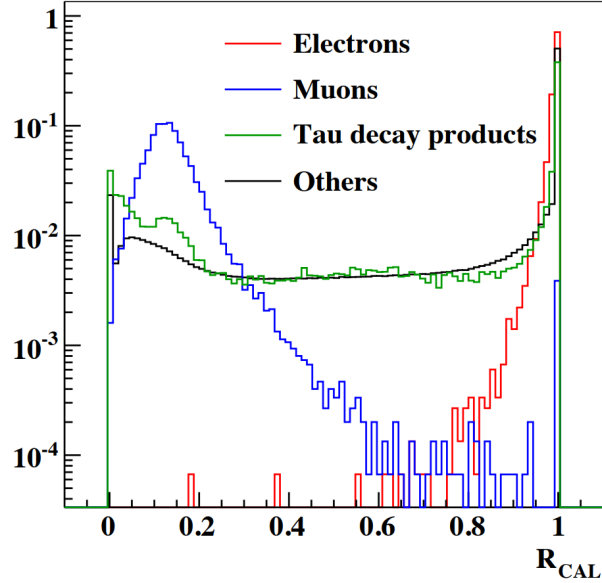


Figure 5.8: Plot of the calorimeter energy ratio R_{CAL} for truth-matched reconstructed electrons, muons and tau decay products, and all other reconstructed particles that were not truth-matched to a lepton, unit normalised. Electrons and muons from W boson decays can be clearly distinguished from each other, and from other particles.

5.4.3 Jet clustering

Any detected isolated leptons are removed from the event, then the event is run through jet clustering using the k_t algorithm [84] with $R = 1.0$. The algorithm is run in exclusive mode, forcing the event into a specific number of jets – in the case of the hadronic analysis, eight jets – plus an additional two beam jets, which are determined by finding the two jets with the lowest angles relative to the beam axis. The beam jets are due to beam-beam backgrounds, and once they have been identified they are removed. Once this is complete, the jet particles are then reclustered using the Durham algorithm [85].

5.4.4 Flavour tagging

The majority of the backgrounds for this analysis do not have four b-jets in the final state. Therefore reliable b-tagging is an important source of discriminating power.

For this analysis, b-tagging is done in the LCFIPlus package [86] which tunes its flavour-tagging using simulated samples of $e^+e^- \rightarrow qqqqqq$ where all quarks have the same flavour. The high number of jets in the final state means that the kinematic properties of the jets are similar to those in the analysis samples. LCFIPlus trains four Boosted Decision Trees (BDT)s for b-tagging, and four for c-tagging, trained using jet properties. These BDTs then give b-tag and c-tag probabilities for each jet, which are used for event selection in the next step.

One of the major differences in this analysis was the upgrade of the flavour-tagging, which removed a bug that influenced the performance of b-tagging [67].

An important variable to select the signal events is the b-tag probabilities of the jets with the four highest b-tags, as well the corresponding c-tag probabilities of these four jets.

5.4.5 Reconstruction of Higgs, top and W boson candidates

After the flavour tagging is completed, the jet energies are used to reconstruct candidates for the Higgs boson, top quarks, and W bosons. The invariant masses of the tops, W bosons, and Higgs are computed, resulting in a χ^2 value. By computing this χ^2 value for all possible combinations of jets and finding the combination that results in the minimum, the jets can be matched to which particles produced them. The χ^2 is calculated as:

$$\chi^2 = \frac{(m_{12} - m_W)^2}{\sigma_W^2} + \frac{(m_{123} - m_t)^2}{\sigma_t^2} + \frac{(m_{45} - m_W)^2}{\sigma_W^2} + \frac{(m_{456} - m_t)^2}{\sigma_t^2} + \frac{(m_{78} - m_H)^2}{\sigma_H^2} \quad (5.5)$$

where the numbered subscripts are labels for the jets used in any particular grouping. A similar equation is used for the semi-leptonic channel, using only the 6 jets present in that process. The χ^2 values are extremely useful for selection, as events that are not ttH, or are ttH events without the fully hadronic decay channel, will have poor χ^2 values, as the jets the event was forced into do not represent physical jets.

5.5 Event selection

The final event selection is done using Boosted Decision Trees, implemented in the Toolkit for Multi-Variate Analysis (TMVA) [87]. In this method, a large number of event variables are fed into the toolkit, which are used to train BDTs to distinguish signal events from background events. The generated events are split randomly into two halves. The first half is used for training the BDTs, and the other becomes the samples used by the BDT. In this analysis, the BDTs are trained separately for each channel.

The BDTs then produce a BDT response value (Fig. 5.16) and a value for this is chosen to optimise the event selection. The criteria for an optimal event selection is the maximal significance:

$$\frac{S}{\sqrt{S + B}} \quad (5.6)$$

where S is the number of signal events selected, and B is the number of background events selected.

For the hadronic channel, the following variables were used request, where some of these are introduced in Sections 5.5.1, 5.5.2, and 5.5.3:

- Reconstructed Higgs mass (Fig. 5.10)
- Number of reconstructed PandoraPFOs in the event (see 5.5.1 and Fig. 5.10)
- Visible jet energy (Fig. 5.10)
- Missing transverse momentum p_T (Fig. 5.10)
- χ^2 of the jet grouping (see 5.4.5 and Fig. 5.10)
- Event shape variables – thrust, sphericity, aplanarity, and oblateness (see 5.5.2 and Figs. 5.10 and 5.11)
- Four highest b-tag values and their corresponding c-tags (see 5.4.4 and Figs. 5.11 and 5.12)

- The cosine of the decay angle of the $h \rightarrow b\bar{b}$, and the cosine of the angles between the Higgs and each top quark (Fig. 5.12)
- The distance between the two closest jets, as defined by the Durham jet clustering algorithm (see 5.5.3 and Fig. 5.13)
- The energy of the four lowest-energy jets (Figs. 5.13 and 5.14)
- The cosine of the angle of the two jets closest to the beam-axis

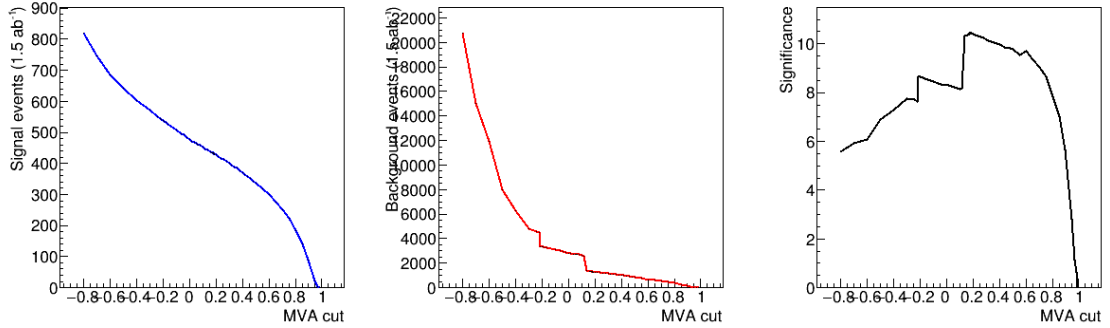


Figure 5.9: Plot showing number of signal events (left) and background events (right) passing the MVA for given cut values; plot showing the significance as a function of MVA cut (right).

5.5.1 PandoraPFOs

The number of particles reconstructed as PandoraPFOs is highly correlated with the number of jets in the event. As the number of jets in the event is not directly measured, since the jet clustering and re-clustering forces the event into a specific number of jets, the number of PFOs can be used to help infer whether the event was a signal event with 8 jets, or a background event with fewer jets.

5.5.2 Event shape

The thrust of event characterises the event shape with respect to the distribution of its momentum. An event's thrust is given by:

$$T = \max \frac{\sum_i |\hat{n} \cdot \vec{p}_i|}{\sum_i |\vec{p}_i|} \quad (5.7)$$

where i is the value for each jet, \vec{p}_i is the momentum of the jet and \hat{n} is the thrust major axis. For example, an event with two jets emitted in exactly opposite directions

would have a thrust of 1. An event with several jets that are spherically symmetric would have a thrust of 0.5. The event thrust is thus a good discriminating variable for the $t\bar{t}$ background, as this is a dijet system and will have much a larger thrust than for the signal event $t\bar{t}h$, or for similar final states like $t\bar{t}Z$ or $t\bar{t}bb$. The effect of the event thrust can be seen in Fig. 5.10.

Also used is the sphericity, which is a measurement of how spherical the event is, when taking into account all the jets. For example, an event with high sphericity would have many jets arrange in a spherically-symmetric manner. The sphericity is given by:

$$S = \frac{\sum_i p_i^\alpha p_i^\beta}{\sum_i |p_i|^2} \quad (5.8)$$

Aplanarity is related to sphericity, and is given by:

$$A = \frac{3}{2} \lambda_3 \quad (5.9)$$

The effects of sphericity and aplanarity can be seen in Fig. 5.11. Also used is the oblateness, a measure of the flattening of sphericity.

5.5.3 Durham jet distance parameter

The Durham jet clustering algorithm defines a distance parameter Y_{ij} such that:

$$Y_{ij} = \frac{\min(E_i^2, E_j^2)(1 - \cos\theta_{ij})}{E_{CM}^2} \quad (5.10)$$

where i represents the n^{th} jet, and j represents the $(n+1)^{\text{th}}$ jet. When the event is forced into an incorrect number of jets – such as when a $t\bar{t}$ event is clustered into eight jets as if it were a fully hadronic $t\bar{t}h$ event – the values of the distances Y_{45} , Y_{56} , and Y_{67} will be smaller than in true eight-jet final states.

5.6 Results

In order to find the value of the cut on the BDT response that gives the maximal significance, the different possible values are looped over. A plot of the MVA cut against the significance can be found in Fig. 5.9. For the the fully hadronic channel, the cut giving the maximum significance was found to be > 0.18 . This corresponds to a significance of 10.4. The result of applying this selection to the BDT response on the event samples can be seen in Table 5.3.

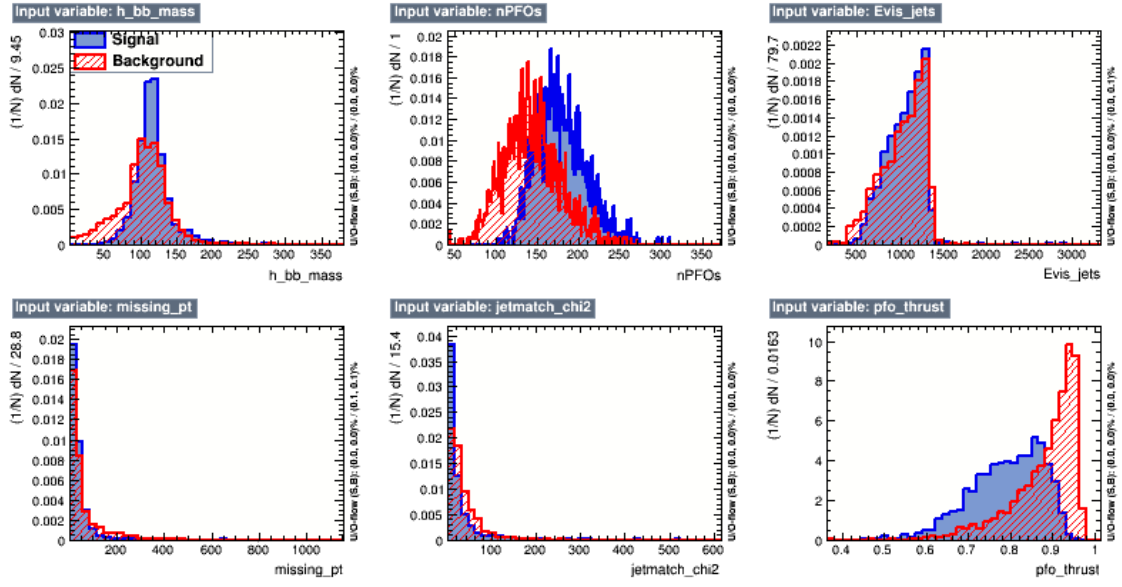


Figure 5.10: Input variables for the BDTs: Higgs mass from $b\bar{b}$ jets; number of particle flow objects; visible jet energy; missing transverse momentum; χ^2 value from jets (from Eq. 5.5); event thrust.

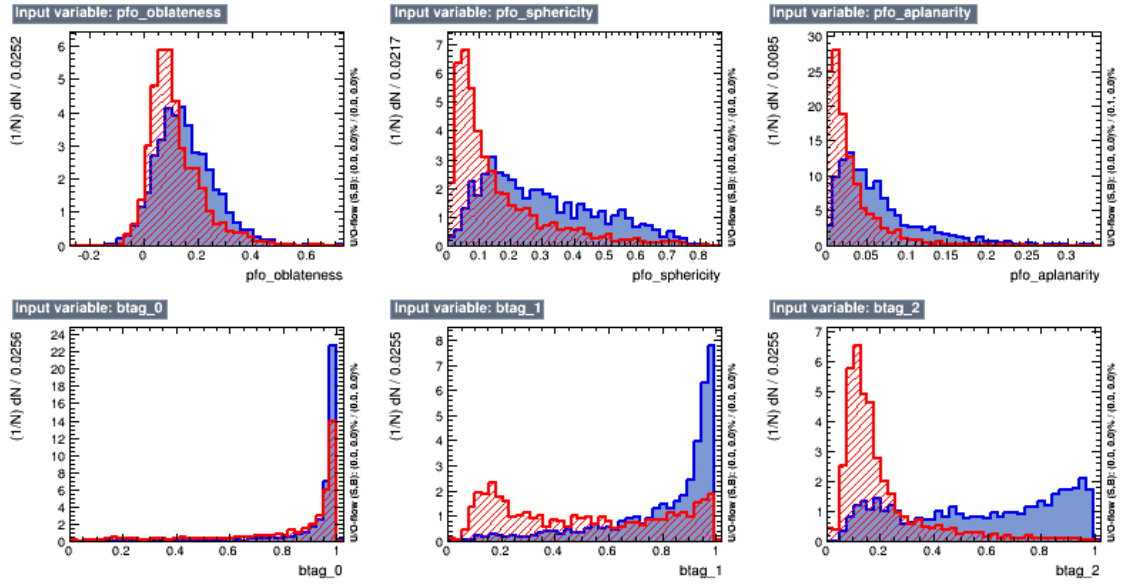


Figure 5.11: Input variables for the BDTs: event oblateness; event sphericity; event aplanarity; first, second and third highest b-tags.

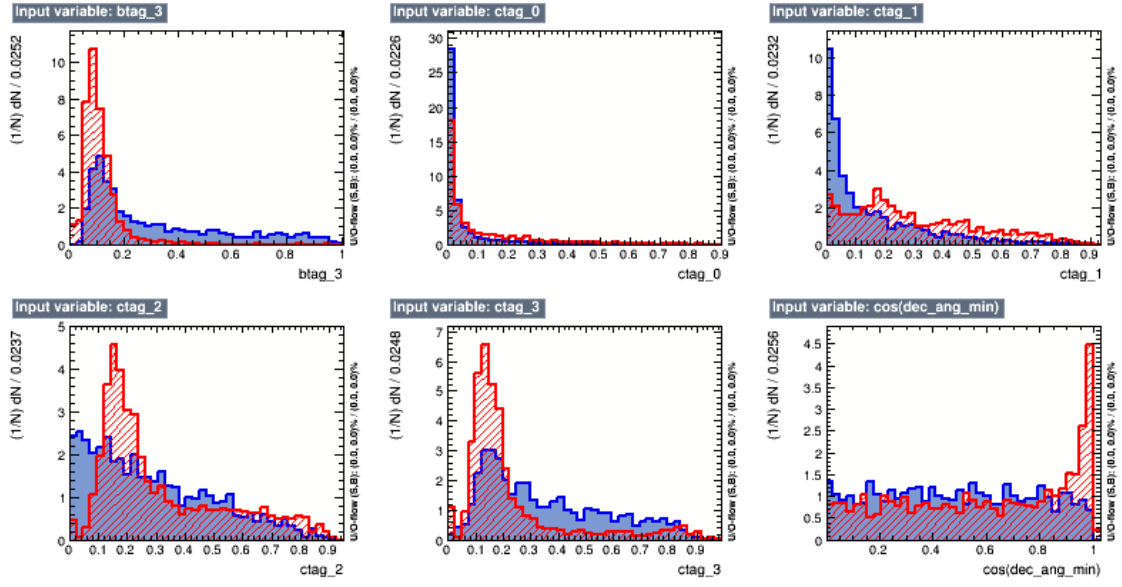


Figure 5.12: Input variables for the BDTs: the fourth highest b-tag; the corresponding c-tags of the jets with the four highest b-tags; the cosine of the Higgs decay angle.

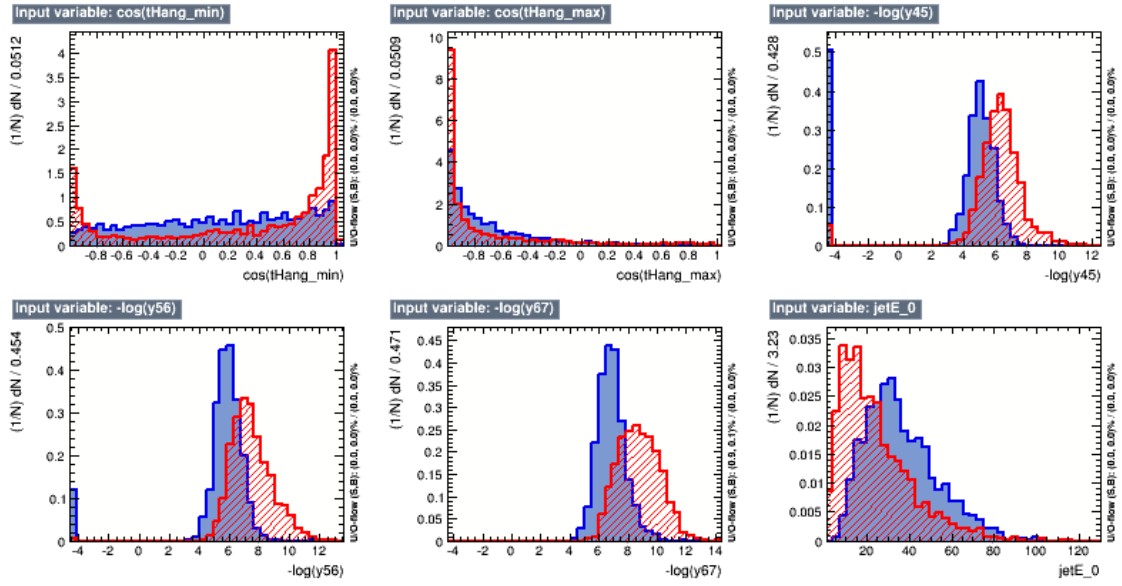


Figure 5.13: Input variables for the BDTs: the cosine of the minimum and maximum angles between the top quark and Higgs boson; the Durham distance values Y_{45} , Y_{56} , and Y_{67} ; lowest jet energy

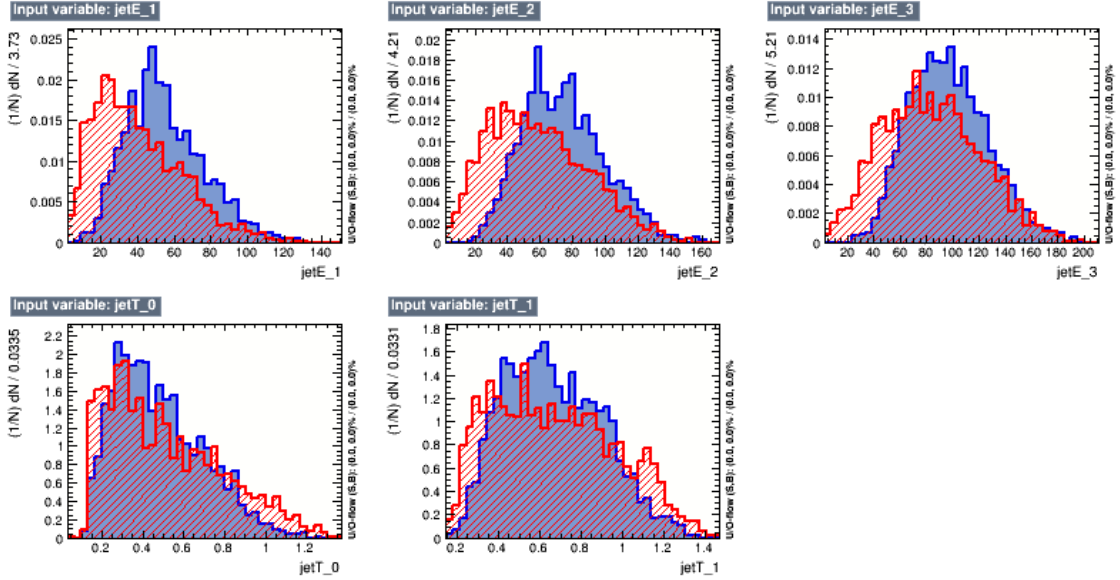


Figure 5.14: Input variables for the BDTs: second, third, and fourth lowest jet energies; the transverse momentum of the first and second jets.

The sensitivity to the top-Higgs Yukawa coupling can then be calculated directly by taking the inverse of the signal significance. With a signal significance of 10.44 in the hadronic channel, the precision on the cross-section is found to be 9.6%. A similar analysis for the semi-leptonic channel found a signal significance of 9.0 and thus a precision on the cross-section of 11.1%. The combined uncertainty for the cross-section of both decay channels is: $\Delta\sigma = 7.5\%$.

In order to use the precision on the measurement of the cross-section to calculate the precision on the measurement of the top-Higgs Yukawa coupling, the contribution of the higgstrahlung diagram must be taken into account, as explained in Section 5.2.1. The value of κ had been determined to be 0.503, therefore the uncertainty on the top-Higgs Yukawa coupling is:

$$\frac{\Delta y_t}{y_t} = 0.503 \frac{\Delta\sigma}{\sigma} = 3.8\% \quad (5.11)$$

This represents an improvement over the previous study [67] where the cross-section could be measured with an accuracy of 10.8% in the fully hadronic channel and 12.0% in the semi-leptonic channel, giving a combined precision of 8.1%. This then translated to the precision on the coupling of 4.27%. Therefore the study presented above represents an improvement of almost 11% from the previous analysis.

These studies also represent a significant increase over the precision the LHC experiments. The full LHC programme, including the high luminosity upgrade (HL-LHC), is

Process	N	Fully hadronic	Semi-leptonic
$t\bar{t}h$, 6 jets, $h \rightarrow b\bar{b}$	647	367	38
$t\bar{t}h$, 4 jets, $h \rightarrow b\bar{b}$	623	1	270
$t\bar{t}h$, 2 jets, $h \rightarrow b\bar{b}$	150	2	22
$t\bar{t}h$, 6 jets, $h \not\rightarrow b\bar{b}$	473	54	11
$t\bar{t}h$, 4 jets, $h \not\rightarrow b\bar{b}$	455	8	22
$t\bar{t}h$, 2 jets, $h \not\rightarrow b\bar{b}$	110	0	1
$t\bar{t}Z$, 6 jets	2843	345	34
$t\bar{t}Z$, 4 jets	2738	59	217
$t\bar{t}Z$, 2 jets	659	1	16
$t\bar{t}b\bar{b}$, 6 jets	824	326	26
$t\bar{t}b\bar{b}$, 4 jets	794	57	226
$t\bar{t}b\bar{b}$, 2 jets	191	2	18
$t\bar{t}$	203700	498	742
total $t\bar{t}H$ signal	2458	433 (17.6%)	365 (14.8%)
total background	211749	1287 (0.61%)	1280 (0.60%)
Significance		10.44	9.00

Table 5.3: Expected numbers of signal and background events classified by the BDTs as either fully hadronic or semi-leptonic in 1.5 ab^{-1} at $\sqrt{s} = 1.4 \text{ TeV}$.

expected to accumulate 3000 fb^{-1} of data at $\sqrt{s} = 14 \text{ TeV}$, and achieve an uncertainty on the top-Higgs Yukawa coupling of between 7-10% [88].

The systematic uncertainties for this study from flavour tagging, lepton reconstruction, and jet energy scale are all expected to be below 10%, making them significantly smaller than the statistical uncertainty of the cross-section [67].

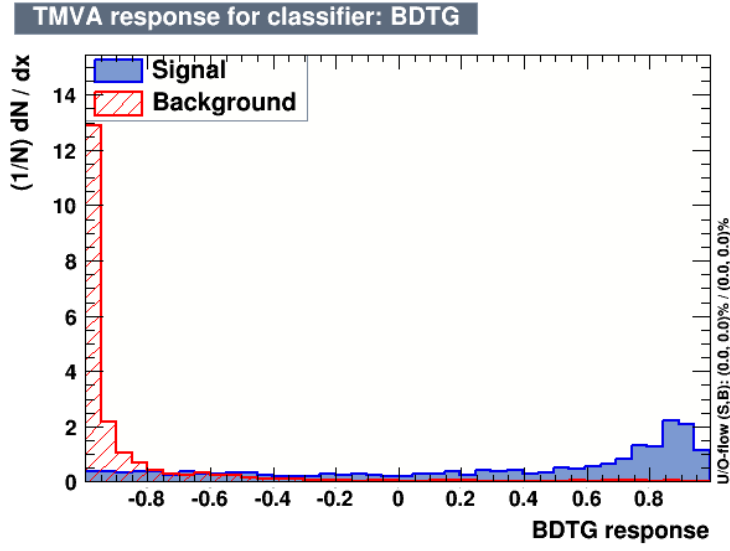


Figure 5.15: Normalised BDTG response for signal and background.

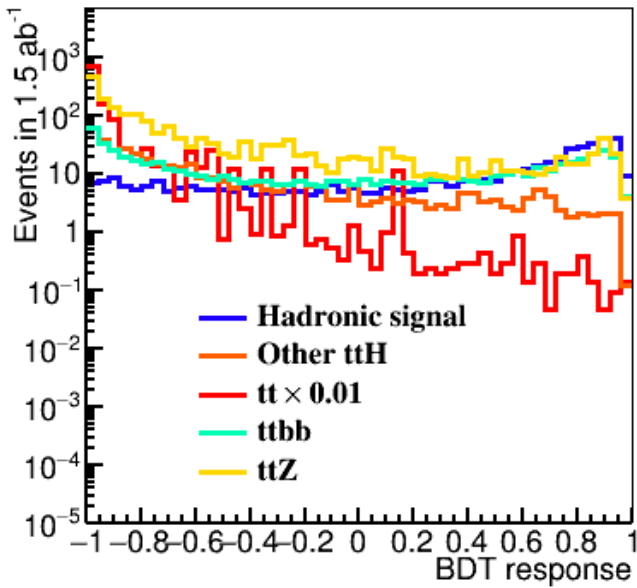


Figure 5.16: BDTG scaled to the number of events expected in 1.5 ab^{-1} . The structure is likely due to the $t\bar{t}$ process' high cross-section, resulting in the $t\bar{t}\bar{h}$ events that pass the selection carry a higher weight.

Chapter 6

Discussion

What we know is really very, very little
compared to what we still have to know.

Fabiola Gianotti

Now that the Large Hadron Collider has confirmed the existence of a Standard Model-like Higgs boson, particle physics is at a crossroads. All indications, including the outcome of the recent European Strategy Meeting in Granada, Spain on the 13th May this year [89], point to the fact that the construction and operation of a lepton collider at the energy frontier is the clearest path ahead.

This thesis has documented a small portion of the global effort to make a future lepton collider a reality, and to pave the way for the future of the study of high energy particle physics.

DQM4hep

The Data Quality Monitoring for High-Energy Physics (DQM4hep) tool was introduced and presented in detail, and its role as a generic online monitor for particle physics experiments, especially within the AIDA-2020 collaboration, was discussed. Development of the important aspect of quality tests was presented, which will allow faster and richer examination of testbeam data with the tool in the future.

An important factor for the uptake of new software like DQM4hep is accessibility. A large contribution that has been made in aid of this is in the form of full, in-depth documentation. While there was existing developer documentation, and other team members wrote user-facing guides about the operation of the framework and its structures, it was also necessary to have a much more focused literature aimed at potential users and their immediate experimental needs.

The user guide explaining the structure of analysis modules, and in-depth examples of how to create new ones, will be a critical resource for any new teams attempting to integrate DQM4hep into their experiment workflows, as well as providing vital documentation for new members of teams who already use the framework. By lowering the barrier to entry, it continues the mission of the DQM4hep to let the physicists focus on the physics, rather than engineering software solutions to solve the same problems over and over again.

Likewise, the quality test user guide provides an in-depth guide to a relatively new feature, but one that is especially powerful. The quality testing feature is foreseen to be most useful within more mature testbeam environments, where the structure and characteristics of the data have been set, and there are precedents for how data should look. This foreknowledge allows the quality tests to be best leveraged, where they are focused on acting as automated checks on how the testbeam is proceeding.

With these combined with the upgrades to the user interface, the framework will be even easier to use and manipulate, which can only benefit its uptake in the community.

AIDA-2020 and IDEA testbeams

In the AIDA-2020 testbeams, understanding and experience of the framework was developing alongside its implementation in experiments. This process was the first time the framework had been applied outside of the environment it was developed in, and the experience acquired was invaluable to understanding how the framework needed to evolve and advance. It also highlighted the important role of documentation and user experience.

Following the experience and expertise acquired in deploying DQM4hep on the CALICE-AHCAL testbeams, this experience was then put to the test using the different and multi-faceted environment of the IDEA combined testbeam. This formed a ‘stress-test’ of the framework, using multiple different types of detector on the same testbeam, with each having their own datatypes, structures, and idiosyncrasies. DQM4hep was able to not only monitor all of these detector types, but also proved that it can even be used for online analysis of these detectors.

These implementations have shown that DQM4hep provides everything that is needed from a generic online monitor and data quality monitor. It can adapt to detectors of many types, timing structures, and triggers. There is even ongoing discussion on the possible use of DQM4hep in the DAMIC direct dark matter detection experiment.

Physics studies at the Compact Linear Collider

The performance of the SiD at the Compact Linear Collider was also examined, using simulated physics and detector interactions of the fully hadronic decay channel of the $e^+e^- \rightarrow t\bar{t}H$ process.

Combined with a similar study of the semi-leptonic channel, it was found that CLIC operating at $\sqrt{s} = 1.4$ TeV using the SiD detector concept would be able to determine the cross-section of the $e^+e^- \rightarrow t\bar{t}H$ process with an uncertainty of 7.3%. The measurement of this cross-section can then be used to directly calculate the top-Higgs Yukawa coupling y_t , meaning that the results of this study can also determine the uncertainty of the measurement of this Yukawa coupling directly.

The Yukawa coupling is an important quantity for examining the dynamics of the Higgs mechanism and the associated Higgs sector of the Standard Model, forming an extremely valuable test of the limits of the SM and a probe for the presence of elusive new physics. The Yukawa coupling of the top quark represents the most accessible of these couplings, and has implications for both the SM and many BSM theories. The result of this study was that the top-Higgs Yukawa coupling could be determined with an uncertainty of 3.8%, offering an increase over previous studies of this process [67] and a significant increase over similar studies that can be performed at the existing experiments at the Large Hadron Collider [88].

The ability of the Compact Linear Collider to perform this measurement with an uncertainty at the percent level, using only one-tenth the centre of mass energy and an integrated luminosity seven orders of magnitude lower than the LHC is a perfect demonstration of the physics case for a lepton collider at the energy frontier. This analysis is thus emblematic of the advantages of the significantly cleaner final state of a lepton collider.

Conclusion

It is often said that particle physics is something like trying to discern the exact mechanisms, inner workings, and design of a finely-crafted pocketwatch by firing it from a cannon at a wall, and sifting through the resulting debris.

Many of the results of these experiments are pulverised brick, providing little to no insight. The other glimmering remnants are what we're interested in – the scraps of metal, the fragments of gems, the twisted springs, and the shards of glass. It's these that we use to try to piece together the whole.

This may seem like madness. But we find ourselves in a universe full of an astonishing

variety of fascinating pocketwatches, yet utterly devoid of the tools we might use to cautiously open them up and examine their mechanisms in a more calm manner. So it seems the cannon is all we have.

In which case, we better get started building a bigger one...

Bibliography

- [1] J Maldacena. Gravity, particle physics and their unification. *arXiv preprint hep-ph/0002092*, 2000. [2](#)
- [2] CPDG Patrignani et al. Review of particle physics. *Chin. Phys.*, 40:100001, 2016. [2](#), [6](#)
- [3] MissMJ. Standard Model of Elementary Particles. https://commons.wikimedia.org/wiki/File:Standard_Model_of_Elementary_Particles.svg, 2006. Accessed: 2019-11-28. [16](#)
- [4] J Goldstone. Field theories with «Superconductor» solutions. *Il Nuovo Cimento (1955-1965)*, 19(1):154–164, 1961. [4](#)
- [5] The ATLAS Collaboration. Observation of a new particle in the search for the Standard Model Higgs boson with the ATLAS detector at the LHC. *Physics Letters B*, 716(1):1–29, 2012. [6](#)
- [6] The CMS Collaboration. Observation of a new boson at a mass of 125 GeV with the CMS experiment at the LHC. *Physics Letters B*, 716(1):30–61, 2012. [6](#)
- [7] S Weinberg. Baryon- and lepton-nonconserving processes. *Phys. Rev. Lett.*, 43:1566–1570, Nov 1979. [6](#)
- [8] T2K Collaboration. Evidence of electron neutrino appearance in a muon neutrino beam. *Phys. Rev. D*, 88:032002, Aug 2013. [6](#)
- [9] BC Allanach. Beyond the Standard Model lectures for the 2016 European School of High-Energy Physics. Technical report, 2016. [6](#)
- [10] M Drees and G Gerbier. Mini-Review of Dark Matter: 2012. *arXiv preprint arXiv:1204.2373*, 2012. [6](#)

- [11] AD Sakharov. Violation of CP invariance, C symmetry, and baryon asymmetry of the universe. *Sov. Phys. Usp.*, 34:392, 1991. [6](#)
- [12] CA Argüelles et al. White Paper on New Opportunities at the Next-Generation Neutrino Experiments (Part 1: BSM Neutrino Physics and Dark Matter). *arXiv preprint arXiv:1907.08311*, 2019. [7](#)
- [13] TM Undagoitia and L Rauch. Dark matter direct-detection experiments. *Journal of Physics G: Nuclear and Particle Physics*, 43(1):013001, 2015. [7](#)
- [14] The ATLAS Collaboration. Observation of $h \rightarrow b\bar{b}$ decays and VH production with the ATLAS detector. *Physics Letters B*, 786:59–86, 2018. [7](#)
- [15] A Djouadi et al. The International Linear Collider Reference Design Report – Volume 2: Physics at the ILC. *arXiv preprint arXiv:0709.1893*, 2007. [7, 8](#)
- [16] S Abachi et al. Observation of the top quark. *Physical Review Letters*, 74(14):2632, 1995. [8](#)
- [17] W Bernreuther. Top-quark physics at the LHC. *Journal of Physics G: Nuclear and Particle Physics*, 35(8):083001, 2008. [9](#)
- [18] SP Martin. A supersymmetry primer. In *Perspectives on supersymmetry*, pages 1–98. World Scientific, 1998. [9](#)
- [19] P de Jong. Supersymmetry searches at the LHC. *arXiv preprint arXiv:1211.3887*, 2012. [9](#)
- [20] S Chatrchyan et al. Search for supersymmetry at the LHC in events with jets and missing transverse energy. *Physical review letters*, 107(22):221804, 2011. [9](#)
- [21] L Randall and D Tucker-Smith. Dijet searches for supersymmetry at the Large Hadron Collider. *Physical review letters*, 101(22):221803, 2008. [9](#)
- [22] JA Conley, HK Dreiner, and P Wienemann. Measuring a light neutralino mass at the ILC: testing the MSSM neutralino cold dark matter model. *Physical Review D*, 83(5):055018, 2011. [9](#)
- [23] P Burrows et al. The Compact Linear e^+e^- Collider (CLIC) – 2018 Summary Report. *CERN Yellow Reports: Monographs*, 2018. [18, 91](#)
- [24] T Behnke et al. The International Linear Collider Technical Design Report – Volume 1: Executive Summary. *arXiv preprint arXiv:1306.6327*, 2013. [9, 10](#)

- [25] J Mnich. The International Linear Collider: Prospects and Possible Timelines. *arXiv preprint arXiv:1901.10206*, 2019. [10](#)
- [26] Assessment of the Revised Plan of International Linear Collider Project (Executive Summary). <http://www.scj.go.jp/ja/info/kohyo/pdf/kohyo-24-k273-en.pdf>, 2019. Accessed: 2019-02-07. [10](#)
- [27] Decision on the International Linear Collider: “not what we had hoped for but progress nevertheless”. <http://www.linearcollider.org/content/decision-international-linear-collider-%E2%80%9Cnot-what-we-had-hoped-progress-nevertheless%E2%80%9D>, 2019. Accessed: 2019-05-17. [10](#)
- [28] MA Thomson. Particle flow calorimetry and the PandoraPFA algorithm. *Nuclear Instruments and Methods in Physics Research Section A: Accelerators, Spectrometers, Detectors and Associated Equipment*, 611(1):25–40, 2009. [11](#)
- [29] JS Marshall, A Münnich, and MA Thomson. Performance of particle flow calorimetry at CLIC. *Nuclear Instruments and Methods in Physics Research Section A: Accelerators, Spectrometers, Detectors and Associated Equipment*, 700:153–162, 2013. [19](#)
- [30] T Behnke et al. The International Linear Collider Technical Design Report – Volume 4: Detectors. Technical report, Argonne National Lab.(ANL), Argonne, IL (United States); Pacific Northwest . . . , 2013. [12](#), [20](#)
- [31] The CLIC Collaboration. Updated baseline for a staged Compact Linear Collider. *arXiv preprint arXiv:1608.07537*, 2016. [13](#), [14](#)
- [32] L Linssen, A Miyamoto, M Stanitzki, and H Weerts. Physics and detectors at CLIC: CLIC conceptual design report. *arXiv preprint arXiv:1202.5940*, 2012. [13](#)
- [33] CLIC Schematic. <http://clic-study.web.cern.ch/content/ctf3>. Accessed: 2019-11-28. [21](#)
- [34] M Benedikt et al. Future Circular Collider: Conceptual Design Report Volume 2. Technical report, FCC-DRAFT-ACC-2018-012, 2018. [14](#)
- [35] M Mangano et al. Future Circular Collider: Conceptual Design Report Volume 1. Technical report, FCC-DRAFT-PHYS-2018-010, 2018. [14](#)

- [36] FCC Schematic. <https://home.cern/science/accelerators/future-circular-collider>. Accessed: 2019-11-28. 21
- [37] CEPC Study Group. CEPC Conceptual Design Report: Volume 1 – Accelerator. *arXiv preprint arXiv:1809.00285*, 2018. 15
- [38] CEPC Study Group. CEPC Conceptual Design Report: Volume 2 – Physics & Detector. *arXiv preprint arXiv:1811.10545*, 2018. 15
- [39] Q Qin et al. Overview of the CEPC Accelerator. 2015. 22
- [40] T Coates et al. DQM4HEP - A Generic Online Monitor for Particle Physics Experiments. In *2017 Topical Workshop on Electronics for Particle Physics*, number PoS(TWEPP-17)050. PoS, 2017. 23, 57
- [41] T Coates et al. DQM4HEP - A Generic Online Monitor for Particle Physics Experiments. In *2017 IEEE Nuclear Science Symposium and Medical Imaging Conference (NSS/MIC)*, pages 1–4. IEEE, 2017. 23, 57
- [42] E Corrin. EUDAQ software user manual. *EUDET-Memo-2010-01*, 2010. 25
- [43] CC Almenar, A Corso-Radu, H Hadavand, Y Ilchenko, S Kolos, K Slagle, and A Taf-fard. ATLAS online data quality monitoring. In *2010 17th IEEE-NPSS Real Time Conference*, pages 1–5. IEEE, 2010. 26
- [44] AIDA-2020 Project Webpage. <http://aida2020.web.cern.ch>. Accessed: 2019-07-02. 26, 57
- [45] R Ete, T Coates, and A Pingault. DQM4HEP: A generic data quality monitoring framework for HEP. Technical report, 2018. 27
- [46] C Gaspar, M Dönszelmann, and P Charpentier. DIM, a portable, light weight package for information publishing, data transfer and inter-process communication. *Computer Physics Communications*, 140(1-2):102–109, 2001. 27
- [47] Qt. <https://www.qt.io/qt-framework>, 2015. Accessed: 2019-11-27. 30
- [48] DQM4hep User Manual – Event Definition. <https://dqm4hep.readthedocs.io/en/latest/user-manual/event-interface/#a-built-in-event-type-generic-event>. Accessed: 2019-02-07. 38
- [49] DQM4hep User Manual – Core Tools. <https://dqm4hep.readthedocs.io/en/latest/user-manual/core-tools/#the-logging-tools>. Accessed: 2019-02-07. 40

- [50] DQM4hep User Manual – Plugin System. <https://dqm4hep.readthedocs.io/en/latest/user-manual/plugin-system/>. Accessed: 2019-02-07. 51
- [51] DQM4hep Doxygen Pages. <https://dqm4hep.github.io/dqm4hep-doxygen/doxygen/dqm4hep/master/index.html>. Accessed: 2019-02-07. 54
- [52] DQM4hep User Manual. <https://dqm4hep.readthedocs.io/en/latest/>. Accessed: 2019-02-07. 55
- [53] V Balagura, S Bilokin, J Bonis, V Boudry, J-C Brient, S Callier, T Cheng, R Cornat, C De La Taille, TH Doan, et al. SiW ECAL for future e+ e- collider. *Journal of Instrumentation*, 12(07):C07013, 2017. 58
- [54] F Sefkow, F Simon, and the CALICE Collaboration. A highly granular SiPM-on-tile calorimeter prototype. In *Journal of Physics: Conference Series*, volume 1162, page 012012. IOP Publishing, 2019. 58
- [55] T Behnke et al. Test Beams at DESY. *EUDET-Memo-2007-11*, 2007. 59
- [56] Introduction to the use of the H6 beam. <http://sba.web.cern.ch/sba/BeamsAndAreas/h6/H6manual.pdf>, 2000. Accessed: 2019-06-21. 59
- [57] Introduction to the use of the H8 beam. <http://sba.web.cern.ch/sba/BeamsAndAreas/h8/H8manual.pdf>, 2000. Accessed: 2019-06-21. 59
- [58] AHCAL beam interface (BIF). https://indico.cern.ch/event/468478/contributions/2197579/attachments/1290870/1923089/2016-06-14_AIDA_BIF.pdf. Accessed: 2019-07-04. 60
- [59] S Lee, M Livan, and R Wigmans. Dual-readout calorimetry. *Reviews of Modern Physics*, 90(2):025002, 2018. 74
- [60] S Lee et al. Hadron detection with a dual-readout fiber calorimeter. *Nuclear Instruments and Methods in Physics Research Section A: Accelerators, Spectrometers, Detectors and Associated Equipment*, 866:76–90, 2017. 74
- [61] F Sauli. The gas electron multiplier (GEM): Operating principles and applications. *Nuclear Instruments and Methods in Physics Research Section A: Accelerators, Spectrometers, Detectors and Associated Equipment*, 805:2–24, 2016. 74

- [62] G Bencivenni, R De Oliveira, G Morello, and MP Lener. The micro-Resistive WELL detector: a compact spark-protected single amplification-stage MPGD. *Journal of Instrumentation*, 10(02):P02008, 2015. [74](#)
- [63] G Chiarello. The full stereo drift chamber for the MEG II experiment. *Journal of Instrumentation*, 12(03):C03062, 2017. [75](#)
- [64] T Coates and I Vivarelli. Private communication. [77](#)
- [65] DREAM Event Selection. https://indico.cern.ch/event/771372/contributions/3204780/attachments/1748752/2832603/SJ_DREAM_slides.pdf. Accessed: 2019-06-27. [83](#)
- [66] RD52 calorimeter – equalisation and electron response vs. material. https://indico.cern.ch/event/771372/contributions/3204780/attachments/1748752/2832603/SJ_DREAM_slides.pdf. Accessed: 2019-06-27. [85](#)
- [67] S Redford, P Roloff, and M Vogel. Physics potential of the top-Yukawa coupling measurement at a 1.4 TeV Compact Linear Collider using the CLIC SiD detector. *CLICdp-Note-2014-001*, 2014. [89, 100, 106, 107, 111](#)
- [68] The CLICdp Collaboration. Top-Quark Physics at the CLIC Electron-Positron Linear Collider. *arXiv preprint arXiv:1807.02441*, 2018. [89](#)
- [69] The CLIC Collaboration. The Compact Linear Collider (CLIC) – 2018 Summary Report. Technical report, 2018. [89](#)
- [70] A Broggio, EJ Chun, M Passera, KM Patel, and SK Vempati. Limiting two-Higgs-doublet models. *Journal of High Energy Physics*, 2014(11):58, 2014. [90](#)
- [71] P Draper and H Rzehak. A review of Higgs mass calculations in supersymmetric models. *Physics Reports*, 619:1–24, 2016. [90](#)
- [72] D Marzocca, M Serone, and J Shu. General composite Higgs models. *Journal of High Energy Physics*, 2012(8):13, 2012. [90](#)
- [73] M Perelstein. Little Higgs models and their phenomenology. *Progress in Particle and Nuclear Physics*, 58(1):247–291, 2007. [90](#)
- [74] Particle Data Group. Review of Particle Physics. *Physical Review D-Particles, Fields, Gravitation and Cosmology*, 86(1):010001, 2012. [91](#)

- [75] D Schulte. High energy beam-beam effects in CLIC. In *Proceedings of the 1999 Particle Accelerator Conference (Cat. No. 99CH36366)*, volume 3, pages 1668–1670. IEEE, 1999. [93](#)
- [76] BC Nejad, W Kilian, JM Lindert, S Pozzorini, J Reuter, and C Weiss. NLO QCD predictions for off-shell $t\bar{t}$ and $t\bar{t}h$ production and decay at a linear collider. *Journal of High Energy Physics*, 2016(12):75, 2016. [93](#)
- [77] C Grefe, S Poss, A Sailer, and A Tsaregorodtsev. ILCDIRAC, a DIRAC extension for the linear collider community. In *Journal of Physics: Conference Series*, volume 513, page 032077. IOP Publishing, 2014. [93](#)
- [78] W Kilian, T Ohl, and J Reuter. WHIZARD — simulating multi-particle processes at LHC and ILC. *The European Physical Journal C*, 71(9):1742, 2011. [93](#)
- [79] T Sjöstrand, S Mrenna, and P Skands. PYTHIA 6.4 physics and manual. *Journal of High Energy Physics*, 2006(05):026, 2006. [93](#)
- [80] Physsim. <https://www-jlc.kek.jp/subg/offl/physsim/>. Accessed: 2019-06-27. [93](#)
- [81] S Agostinelli et al. GEANT4 — a simulation toolkit. *Nuclear instruments and methods in physics research section A: Accelerators, Spectrometers, Detectors and Associated Equipment*, 506(3):250–303, 2003. [93](#)
- [82] F Gaede and J Engels. Marlin et al - A Software Framework for ILC detector R&D. *EUDET-Report-2007-11*, 2007. [94](#)
- [83] A Münnich. TauFinder: A reconstruction algorithm for τ leptons at linear colliders. Technical report, 2010. [98](#)
- [84] S Catani, YL Dokshitzer, MH Seymour, and BR Webber. Longitudinally-invariant k_t -clustering algorithms for hadron-hadron collisions. *Nuclear Physics B*, 406(1-2):187–224, 1993. [100](#)
- [85] S Catani, YL Dokshitzer, M Olsson, G Turnock, and BR Webber. New clustering algorithm for multijet cross sections in e^+e^- annihilation. *Physics Letters B*, 269(3-4):432–438, 1991. [100](#)
- [86] T Suehara and T Tanabe. LCFIPlus: A framework for jet analysis in linear collider studies. *Nuclear Instruments and Methods in Physics Research Section A: Accelerators, Spectrometers, Detectors and Associated Equipment*, 808:109–116, 2016. [100](#)

- [87] S Hoecker et al. TMVA – Toolkit for multivariate data analysis. *arXiv preprint physics/0703039*, 2007. 101
- [88] S Dawson, A Gritsan, H Logan, J Qian, C Tully, and R Van Kooten. Working group report: Higgs boson. Technical report, Fermi National Accelerator Lab.(FNAL), Batavia, IL (United States), 2013. 107, 111
- [89] Summary: Electroweak session. <https://indico.cern.ch/event/808335/contributions/3365082/attachments/1845504/3028247/SummaryTalk.pdf>. Accessed: 2019-07-04. 109

Acronyms

μ -RWELL Micro-Resistive WELL. 74

ADC Analogue to Digital Conversion. 38, 39, 42, 44, 61, 63, 64, 66, 67, 76–82, 84, 85, 87

AHCAL Analogue Hadronic Calorimeter. 12, 58–60, 63, 66, 68, 69, 110

AIDA Advanced Infrastructures for Detectors at Accelerators. v, vi, 23, 25, 26, 56–60, 71, 72, 109, 110

ATLAS A Toroidal LHC Apparatus. 7, 26

BDT Boosted Decision Trees. 9, 100, 101, 103, 107

BIF Beam Interface. 59, 60

BSM Beyond the Standard Model. 1, 7, 9, 111

CALICE Calorimeter for Linear Collider Experiment. 58, 68, 69, 72, 110

CDR Conceptual Design Report. 14, 15

CEPC Circular Electron Positron Collider. 2, 15, 22, 72, 91

CERN *Conseil européen pour la recherche nucléaire*. 10, 13, 24, 26, 33, 58, 59, 66, 68, 69, 72, 73, 77, 89

CLIC Compact Linear Collider. 1, 13, 14, 18, 19, 21, 89, 111

CLICdp CLIC detector and physics. 89

CSV Comma-Separated Values. 76

DAMIC Dark Matter in CCDs. 110

DAQ Data Acquisition. 24, 26

DESY *Deutsches Elektronen-Synchrotron*. 10, 24, 33, 58, 59

DIM Distributed Information Management System. 27, 45

DQM Data Quality Monitoring. 25, 46

DQM4hep Data Quality Monitoring for High-Energy Physics. 23, 25–31, 33, 36–39, 45, 46, 48, 51, 54–57, 59–61, 63, 65, 66, 71, 72, 75–77, 80, 85, 109, 110

DQMF Data Quality Monitoring Framework. 26

DREAM Dual Readout Method. 74

DWC Delay Wire Chamber. 75

ECAL Electromagnetic Calorimeter. 12, 13, 97

EDM Event Data Model. 28

EUDAQ EU Data Acquisition. 25, 26, 59

FCC Future Circular Collider. 2, 14, 15, 21, 72, 91

FLC *Forschung mit Lepton Collidern*. 58

GEM Gas Electron Multiplier. 76

GUI Graphical User Interface. 30, 32, 33

HCAL Hadronic Calorimeter. 12, 13

HL-LHC High Luminosity Large Hadron Collider. 1, 10, 18, 106

IDEA Innovative Detector for Electron-positron Accelerators. vi, 71–73, 80, 110

IEEE Institute of Electrical and Electronics Engineers. 23

ILC International Linear Collider. 1, 9–12, 14, 15, 17

ILD International Large Detector. 11–13, 15, 19, 20

IP Impact Parameter. 97

IP Interaction Point. 10

JINR Joint Institute for Nuclear Research. 10

JSON Javascript Object Notation. 49, 50

LCIO Linear Collider Input/Output. 30, 60

LEP Large Electron Positron Collider. 15

LHC Large Hadron Collider. 1, 6, 7, 9, 10, 13, 15, 26, 59, 106, 109, 111

MAPS Monolithic Active Pixel Sensor. 12

MIP Minimum Ionising Particle. 60, 64, 65, 83

MSSM Minimal Supersymmetric Standard Model. 90

PFO Particle Flow Object. 102

QCD Quantum Chromodynamics. 7, 8, 93

qtest quality test. 46, 49–53

RF radio frequency. 13

RPC resistive plate chambers. 12

SCRF Superconducting Radio Frequency. 9

SDHCAL Semi-Digital Hadronic Calorimeter. 12, 32

SiD Silicon Detector. 11, 12, 20, 89, 111

SiPM Silicon Photomultipliers. 12, 58, 62, 69

SiWECAL Silicon Tungsten Electronic Calorimeter. 58, 60

SM Standard Model. v, 1–4, 6, 8, 9, 18, 90, 109, 111

SPPC Super Proton Proton Collider. 15

SPS Super Proton Synchrotron. 24, 58, 59, 66, 68, 69, 72, 73, 77, 78

SUSY Supersymmetry. 9

TDC Time to Digital Conversion. 60, 61, 76, 77

TDR Technical Design Report. 10

TMVA Toolkit for Multi-Variate Analysis. 101

TPC Time Projection Chamber. 12, 15

XML Extensible Markup Language. 35, 39, 44, 49, 50, 52, 53, 55, 56, 63, 65, 76, 80